INFORMATION TO USERS

While the most advanced technology has been used to photograph and reproduce this manuscript, the quality of the reproduction is heavily dependent upon the quality of the material submitted. For example:

- Manuscript pages may have indistinct print. In such cases, the best available copy has been filmed.
- Manuscripts may not always be complete. In such cases, a note will indicate that it is not possible to obtain missing pages.
- Copyrighted material may have been removed from the manuscript. In such cases, a note will indicate the deletion.

Oversize materials (e.g., maps, drawings, and charts) are photographed by sectioning the original, beginning at the upper left-hand corner and continuing from left to right in equal sections with small overlaps. Each oversize page is also filmed as one exposure and is available, for an additional charge, as a standard 35mm slide or as a 17"x 23" black and white photographic print.

Most photographs reproduce acceptably on positive microfilm or microfiche but lack the clarity on xerographic copies made from the microfilm. For an additional charge, 35mm slides of 6"x 9" black and white photographic prints are available for any photographs or illustrations that cannot be reproduced satisfactorily by xerography.

Schnitzlein, Michael Georg

THE HYDRODYNAMICS OF A FAST FLUIDIZED BED CHARACTERIZED BY ITS PRESSURE SIGNALS

City University of New York PH.D. 1987

PLEASE NOTE:

In all cases this material has been filmed in the best possible way from the available copy. Problems encountered with this document have been identified here with a check mark __✓__.

1. Glossy photographs or pages _____
2. Colored illustrations, paper or print _____
3. Photographs with dark background _____
4. Illustrations are poor copy _____
5. Pages with black marks, not original copy _____
6. Print shows through as there is text on both sides of page _____
7. Indistinct, broken or small print on several pages __✓__
8. Print exceeds margin requirements _____
9. Tightly bound copy with print lost in spine _____
10. Computer printout pages with indistinct print _____
11. Page(s) _____ lacking when material received, and not available from school or author.
12. Page(s) _____ seem to be missing in numbering only as text follows.
13. Two pages numbered _____. Text follows.
14. Curling and wrinkled pages _____
15. Dissertation contains pages with print at a slant, filmed as received __✓__
16. Other _____

_____

_____

University
Microfilms
International

THE HYDRODYNAMICS OF A FAST FLUIDIZED BED CHARACTERIZED BY ITS PRESSURE SIGNALS

by

MICHAEL G. SCHNITZLEIN

A dissertation submitted to the Graduate Faculty in Engineering in partial fulfillment of the requirements for the degree of Doctor of Philosophy, The City University of New York.

1987

This manuscript has been read and accepted for the Graduate Faculty in Engineering in satisfaction of the dissertation requirement for the degree of Doctor of Philosophy.

2/6/87 — Chairman of Examining Committee
Date

2/6/87 — Executive Officer
Date

Dr. J.M. Matsen
Prof. R. Shinnar
Prof. G. Tardos
Prof. R.A. Graff
Prof. R. Mauri

Supervisory Committee

The City University of New York

Abstract

THE HYDRODYNAMICS OF A FST FLUIDIZED BED
CHARACTERIZED BY ITS PRESSURE SIGNALS

by

Michael G. Schnitzlein

Advisor: Professor H. Weinstein

Fast fluidization flow characteristics were studied using instantaneous pressure signals in a fast fluidization unit with 0.152 m I.D. and 8.4 m height using as a solid a Zeolite FCC catalyst, HFZ-33 (dp = 59 um).

The data confirmed that a fast fluidized bed can usually be clearly divided into two main regions, a dense region at the bottom and a dilute region at the top of the bed. Within both regions the mean void fractions are essentially constant along the height and only dependent on flow parameters, i.e. superficial gas velocities and solid rate. In particular the void fraction in the dense region is even independent of the solid rate and varies only slightly with the superficial gas velocity.

The bed height, taken as the transition between dense and dilute regions, is clearly influenced both by flow parameters and flow conditions in the gas entrance section. This leaves the latter as a powerful tool for variations in solid hold-up under otherwise constant gas velocities and solid rates.

Upward moving instabilities were detected within the dense region of the bed with a wave speed being fairly constant over a wide range of flow parameters. There is a clear similarity to phenomena in slugging fluidized beds.

The presented results suggest that the solid in the dense regions of high-velocity fluidized beds is present in three different forms; fairly stagnant in a dense annulus region, very dilute in a core region and in the form of waves rolling upward between the core and dense annulus.

A C K N O W L E D G M E N T S

I am grateful to my mentor, Professor Herbert Weinstein, for his support, encouragement and guidance throughout the research project as also for his personal interest in me.

I would like to thank Professor J. Werther for my early exposure and training in fluidization which paved the way to many of the concepts developed in this work.

I wish to acknowledge the members of my thesis committee, Professor R. Shinnar, Professor R.A. Graff, Professor G. Tardos, Professor R. Mauri and Dr. J.M. Matsen for their interest in this work and helpful suggestions.

Valuable contributions to this work were made by my friends: P. Sacker performed the many experimental runs on the fluidization rig, E. Bandlamudi developed a great deal of the data base management system and H.-J. Feindt helped with the lay-out of this dissertation.

To my colleagues and the technical and administrative staff of the Chemical Engineering Department of the City College thank you very much for your support and assistance.

Financial support for this project was given by the National Science Foundation under Grant # CBT-8103627A.

Finally, the completion of this work was specially made possible by the love, patience and able help of my wife, Bethel.

Above all I acknowledge my Lord and God, Jesus Christ, without whom, even this work would be meaningless for me.

To my father,

Ingenieur Otto W. Schnitzlein,

whose great ingenuity

inspired me for

innovative and creative

engineering

T A B L E O F C O N T E N T S

ABSTRACT iv

ACKNOWLEDGMENTS v

TABLE OF CONTENTS vi

LIST OF TABLES ix

LIST OF FIGURES x

NOMENCLATURE xxi

1 INTRODUCTION 1

2 LITERATURE REVIEW 4

2.1 APPLICATION OF CIRCULATING FLUIDIZED BEDS 5

2.1.1 COAL COMBUSTION
IN CIRCULATING FLUIDIZED BEDS 9

2.1.2 CALCINATION
IN CIRCULATING FLUIDIZED BEDS 13

2.1.3 GAS ABSORPTION
IN CIRCULATING FLUIDIZED BEDS 15

2.2 REVIEW ON HYDRODYNAMCS OF GAS-SOLIDS UP-FLOW
IN VERTICAL PIPES 17

2.2.1 FAST FLUIDIZATION 17

2.2.2 PNEUMATIC TRANSPORT OF SOLIDS 27

2.3 DISCUSSION ON HYDRODYNAMICS
OF FAST FLUIDIZED BEDS 37

3 EXPERIMENTAL EQUIPMENT 40

3.1 THE CIRCULATING FLUIDIZED BED SYSTEM 40

T A B L E O F C O N T E N T S (CONT.)

3.2 DATA ACQUISITION OF BASIC PRESSURE READINGS 42
3.3 TIME SERIES MEASUREMENTS
FOR PRESSURE FLUCTUATIONS 45
4 EXPERIMENTAL RESULTS 49
4.1 TIME AVERAGED VOID FRACTION IN THE TOP AND
BOTTOM REGION OF THE FAST FLUIDIZED BED 51
4.1.1 THE VOID FRACTION IN THE BOTTOM REGION
OF A FAST FLUIDIZED BED 67
4.1.2 THE VOID FRACTION IN THE TOP REGION
OF A FAST FLUIDIZED BED 82
4.2 VARIATIONS OF THE BED HEIGHT
IN A FAST FLUIDIZED BED 92
4.3 FFT ANALYSIS OF PRESSURE SIGNALS
IN THE FAST FLUIDIZED BED 104
4.3.1 PREDOMINANT FREQUENCIES
OF PRESSURE SIGNALS 105
4.3.2 WAVE SPEED IN FAST FLUIDIZED FLOW 110
4.4 DISCUSSION OF EXPERIMENTAL RESULTS 122
5 CONCLUSIONS 134
APPENDIX A (SUMMARY OF EXPERIMENTAL RUNS) 137
APPENDIX B (INFORMATION ON PRESSURE DIFFERENTIALS) 145
REFERENCES 147

L I S T O F T A B L E S

Page

Tab. 1 Comparision of different gas-solid reactors 7

Tab. 2 Comparision between combustion of solid fuel in bubbling and circulating fluidized beds 11

L I S T O F F I G U R E S

		Page
Fig. 1	Comparision of different gas-solid reactors by solid retention time and particle size	8
Fig. 2	Process schematic of a circulating fluidized bed combustor (steam generation for 230t/h, build in Duisburg, West Germany)	12
Fig. 3	Process schematic for a circulating fluidized bed calciner	14
Fig. 4	Process schematic circulating fluidized bed for gas adsorption	16
Fig. 5	Void fraction profiles in fast fluidized beds (Li et al., 1982)	21
Fig. 6	Hydrodynamic Model by Li and Kwauk, 1980	23
Fig. 7	Reduced mass flux profiles in a fast fluidized bed (Ug = 3.2 m/s) for various solid rates (Monceaux et al.(1985)	26
Fig. 8	Pressure fluctuations in a 3-in pneumatic transport line (Capes, 1971)	29
Fig. 9	Pressure gradient vs. height in a pneumatic transport line (Capes and Nakamura, 1973)	31
Fig. 10	Particle velocities as a function of radius in the freeboard of a fluidized bed for different gas velocities (Morooka, 1983)	33

L I S T O F F I G U R E S (cont.)

Page

Fig. 11 Particle velocities as a function of height in a vertical pneumatic conveying line for different fractions of particle size (Arastroopour, 1979) 35

Fig. 12 Laboratory system for fast fluidization experiments 41

Fig. 13 Power sprectum of a 110 Hz pressure signal (Fan-test arrangement), window of 8192 data points 46

Fig. 14 Auto correlation function of a gauge pressure signal in a slugging fluidized bed 46

Fig. 15 Cross correlation function of gauge pressure signals in a slugging fluidized bed 46

Fig. 16 Typical void fraction profile in a fast fluidized bed 50

Fig. 17 Void fraction profile of a bubbling fluidized bed (Ug = 0.03 m/s) 52

Fig. 18 Void fraction profile of a slugging fluidized bed (Ug = 0.7 m/s) 53

Fig. 19 Void fraction profile in a high velocity fluidized bed (Ug = 1.5 m/s, Gs = 65 kg/m2s) 54

L I S T O F F I G U R E S (cont.)

Page

Fig. 20 Void fraction profile in a high velocity fluidized bed (Ug = 3.0 m/s, Gs = 133 kg/m2s) 55

Fig. 21 Probability density functions of differential pressures in a bubbling fluidized bed (Ug = 0.03 m/s) 57

Fig. 22 Probability density functions of differential pressures in a slugging fluidized bed (Ug = 1.0 m/s) 58

Fig. 23 Probability density functions of differential pressures in a high velocity fluidized bed (Ug = 2.0 m/s, Gs = 88 kg/m2s) 59

Fig. 24 Probability density functions of differential pressures in the top section of a slugging fluidized bed (Ug = 1.0 m/s) 60

Fig. 25 Probability density functions of differential pressures in the top section of a high velocity fluidized bed (Ug = 2.0 m/s, Gs = 88 kg/m2s) 61

L I S T O F F I G U R E S (cont.)

Page

Fig. 26 Difference between the mean and median of the differential pressure readings along the height in a high velocity fluidized bed (FFB2090P, Ug = 2.0 m/s, Gs = 88 kg/m2s) (FFB2065P, Ug = 2.0 m/s, Gs = 67 kg/m2s) 64

Fig. 27 Difference between the mean and median of the differential pressure readings along the height in a high velocity fluidized bed (FFB50A5P, Ug = 5.0 m/s, Gs = 150 kg/m2s) (FFB50A3D, Ug = 5.0 m/s, Gs = 132 kg/m2s) 65

Fig. 28 Difference between the minmax-average and the median of the differential pressure readings along the height in a high velocity fluidized bed (FFB2090P, Ug = 2.0 m/s, Gs = 88 kg/m2s) (FFB50A5P, Ug = 5.0 m/s, Gs = 150 kg/m2s) 66

Fig. 29 Void fraction profile in a fast fluidized bed, with values obtained by three different methods (SLOWG15A, Ug = 1.5 m/s, Gs = 65 kg/m2s) 68

Fig. 30 Void fraction profile in a fast fluidized bed, with values obtained by three different methods (FFB25FFA, Ug = 2.5 m/s, Gs = 83 kg/m2s) 69

L I S T O F F I G U R E S (cont.)

Page

Fig. 31 Mean difference between the mean and median of the differential pressure readings in the dense fluidized region as a function of gas velocity 71

Fig. 32 Mean difference between the mean and median of the differential pressure readings in the dense fluidized region as a function of gas velocity (range of high velocity fluidized beds) 73

Fig. 33 Mean standard deviation of the differential pressure readings in the dense fluidized region as a function of gas velocity 74

Fig. 34 Mean difference between the minmax-average and the median of the differential pressure readings in the dense fluidized region as a function of gas velocity 75

Fig. 35 Mean void fraction in the dense bottom region of gas fluidized beds as a function of the gas velocity, values obtained by three different methods 77

Fig. 36 Mean void fraction in the dense bottom region of gas fluidized beds as a function of the solid rate, values obtained by three different methods 79

L I S T O F F I G U R E S (cont.)

Page

Fig. 37 Mean void fraction in the dense bottom region of gas fluidized beds as a function of the gas velocity. Mean values compared with model by Kwauk (eq. (2) - (4)) 81

Fig. 38 Void fraction profile in a fast fluidized bed, with values obtained by three different methods (FFB50A3D, Ug = 5.0 m/s, Gs = 132 kg/m2s) 83

Fig. 39 Mean void fraction in the top dilute region of at fast fluidization, experimental data compared with calculated data (eq. (6)) 86

Fig. 40 Mean void fraction in the top dilute region of at fast fluidization, experimental data compared with calculated data (eq. (6) and (7)) 87

Fig. 41 Radial voidage distribution in the dilute top region of a fast fluidized bed (Shao, 1986) 89

Fig. 42 Mean void fraction in the top dilute region of at fast fluidization, experimental data compared with calculated data from model by Kwauk et al. (eq. (9) - (11)) 91

Fig. 43 Void fraction profile and pressure distribution in system, solid control valve fully open.
(SLOWG10A, Ug = 1.0 m/s)
(FFB20FFE, Ug = 2.0 m/s)
(FFB30FFE, Ug = 3.0 m/s) 95

L I S T O F F I G U R E S (cont.)

Page

Fig. 44 Void fraction profile and pressure distribution in system, solid control valve fully open.
(FFB40FFA, Ug = 4.0 m/s)
(FFB45FFA, Ug = 4.5 m/s)
(FFB50FFA, Ug = 5.0 m/s) 96

Fig. 45 Void fraction profile and pressure distribution in system for varying gas velocities
(FFB2090D, Ug = 2.0 m/s, Gs = 94 kg/m2s)
(FFB2590D, Ug = 2.5 m/s, Gs = 93 kg/m2s)
(FFB3090D, Ug = 3.0 m/s, Gs = 89 kg/m2s) 99

Fig. 46 Void fraction profile and pressure distribution in system for varying solid rates
(FFB3090D, Ug = 3.0 m/s, Gs = 89 kg/m2s)
(FFB30A1D, Ug = 3.0 m/s, Gs = 113 kg/m2s)
(FFB30A3D, Ug = 3.0 m/s, Gs = 133 kg/m2s) 100

Fig. 47 Void fraction profile and pressure distribution in system for varying entrance conditions
(Ug = ca. 4.0 m/s, Gs = ca. 90 kg/m2s)
(FFC4090A, 0% of air at nozzle N3)
(FFC4090C, 20% of air at nozzle N3)
(FFC4090E, 40% of air at nozzle N3) 102

Fig. 48 Void fraction profile and pressure distribution in system for varying solid inventory in system
(Ug = ca. 4.0 m/s, Gs = ca. 90 kg/m2s)
(FFC4090B, 70 in. of solid in storage)
(FFC4090K, 90 in. of solid in storage)
(FFC4090E, 115 in. of solid in storage) 103

L I S T O F F I G U R E S (cont.)

Page

Fig. 49 Power spectra of gauge pressure signals in a fast fluidized bed at pressure tap 1
(FFB40A1C, Ug = 4.0 m/s, Gs = 110 kg/m2s)
(FFB40A3C, Ug = 4.0 m/s, Gs = 130 kg/m2s)
(FFC40FFE, Ug = 4.0 m/s, Gs = 190 kg/m2s) 106

Fig. 50 Auto correlation functions of gauge pressure signals at different location within the system
(FFB35FFD, Ug = 3.5 m/s, Gs = 143 kg/m2s) 107

Fig. 51 Power spectra of differential pressure signals in a fast fluidized bed at pressure between taps 2 and 3
(SLOWG10A, Ug = 1.0 m/s, Gs = 0 kg/m2s)
(FFB2090P, Ug = 2.0 m/s, Gs = 88 kg/m2s)
(FFC4090P, Ug = 4.0 m/s, Gs = 93 kg/m2s) 109

Fig. 52 Cross correlation function of differential pressure signals in a fast fluidized bed at different heights within the dense region
(FFB30A3D, Ug = 3.0 m/s, Gs = 133 kg/m2s) 111

Fig. 53 Cross correlation function of differential pressure signals in a fast fluidized bed at different heights within the dilute region
(FFB30A3D, Ug = 3.0 m/s, Gs = 133 kg/m2s) 113

Fig. 54 Interpretation of cross correlation functions of differential pressures within a fast fluidized bed, denser solid (A) moving upward 114

L I S T O F F I G U R E S (cont.)

Page

Fig. 55 Cross correlation function of differential pressure signals in a fast fluidized bed over different heights within the dense region, first pressure differential over taps 1 and 2 (SPC20FFA, Ug = 2.0 m/s, Gs = 108 kg/m2s) 116

Fig. 56 Cross correlation function of differential pressure signals in a fast fluidized bed over different heights within the dense region, first pressure differential over taps 2 and 3 (SPC20FFC, Ug = 2.0 m/s, Gs = 131 kg/m2s) 117

Fig. 57 Cross correlation function of differential pressure signals in a fast fluidized bed over different heigths within the dense region, first pressure differential over taps 3 and 4 (SPC20FFC, Ug = 2.0 m/s, Gs = 131 kg/m2s) 118

Fig. 58 Wave speed in two fast fluidized beds as a function of height (FFB2090P, Ug = 2.0 m/s, Gs = 88 kg/m2s) (FFB30A3D, Ug = 3.0 m/s, Gs = 133 kg/m2s) 119

Fig. 59 Wave speed in the dense fluidized regions in various fluidized beds as a function of gas velocitiy, with theoretical slug velocity by Matsen (eq. (1)) 121

Fig. 60 Standard deviation of differential pressure signals within the dense fluidized region, normalized by the mean pressure difference 124

L I S T O F F I G U R E S (cont.)

Page

Fig. 61 Difference between the absolute minimum and maximum of differential pressure signals within the dense fluidized region, normalized by the mean pressure difference 125

Fig. 62 Construction of transition velocity deviding low and high velocity fluidization on the basis of the mean void fraction in the dense fluidized region 127

Fig. 63 Construction of transition velocity deviding low and high velocity fluidization on the basis of the mean wave speed in the dense fluidized region 129

N O M E N C L A T U R E

AR	-	Archimedes number
dp	-	mean particle size of solid
Dt	-	diameter of fluidization column
E	-	crosssectional mean void fraction in fluidized flow
Ebot	-	void fraction in the bottom region of a fast fluidized bed
Etop	-	void fraction in the top region of a fast fluidized bed
g	-	gravity
Gs	-	solid rate
mu	-	kinematic viscosity of fluid
Res	-	modified Reynolds number
rof	-	density of fluid
ros	-	apparent density of solid
Ub	-	slug rise velocity
Ug	-	superficial gas velocity
Umf	-	superficial gas velocity at minimum fluidization
Us	-	superficial solid velocity
Usl	-	slip velocity between solid particles and fluid
Ut	-	terminal velocity of mean solid particle

1. INTRODUCTION

The existence of high velocity fluidized beds, although under a variety of different names has been known, for a long time. The first detailed experimental data were published in 1949 by Lewis et al. . It was not before the end of the sixties that studies on the hydrodynamics of high velocity fluidized beds were carried out in more detail and successful applications of these systems as gas-solid reactors emerged. But until now only a relatively few papers on fast fluidized beds have been published and these reported mainly the mean pressure gradient along the column height. The present view is that the published data often illustrate effects of the particular experimental system but provide little physical insight into the flow dynamics. Weinstein et al. (1983) discovered that other parameters in addition to gas velocity and solid rate are needed to descibe the solid hold-up or pressure profile in the bed.

One of the major shortcomings in present day descriptions of the state of fast fluidization is due to the lack of knowledge about the different regions of flow which are present. Since the paper of Li and Kwauk in 1980, where pressure gradient profiles showed large variations in the void fraction along the fast bed, it should be clear that the state of fluidization for such systems cannot be described by one mean bed void fraction. This also has to be kept in mind when fluidization diagrams are presented.

It is obvious from these pressure profiles that two regions of flow typically coexist which have two very different characteristics in terms of gas-solid contact, residence time and backmixing, both for gas and solid. The published pressure profiles suggest that the void fraction in the two different regions may be constant over the height, raising the question whether this is true for the entire spectrum of gas velocities and solid rates and if such can be concluded also for other properties like gas and solid mixing. It seems also likely that the fluidization properties within these regions are functions only of the flow parameters, i.e. gas velocity, solid rate, bed diameter and properties of the solid and the gas. This hypothesis is based on the data published in 1983 by Weinstein et al.. It showed that the solid hold-up in the fast bed is dependent also on operating conditions that were not encountered in experiments before, i.e. the imposed pressure drop across the solid recirculation leg. The void fraction within the regions itself seemed to be independent of the inventory.

The scope of this work is to verify whether a fast fluidized bed can be described in terms of two different flow regions. The pressure signals were studied to find out whether or not characteristics of the flow are constant within these regions and to determine the dependence of these characteristics on the flow parameters. The impact of

both flow parameters and design characteristics of the fluidization equipment on the total solid hold-up in the fast bed is depicted in detail.

The experimental work was carried out in fluidization equipment containing as an upflow section a round column of 0.152 m I.D. and 8.4 m height. A detailed analysis of the differential pressures drops and the pressure fluctuations in the fast fluidized bed was accomplished using pressure transducers and a computer-based data aquisition system for data analysis in the time and frequency domains.

2. LITERATURE REVIEW ON FAST FLUIDIZATION

In contrast to topics dealing with bubbling fluidized beds, only a relatively small number of publications can be found on fast fluidization. In addition, the term fast fluidization, first mentioned by Yerushalmi et al. in 1974 has been used for a variety of gas-solid flows because clear regime definitions in the high velocity fluidization range are still lacking. To avoid confusion, the following chapters will seek to clarify the term of fast fluidization in order to set the stage for the investigations of the present research work.

It is at first necessary to distinguish the terms fast fluidized bed and circulating fluidized bed from each other. For our purpose the term fast fluidization will be used only when the fluid bed exhibits certain properties of the flow, which will be discussed in detail in Chapter 2.3. On the other hand, the term circulating fluidized bed will be used in a more general way to describe gas solid up-flow systems that exhibit a significant carry-over of solid and an external solid recirculation leg.

A number of publications deal with high velocity fluidized beds with internal solid recirculation (Bergreen, 1981, Kuramoto, 1981, Hofbauer, 1982, Mohamed, 1985). Although these systems can be referred to as circulating fluidized beds and even show some flow properties similar to those found in fast fluidized beds, they will not be

considered in the following discussions. The reason for this is that the behavior of these fluidized bed systems is based on a number of design parameters that are inherent for the special design of these systems.

2.1. APPLICATION OF CIRCULATING FLUIDIZED BEDS

The first circulating fluidized bed was part of the FCC unit built during World War II by Standard Oil of New Jersey (Murphee, 1943) and was called a gas-solid up-flow reactor. The plant however failed due to severe problems in regulating the solid hold-up in the bed and in the recovery of the solid through cyclones. Nevertheless, from this, modern FCC technology emerged. Fluid cat-cracking units can be considered the most important commercial application of circulating fluidized beds. Because of large volume changes of the gas due to reaction, the FCC riser however represents a system with gas velocities varying over a wide range of flow conditions, one of which would be fast fluidized flow. However, the lack of data on the operation and hydrodynamics of such systems makes it difficult to include riser technology in the following discussion.

Circulating fluidized beds have found large scale application in other processes only during the last 15 years (Reh, 1971). Squires et al.(1975) and Liss et al.(1981) proposed a new concept of coal gasification on the basis of a fast fluidized bed. Until now, no experimental data have

been reported that would result in an understanding of the hydrodynamics of such a system.

The following review focuses only on circulating fluidized bed units in pilot or industrial scale that were parts of successful processes. Restrictions are made by defining the circulating fluidized bed as a state of two-phase flow lying, in terms of the gas velocity, between the turbulent fluidized bed and the very dilute transport reactor (e.g. powdered coal combustion unit). The limits are somewhat unclear, but qualitative characteristics of these reactors can be assigned as was done by Reh (1981) and shown in Table 1.

The given comparision is made using a number of process parameters such as gas and solid retention time. The gas retention time in a fast fluidized bed system seems comparable to the one obtained in the bubbling fluidized bed. For many applications, the solid retention time is on the order of several minutes compared to several hours in the bubbling fluid bed. It can however be varied independently over a wide range through the solid recirculation rate. Due to the small particle sizes possible, the circulating fluidized bed can exhibit much higher mass and heat transfer rates than the classical fluidized bed. Temperature control is therefore excellent and a high temperature uniformity within the fast bed is achieved.

Type of reactor	FIXED BED		FLUID BED		TRANSPORT
	over flowed 	permeated 	Fluidized bed 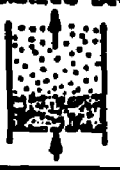	Entrained fluid bed 	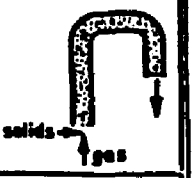
Typical reaction devices	Multiple hearth Rotary kiln Belt dryer	Shaft furnace Travelling grate Grate firing boiler	Fluid cracker Fluid bed roaster Multistage fluidized bed furnace	Circulating fluid bed Venturi fluid bed	Flash dryer Cyclone preheater Melting cyclone Burner
Solids movement by	Mechanics	Gravitation Mechanics	Gravitation Drag force		Gravitation Drag force
Gas solids flow	Co-current Counter-current Cross-current		Well mixed Counter-current in stages Cross-current in stages		Co-current Well mixed by recycle Counter c. in stages
Particle diameter	small-very large	medium-very large	small-medium	very small-small	very small
Solids retention time	hours-days		hours	minutes	seconds and less
Gas retention time	seconds		seconds		fractions of seconds
Heat+mass-transfer	very low	low-medium	high	very high	very high
Temperature control	medium-good	medium	good	excellent	medium-good
Volume-time efficiency	very low-medium	medium	medium-high	high	very-high

Tab. 1 Comparision of different gas-solid reactors

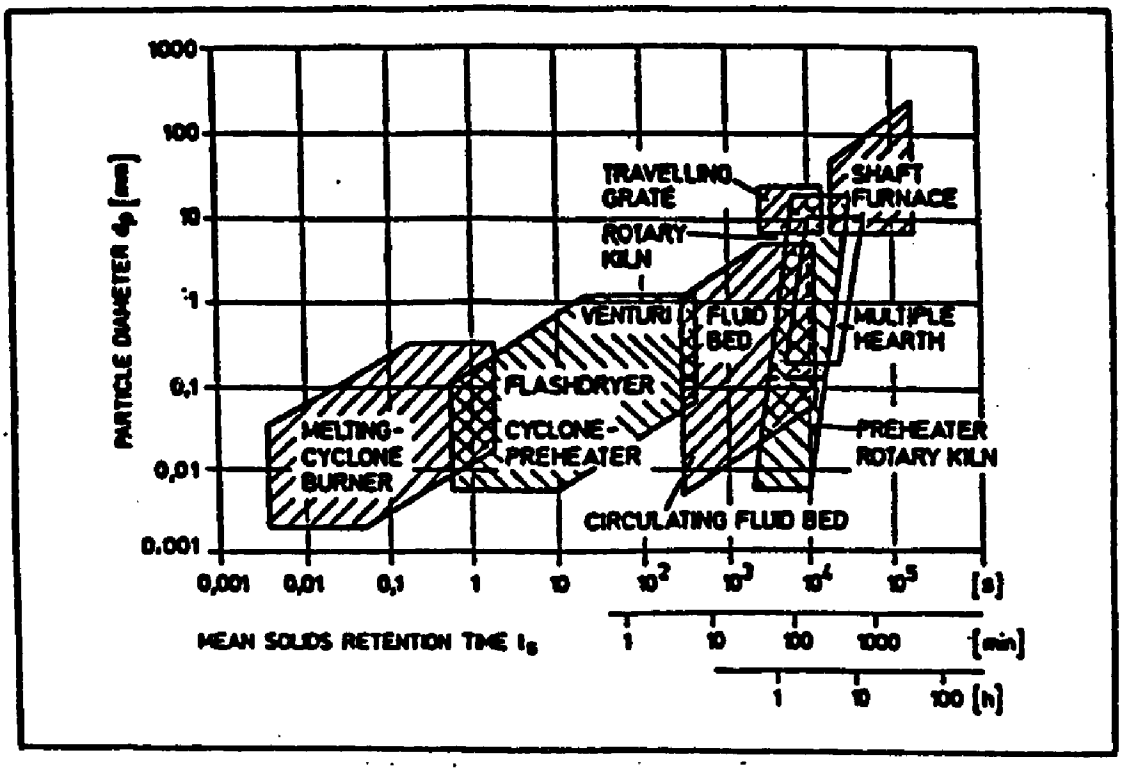

Fig. 1 Comparision of different gas-solid reactors by solid retention time and particle size

These more general features which characterize the circulating fluidized bed as a reactor for gas-solid reactions fill the gap between the features of turbulent fluidized beds and those of dilute transport reactors (Figure 1). Although many of the features describe an excellent gas-solid reaction system, it is clear that due to the required higher gas velocities and elaborate solid recirculation system, investments and power requirements are much higher than those of bubbling fluidized beds. These requirements consequently leave the circulating fluidized bed for particular applcations where other systems lack either flexibility, ease in scale-up or a sufficiently high level of conversion. Recently Squires and Avidan (1985) stated that investment costs for circulating fluidized beds are equal or even less than those of a bubbling fluidized bed in application as a coal combustor. A cost analysis for the verification of this statement is however missing.

2.1.1. COAL COMBUSTION IN CIRCULATING FLUIDIZED BEDS

One of the areas, where circulating fluidized beds found industrial application is in combustion, in particular for low-grade brown coal. Also wood, waste and even sewage sludge (Beisswenger, 1980) can be used as fuels. The versatility of the reactor plays an important role. Tight exhaust regulations in several European countries and Canada make the fluid bed combustor a competitive unit to powdered

coal combustion units and traveling grate furnaces. This is because both of these require additional units for the removal of sulfur dioxide from the exhaust gas.

In contrast, fluid bed combustors can be designed for an in-situ sulfur removal by adding limestone to the bed material which in itself consists mainly of ash. The advantage of the circulating fluidized bed over the bubbling fluidized bed is based on the higher mass transfer rates possible which allow a significant reduction in the amount of limestone added. Further comparisions to bubbling fluidized beds are given in Table 2. It should be noted that most of the advantages of the circulating fluid bed are a result of a few characteristics (Beisswenger, 1981) such as:

- high temperature uniformity within the bed
- small particle size
- high solid inventory per unit cross section
- variable solid recirculation
- possible staged combustion with secondary gas inlet

The utilization of a circulating fluid bed combustor is shown in Figure 2 (Wein, 1980). The figure includes a coal processing unit with an additional heat exchanger unit for the exhaust gas. It is interesting that only 20% of the total heat is removed within the fast bed. Another 45% is transferred in the fluid bed coolers within the solid recirculation leg. The remaining 35% is transferred in the

Criterion	Bubble-forming fluidized bed (FB)	Circulating fluidized bed (CFB)
Heating surfaces	Immersed in fluidized bed. Difficult to adapt heat transfer to load variation. Erosion problems with tube bundles	Pipe walls utilizable for circulating fluid bed reactor, no losses. Separation of heat transfer and combustion by separate fluidized bed heat exchanger
Gas – solids contact	Restricted to a bed height of about 0.5–2 m, large free space (over bed burning)	Distributed over the entire reactor height of 20–30 m
Pressure drop	Comparable	Comparable, to a limited extent adjustable by solids recirculation
Partial load control	Up to 70% of nominal load in a single module, limited reactor's temperature variation. Complicated controls	Up to 40% of nominal load without adverse effect on combustion process. Small number of controls
Bed material	Relatively coarse-grained	fine grain size
Mean grain size	2–4 mm	0.2–0.4 mm
Upper limiting grain size	about 6 mm	about 2mm
Comminution	Not extensive, crushers without drying possibly sufficient	Medium, not as fine as for pulverized coal firing. Use of ball mill possible
Fuel supply	Difficult, distribution over numerous feed points owing to unsatisfactory radial mixing and large bed cross-sections	Simple, only a few feed points with a satisfactory radial mixing and smaller reactor cross-sections
Combustion air	1–2 m/s, at high velocities loss of unburnt fines	5–8 m/s, primary and secondary air supply
Fuel – air ratio	λ above 1.2 due to large bed cross-section and unsatisfactory radial mixing	$\lambda = 1.1$, good gas-solids mixing, long contact zone over the entire reactor height
Temperature distribution	Uniform in fluidized bed, over bed burning	Very uniform due to solids recirculation
Heat flux	1–3 MW/m^2	3–8 MW/m^2 and above
Fuel burnout ratio	High carbon content in flue dust, recycle to separate burnout fluidized bed chamber possibly required	Above 99%, high solids residence time due to direct recirculation
Emissions SO_2 decrease at 90% Ca/S	3 and above	1.5–2, finer limestone size and long residence time
NO_X	300–400 ppm	100–200 ppm by controlled stage combustion
Waste gas cleaning	Comparable	Comparable

Tab. 2 Comparision between combustion of solid fuel in bubbling and circulating fluidized beds

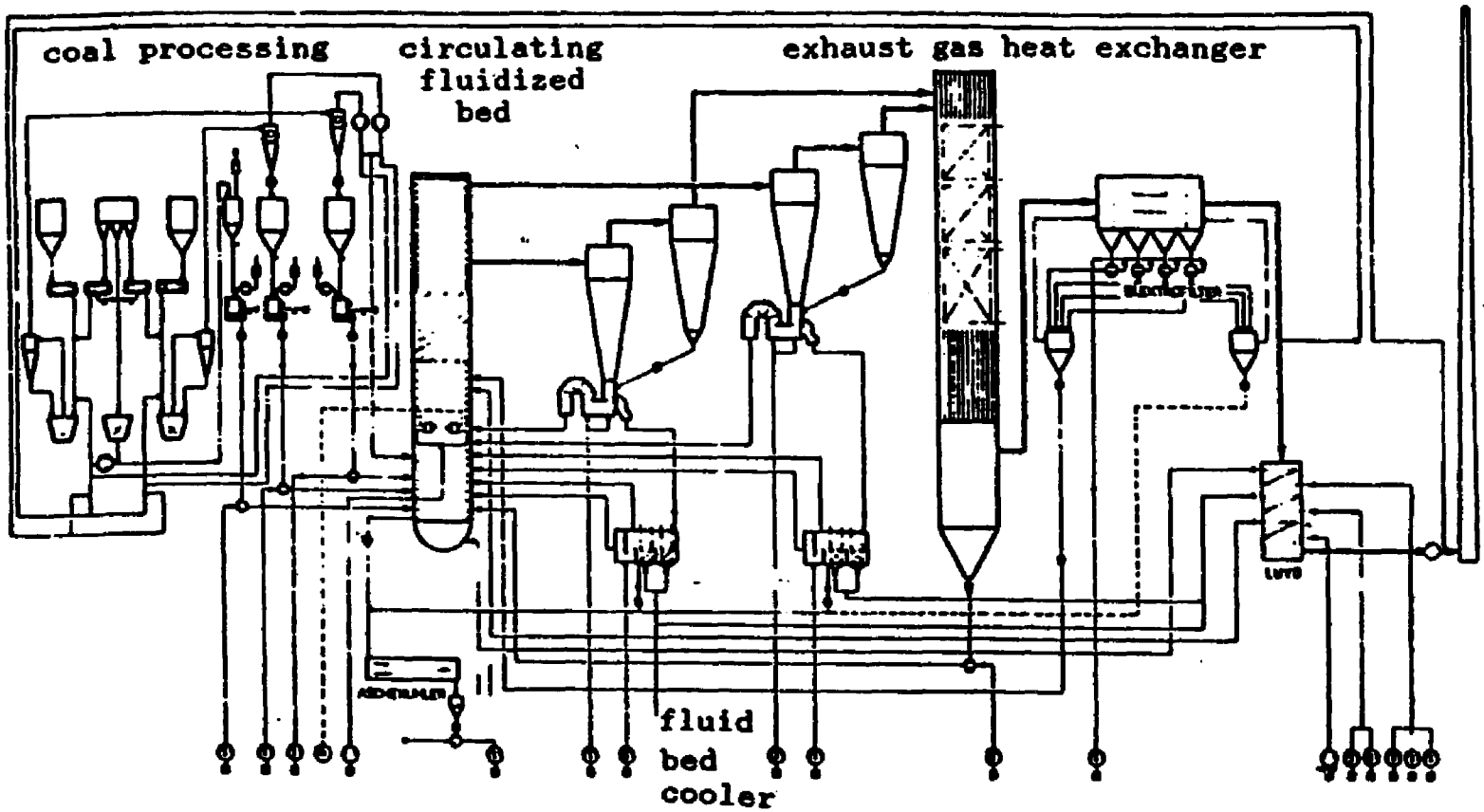

Fig. 2 Process schematic of a circulating fluidized bed combustor (steam generation for 230t/h, build in Duisburg, West Germany)

exhaust gas heat exchanger (Wein, 1980). A similar design is reported by Engstrom (1981). This utilization of the additional fluid bed cooler improves temperature control and reduces the attrition rate.

The properties of the fluidized bed are:

temperature	gas velocity	particle size	tot.pressure drop
ca. 1200 K	6.0-8.0 m/s	200-300 microns	not available

It seems questionable that this operation represents fast fluidized conditions for the gas velocities and particle sizes given. From the published data it is however not possible to prove such a statement. The characteristics of fast fluidized flow will be discussed in detail in Chapter 2.3.

2.1.2. CALCINATION IN CIRCULATING FLUIDIZED BEDS

The first commercial circulating fluidized bed, excluding FCC units, was designed for the calcination of aluminium hydroxide to alumina. Thermal uniformity and the existence of an easily accessable solid recirculation leg made the circulating fluidized bed an economically attractive reactor type (Reh, 1971). A wide flexibility in load is achieved by introducing a fluid bed cooler into the solid recirculation leg, which keeps the thermal efficiency high. The scheme shown in Figure 3 is practically the same as for the combustion unit shown in Figure 2. In this case

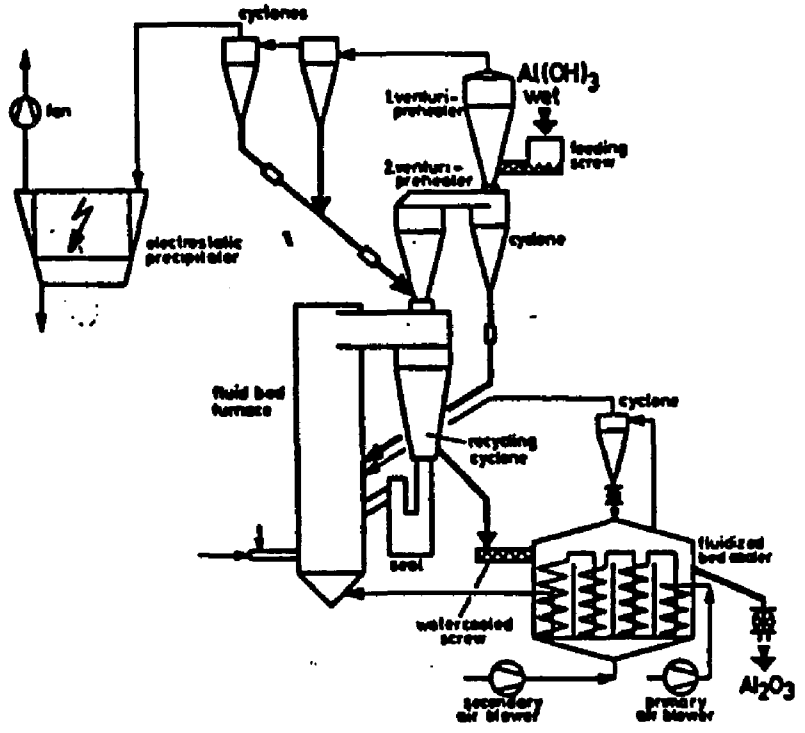

Fig. 3 Process schematic for a circulating fluidized bed calciner

however two venturi reactors are included. It is not clear, whether the main reaction takes place in the fluid bed itself or in the venturi reactors.

The properties of the fluid bed are:

temperature	gas velocity	void fractions		tot.pressure drop
		bottom	top	
1420 K	3.0 m/s	.94	.982	70 - 200 mbar

A mean particle size of 45 microns is reported. The pressure drop corresponds to a mean void fraction in the bed of a maximum of 0.95. These data however do not represent a fast fluidized bed with a characteristic high solid fraction. The characteristics of the special design mentioned in 2.1.1. apply equally to this reactor.

2.1.3. GAS ABSORPTION IN CIRCULATING FLUIDIZED BEDS

Using as a basis the calcination unit shown in Figure 4, several dry gas cleaning units were built over the past years for absorption of HF and HCL with aluminium hydroxide for the production of aluminium fluoride (Reh, 1971). In recent years, similar units were constructed for exhaust gas cleaning in waste combustion units.

High reactivity due to the small particle size possible and the ease of control of the system's solid recirculation rate made the circulating fluidized bed a competing alternative to spray tower absorption. A process scheme is

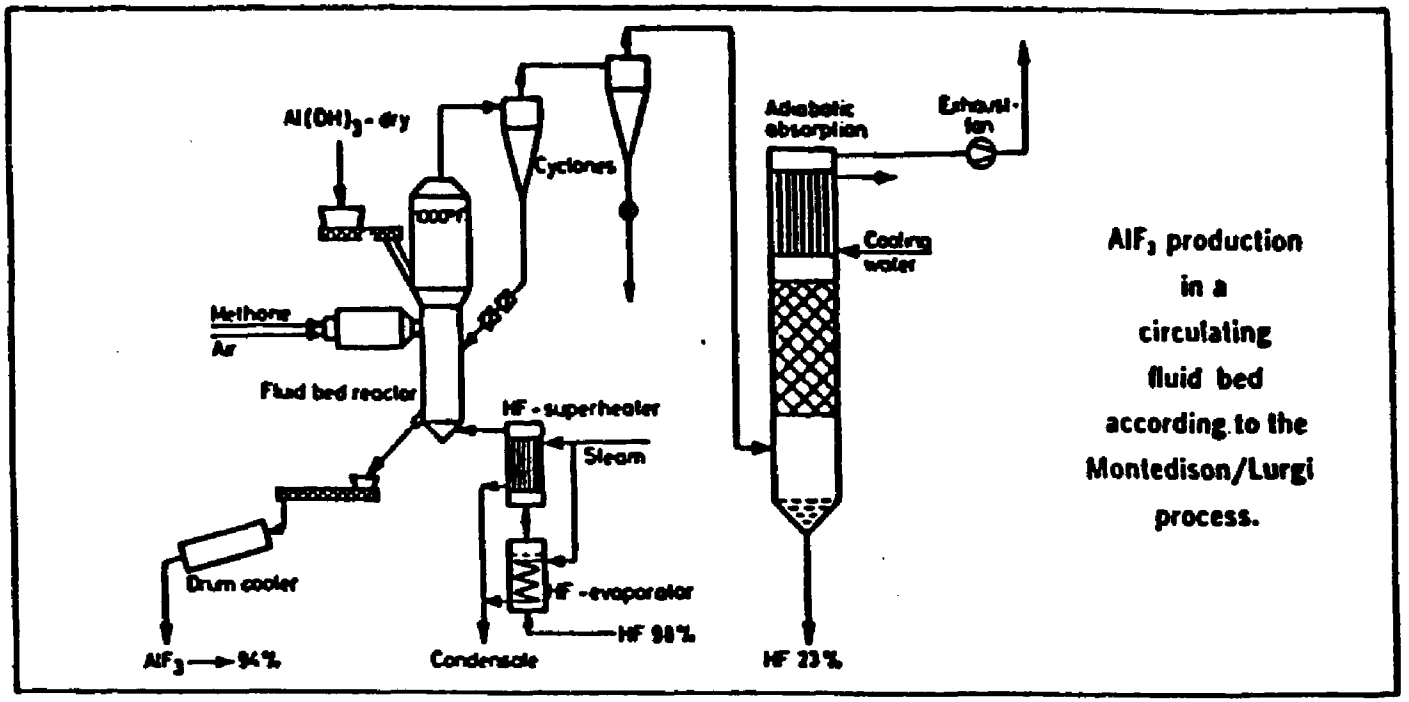

Fig. 4 Process schematic
circulating fluidized bed for gas adsorption

given in Figure 4. For a discussion refer to Chapters 2.1.1 and 2.1.2, since the process itself is very similar to those mentioned therein.

2.2 REVIEW ON HYDRODYNAMICS OF GAS-SOLID UP-FLOW IN VERTICAL PIPES

2.2.1 FAST FLUIDIZATION

The behavior of fast fluidized beds was first described by Lewis et al. in 1949. It was noted that by increasing the gas velocity in a bubbling fluidized bed, a relatively dense gas-solid flow can be obtained in the vertical column. This requires that solid be fed at the bottom from the bed to balance the significantly large carry-over of the bed. Several advantages of this fluidization regime over the bubbling bed are reported.

Later Lanneau(1960) observed further advantages in the operation of a fluidized bed at higher gas velocities particularly for gas-solid catalytic reactions. His small scale fluidization column clearly operated more smoothly compared to the bubbling bed and backmixing of gas was also reported to be significantly smaller. Although those characteristics are typical for fast fluidized beds, Lanneau did not encounter the high solid carry-over that is tyical of the fast fluidized bed. His fluid bed is considered from the present point of view to be a turbulent fluidized bed.

In spite of the promising ideas for the operation of high velocity fluidized beds, it remained for Reh (1971) to set the stage for the first discussion on the characteristics of fast fluidized beds in view of his first large scale application. In his publication, Reh presented limits for operational conditions in a fluidization diagram, which was originally established for low velocity fluidized beds. The limits for fast fluidization are given in form of the Archimedes number and a coefficient related to the Froude number. For a given pair of gas and solid, the gas velocity is taken as the only process parameter for the fast fluidized bed.

This first approach to define a certain range for high velocity fluidization, although this term was still to be invented, was followed by a number of more elaborate studies conducted by Yerushalmi et al. (1974 - 1979). These studies mainly focused on definitions for the different fluidization regimes and their limits based on two parameters: gas velocity and solid rate.

In a paper published in 1978, Yerushalmi et al. defined three different regimes for high velocity fluidization valid for particle sizes in the range of about 50 to 250 microns and solid densities in the range aroud 1000 kg/m3, in other words, solid of Geldart's classification A (Geldart, 1973, Molerus, 1982). Increasing the gas velocity past the bubbling or slugging fluidized bed's upper limit, the bed

becomes smoother in its operation. In particular, this is seen through a significant reduction in the magnitude of pressure fluctuations in the bed and the breaking up of bubbles into a continous gas-solid dilute phase surrounding strands and clusters. Nevertheless, solid carry-over is reported to be still insignificant and does not demand solid recirculation. The flow regime of turbulent fluidization has been studied by a number of scientists for various particle properties. A more thorough discussion on turbulent fluidized beds can be found in Avidan(1980).

In contrast to the turbulent fluidized bed, fast fluidization is described as a flow regime, where a significant solid carry-over requires solid to be fed at the bottom of the bed and where the solid rate strongly affects the properties of the bed, in particular, the void fraction. If the gas velocity is raised further the so-called transport flow regime can be established. This regime, known also as pneumatic transport is described in Chapter 2.2.2.

Yerushalmi and Cankurt (1979) defined two gas velocities between which the fast fluidization regime can be observed. Utr is the velocity at which fast fluidization is established and where solid recirculation becomes necessary. The recirculation rate becomes an additional parameter determining the solid hold-up in the fluid bed. The transition is relatively sharp and the transition velocity

is solely taken as a function of the gas and solid properties. This is not valid for the second transition velocity, Upt, where the void fraction in the fast fluidized bed decreases to values that are comparable to those found in pneumatic transport lines. Upt however is considered to be a clear function of the solid rate and the transition is reported to be less sharp than the one at Utr. Whereas Reh described the fast bed void fraction by one variable , i.e. gas velocity , the solid rate through the system was used by Yerushalmi as a second parameter.

Although Yerushalmi reported pressure profiles as early as 1976, it remained for Li et al. (1981) to give a detailed description of fast bed behavior by a detailed analysis of the pressure gradient along the bed height. Figure 5 shows that with such an analysis the gradient is more or less constant over the height in two regions of the bed. These are divided by a transition zone, where the profile exhibits an inflection point. Li postulated therefore in the form of a hydrodynamic model that the shape of such a profile in a fast fluidized bed is essentially the same and that the pressure gradient in both regions and the height of the inflection point are functions of the various process parameters.

Later it was found by Weinstein et al. (1983), that the position of the above mentioned inflection point is dependent on additional parameters other then flow

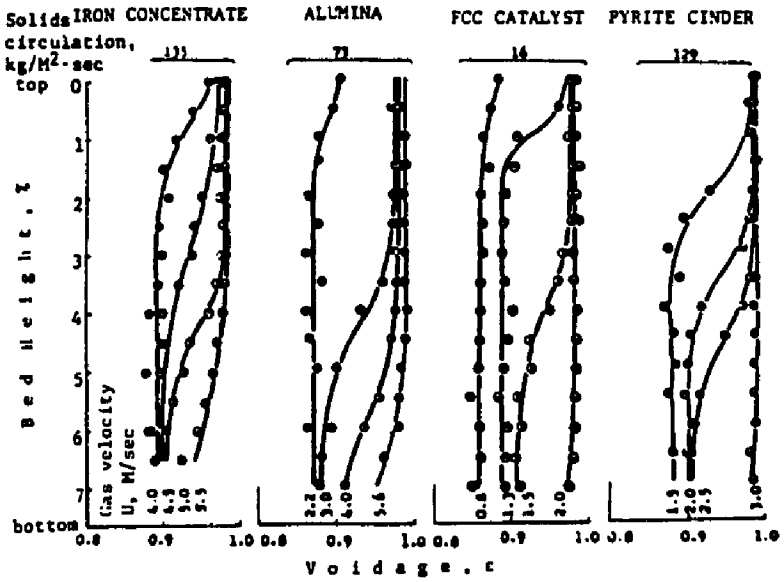

Fig. 5 Void fraction profiles in fast fluidized
(Li et al., 1982)

parameters, e.g. the 'imposed pressure drop' set by the recirculation leg of the fluidization system. In their experiments, an unrestrained or bottom restrained standpipe was used for solid recirculation and it was found that the solid inventory above the standpipe leg clearly affected the height of the inflection point. However the pressure gradient within the bottom and top region of the bed seemed to be unchanged.

With this it can be concluded that a fluidization diagram, as given by Avidan and Yerushalmi(1982) and Li and Kwauk(1982) can not be supported. This is because the mean void fraction of the bed and the void fraction found in any fixed section of the fluidization column are also dependent on other parameters in addition to the gas velocity and solid rate. This is also true for the diagram presented by Reh (1971) unless further definitions are given.

Recently, Kwauk (1985) presented a detailed description of fast fluidized bed flow, whereby empirical correlations were presented to determine the four parameters of a hydrodynamic model necessary to describe the mean void fraction profile over the height. The model is based on the idea that particle lumps evident in the lower part of the bed are diffusing into the top portion of the bed and fall back again into the dense region (Figure 6). At present, this model represents clearly the best description of fast fluidized flow especially since it includes the typical void

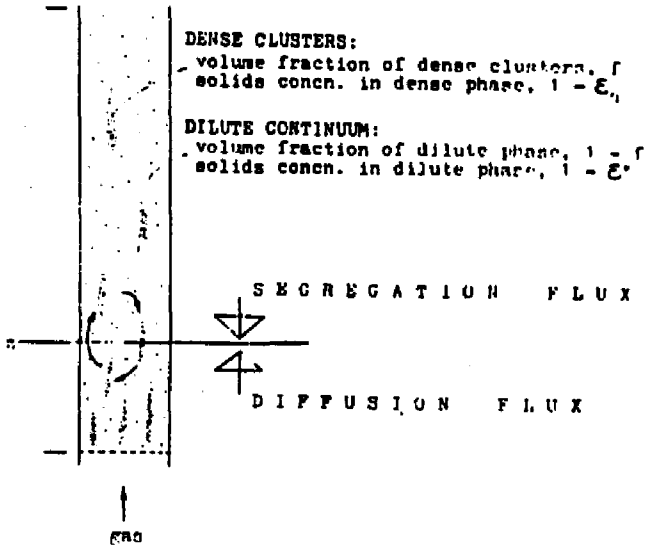

Fig. 6 Hydrodynamic Model by Li and Kwauk, 1980

fraction profile found in the fast fluidized bed. The different aspects of this model will be discussed in Chapter 4 in parallel with experimental results of this investigation.

A number of more detailed experiments on fast fluidized beds have been published. However in many of these the fast fluidized bed's variable inflection point was not considered and hence the results often are of no general use and sometimes even confusing. This might also be the case for the few additional papers which are described below.

Cankurt et al.(1978) measured gas backmixing in a fast fluidized bed of 0.152 m diameter for various velocities. The axial dispersion coefficient was found to be small in the fast fluidized bed regime compared to that in bubbling and turbulent fluidized beds. The results could be described well by plug flow behavior. On the other side, the extremly low bed densities reported suggest that the flow in the bed resembled the flow in a dilute pneumatic conveying line.

Using the same equipment, Avidan(1980) tested solid backmixing and described it to have similarities to liquid-solid systems, because a minimum in the dispersion coefficient could be detected at a distinct gas velocity and solid rate. Another observation was that the dispersion coefficient was constant throughout the fluidized bed. In this case the location of the inflection point was not taken

into consideration.

The mean radial void fraction in the fast fluidized bed measured by X-ray absorption was reported by Weinstein et al. (1985). It is shown that below the inflection point of the pressure gradient profile the void fraction is found to be high near the wall of the 0.152 m round column (0.6 - 0.7). In the center a relatively dilute flow is encountered (> 0.95). The data exhibit a clear distiction between the flow in the dense bottom region and the top region where the void fraction seems to be nearly constant in the radial direction. Comparable profiles were also reported by Hartge et al.(1985), where fiber optic sensors were used to detect the local void fraction. This is of major significance, since Hartge not only used a different technique, but also since his experiments were conducted in a much larger fluid bed of 0.40 m in diameter.

More recently, Monceaux et al.(1985) presented the local solid flux in a fast fluidized bed for solid of Geldart's Class A. It is noted that the experiments were done below the transition zone. The profile given in Figure 7 shows clearly a downflow of solid near the wall, which is balanced by a 1.5 to 2.5 fold increase in the solid flux in the center of the 0.144 m I.D. fluidization column. In connection with data by Weinstein et al. (1985), also done on a 'A-type' catalyst, this result suggests that highly compact solid agglomerates flow down at the wall, while the

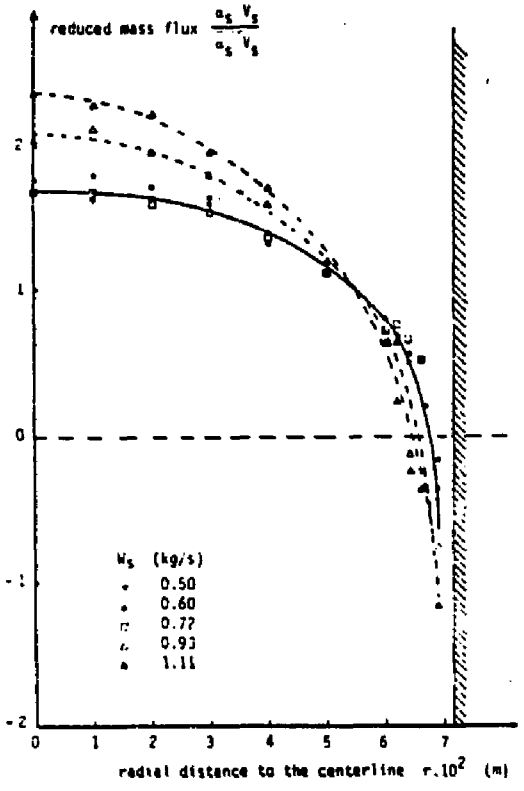

Fig. 7 Reduced mass flux profiles in a fast fluidized bed (Ug = 3.2 m/s) for various solid rates (Monceaux et al.(1985)

overall upward transport of solid is accomplished within the very dilute core. The presentation is clearly preliminary and a more general conclusion on the radial mass flux distribution is yet to come.

Finally, a chemical reaction, decomposition of NAHCO3, was conducted by Helmrich (1979) in a fast fluidized bed. In an overview of a number of different gas-solid reactors, he was able to show that in the fast fluidized bed reaction rates were high, second only to those of a dilute flow transport reactor in magnitude. His system nevertheless showed some special features, one of which was significant gas backflow through the standpipe line, which makes it hard to extrapolate the published results to fast fluidization in general.

2.2.2. PNEUMATIC TRANSPORT OF SOLID

The transport of solid in vertical pipes within the so called transport regime resuts in a flow pattern closely related to that in fast fluidization and often mistaken as the latter. Therefore, it seems appropriate to review some basic properties of pneumatic conveying.

In this type of flow the void fractions are significantly higher than the ones obtained in the dense region of a fast fluidized bed and are found to be in the range above 0.95. At lower gas velocities keeping the solid rate constant, unstable operation can occur (Lewis et al.,

1949). Then the transport of solid is being accomplished through slugs of solid moving upward (Leung, 1971). The phenomenon is known as 'choking' of the transport line. Although the existence of such slugs correlates to certain gas velocities, instabilities of the flow, recognizable as pressure fluctuations increase steadily as the gas velocity is decreased - even far above the choking velocity (the solid rate is held constant in this case).

Capes(1971) reported such pressure fluctuations for the total pressure drop in a 0.075 m I.D. vertical pipe and they are presented in Figure 8. The fluctuations are caused by slugs in the transport line, whereby these slugs can move throughout the total bed height or only a fraction thereof. It becomes clear that at higher solid fractions in the flow (corresponding to lower gas velocities at constant solid throughput) the two-phase flow becomes increasingly unstable.

Another conclusion can be made from the data given by Capes(1971), also Capes and Nakamura(1973). Plotting the pressure in the column against the height, it becomes clear that the pressure gradient in such a two-phase flow is higher at the entrance region, but is steadily decreasing with decreasing slope. Above a certain height, the pressure gradient becomes constant and this is the reason why a definite pressure gradient can be taken to describe the flow in a pneumatic transport line.

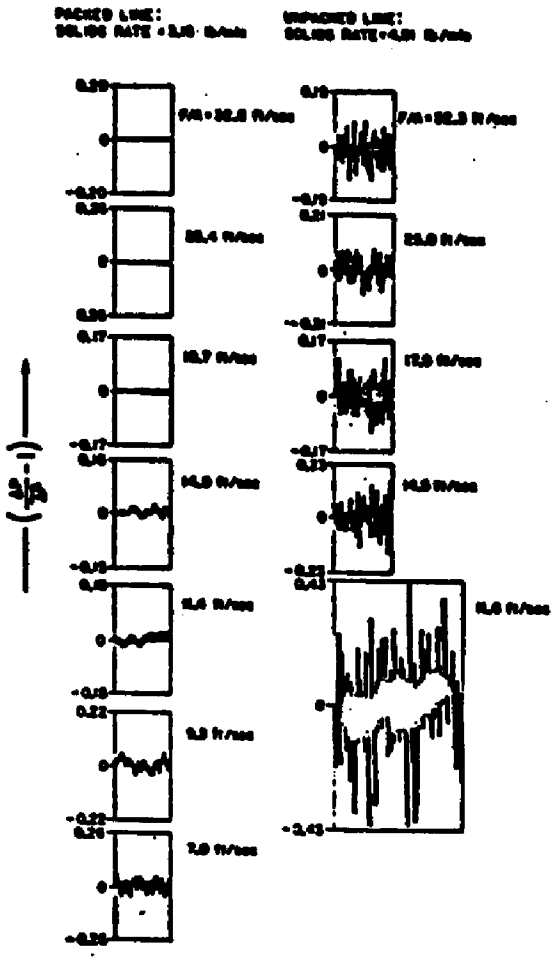

Fig. 8 Pressure fluctuations in a 3-in pneumatic transport line (Capes, 1971)

In Figure 9 data from Capes and Nakamura(1973) are presented for different gas velocities at constant solid rate. The deviation in the entrance region is greatest for small gas velocities. In this diagram the solid rate was held constant at 13.4 kg/m2s, a relative small value compared to solid rates in fast fluidization. The deviation at the entrance region is a result mainly of two factors:

1) The pressure drop due to particle acceleration
2) Increased solid hold-up,

which itself is due to the smaller particle velocities in that region, since the particles are not yet accelerated to their final velocities.

The structure in the flow with constant pressure gradient was examined by Irons and Chang(1983) by means of a capacitance probe. With this they were able to show that the particle velocities across the bed diameter vary only in a small range. This gives evidence for particulate flow in the tranport line although additional solid hold-up within a small distance from the wall can be observed (Berker and Tulig, 1986). Since this assumption was often taken for analytical descriptions of vertical transport lines, this result is of major importance. It should be noted however, that the gas velocities encountered are at the upper limit of the region where fast fluidization flow phenomena usually can be observed.

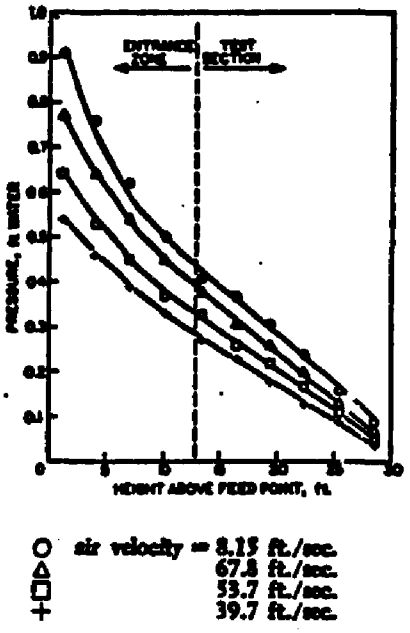

Fig. 9 Pressure gradient vs. height in a pneumatic transport line (Capes and Nakamura, 1973)

It is relevant to mention that a similar flow was observed by Morooka et al.(1983) in the freeboard region of a bubbling fluidized bed, although the gas velocities are in this case much lower than those in the above references and lie below those encountered in fast fluidized beds. In particular particle velocities in different lateral positions are presented. In Figure 10 this distribution is given for different mean solid fractions (<ep> in Figure 10) and a gas velocity of 0.7 m/s. It should be noted that the distribution corresponds to the steady state behavior in the freeboard region and is essentially the same for greater heights in the freeboard. For high solid volume fractions, the flow seems to be composed of two different zones, a core zone with solid upflow and a wall zone with downflow of solid. It becomes clear that the assumption of particulate flow or equally distributed particles holds only in the center portion of the flow and that solid are moving downward near the wall showing a completely different flow pattern. Although this is the case, the pressure drop and the flow pattern above the transport disengaging height is said to be constant over the bed height thus providing evidence that a steady state flow pattern is encountered.

Other effects that occur in the entrance region of a pneumatic transport line due to the particle size distribution were calculated analytically by Arastroopour et al.(1979). In this theoretical paper, segregation effects and particle-particle interaction are the main focus. Yet

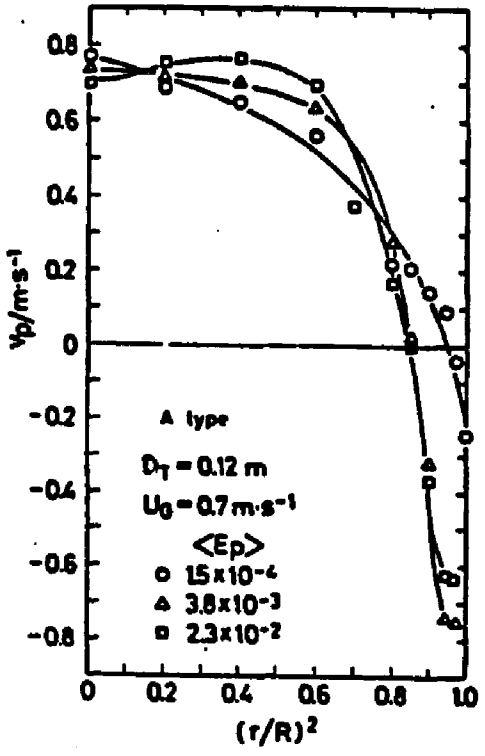

Fig. 10 Particle velocities as a function of radius in the freeboard of a fluidized bed for different gas velocities (Morooka, 1983)

interesting results for further discussion on fast fluidization are given in the form of the different particle velocities over the height of the column. Figure 11 presents the results obtained at a gas velocity of 15.2 m/s and a solid rate of ca. 100 kg/m2s. The different curves correspond to different particle size fractions. (The total length of the column is 15.2 m, the solid density amounts to 1260 kg/m3, and the particle size distribution varies between ca. 50 and 1450 microns with air as gas). It is interesting that in spite of very different free fall velocities of the particles a steady state is obtained due to particle-particle interaction. It is clear that the smaller solid velocities in the entrance region demand higher solid densities, so that a continuity equation can be satisfied for each particle fraction.

From the above mentioned results the following characteristics of pneumatic transport lines are summarized in order of their significance to further discussion of fast fluidization:

1) The flow pattern of a pneumatic transport line can be divided into two regions: an entrance region and a region following down stream, the latter with all differential flow parameters constant (i.e. solid holdup, particle velocities and pressure gradients).

2) The region above the entrance region can be clearly described as particulate flow for higher gas velocities and

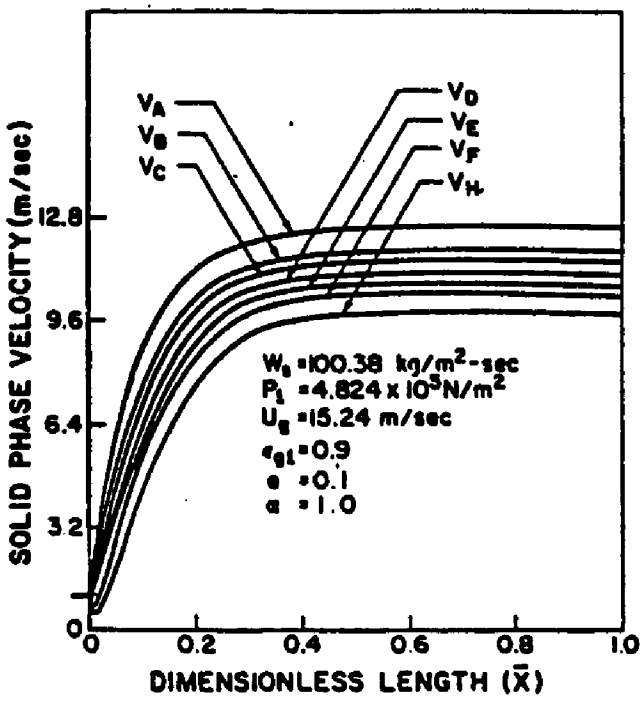

Fig. 11 Particle velocities as a function of height in a vertical pneumatic conveying line for different fractions of particle size (Arastroopour, 1979)

larger particles (Capes: 450 microns, Irons et al. 470 microns). On the other hand, at smaller particle sizes and low gas velocities (Morooka: 60 microns) a segregation of particles towards the wall which is always encountered becomes significant. In the resulting wall zone, particles are moving downward in contrast to the movement in the core zone. Any dependence of these effects on particle sizes, particle densities, Archimedes numbers etc. could not be found in the literature.

3) A clearly higher pressure gradient is found in the entrance region of the transport line. It is caused by acceleration of the solid to the steady state particle velocity and a necessarily increased solid hold-up due to the smaller particle velocities in that region. In contrast to fast fluidized bed behavior the second derivative of the void fraction profile is always positive and no inflection point is encountered.

4) Segregation effects due to a large particle size distribution seem not to lead to different shapes of the pressure gradient profiles and to no unsteady flow pattern through continuous increase of the fraction of large particles in the entrance region. This analytical result is also supplemented by the additional analytical finding. In the case of a particle size distribution constant flow properties are ensured in the region above the entrance region.

2.3 DISCUSSION ON HYDRODYNAMICS OF FAST FLUIDIZED BEDS

With the help of the above review of fast fluidization and pneumatic transport, two conclusions can be drawn that will provide a clear definition of fast fluidization itself and to screen literature data regarding fast fluidization into those that do and those that do not clearly show the basic features of fast fluidized beds. From the conclusions already drawn in the last two chapters, fast fluidization, a flow pattern clearly distinct from pneumatic conveying, seems to be evident under the following conditions:

1) Solid recirculation is necessary to maintain a steady state flow in the fluidization column and the solid rate clearly affects the solid hold-up in the fluid bed.

2) The pressure gradient is typically fairly constant along the bed height in both a dense lower region and a upper dilute region. The plot of the pressure gradient vs. bed height will show an inflection point as long as both regions are present within the total column height. Fast fluidization however is still possible when the dense region is evident throughout the actual column height and therefore an inflection point can no longer be observed. A numerical value for the mean crosssectional void fraction for the discrimination between dilute phase flow and dense flow of a fast fluidized bed is needed in this case. For literature data and the data of this investigation such a boundary

could be given for the crossectional mean void fraction, E < 0.95, for the dense flow. In anticipation of results given in Chapter 4 a more general definition is possible: Dense fast fluidized flow is characterized by a very weak function of the mean void fraction on the solid rate in contrast to the dilute phase flow in the top of the fast fluidized bed.

From these two basic observations alone we will find that a number of reports of data published under the term fast fluidization cannot be considered to be applicable. Typical examples of recently published data supposedly taken in fast fluidized beds are data by Bereton and Stroemberg(1985) and Arena et al.(1985). The data show in particular no inflection point in the pressure gradient profile and often no significantly high void fraction in the bottom of the bed (<0.95). In addition, it can be concluded that the data presented and the often elaborate conclusions made from these represent the behavior of pneumatic conveying lines.

Since the void fraction in the fast fluidized bed is largely different in the two regions of the bed and the total solid hold-up is (Chapter 4.3) dependent on equipment related parameters, it is clearly inappropriate to use the total solid hold-up in the fluidization column or a overall bed void fraction for the desciption of a fast fluidized flow. Such an approach was used by Reh(1971), Yerushalmi(1974-78), Avidan and Yerushalmi(1982) and Li and

Kwauk(1982), to name a few. In the same fashion the void fraction within a fixed section of the fluidization column is not only a function of the flow parameters. Such a void fraction was used to describe the flow by elaborate fluidization diagrams. Cluster sizes for the fast fluidized bed were derived from it (Avidan, 1980). It is clear that without detailed analysis of the data given, conclusions which have been made need thorough revision. This is true for the majority of papers published in the field of fast fluidization.

Finally, one recent approach that encounters the evident pressure gradient profile in the fast bed was made by Rhodes and Geldart(1985). They suggested that the void fraction in the top region of the fast fluidized bed is continuously decreasing. Implicitly, the solid hold-up in the fast fluidized bed is not only dependent on the solid rate and gas velocity, but also the height of the fluidization column. These statements are made by comparing the top region of the fast fluidized bed with the freeboard of a bubbling fluidized bed below the transport disengaging height. This approach is already disproved by Weinstein et al. (1983) who showed that the same solid recirculation rate can be obtained in a fast fluidized bed with varying heights of the 'inflection point'. More details on variations in the inflection point or bed height are given in Chapter 4.3.

3 EXPERIMENTAL EQUIPMENT

3.1 THE CIRCULATING FLUIDIZED BED SYSTEM

The equipment used in this investigation to determine the properties of fast fluidized flow is shown in Figure 12. It consists of a bubbling fluidized bed of 0.343 m in diameter and to the right of the actual fast fluidization column, a 0.152 m round column of 8.4 m height. The solid is carried upward through the latter column, is separated at the top of the bed by a two stage cyclone arrangement and falls back to the bubbling fluidized bed which serves as a storage for the solid. This bed terminates into an aerated standpipe of 0.152 m diameter. This standpipe includes a butterfly valve for the control of the solid rate and full aeration over the total length. It is understood that the standpipe can be operated in a bottom restrained or unrestrained, fully aerated mode by positioning the butterfly valve. The two operating conditions exhibit completely different characteristics (Judd(1978)) particularly in their pressure gradient profiles.

The main air for the fast fluidized bed is introduced in the system within the U-bend section by means of 5 nozzles, which are attached to the U-bend at three different locations (Figure 12). The air supply can be regulated separately over three air supply lines. The solid rate is measured by means of a butterfly valve located in the upper portion of the storage bed. The valve is made out of a

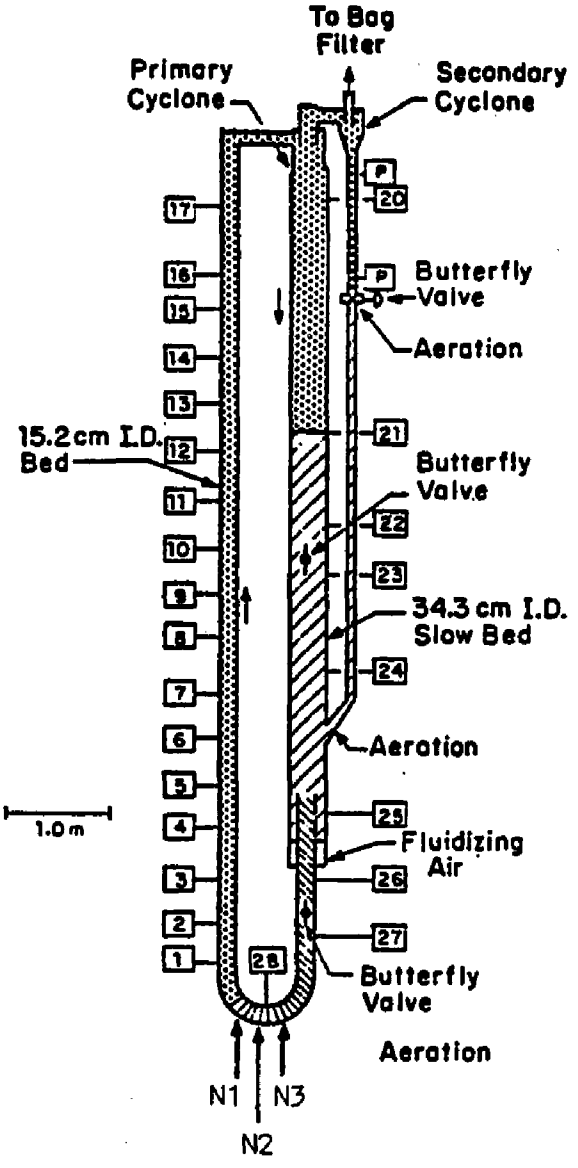

Fig. 12 Laboratory system for fast fluidization experiments

porous sintered plate so that when closed, the recirculated solid from the primary cyclone will be fluidized above it as in the actual bubbling bed below. With this arrangement the total pressure drop is essentially constant during the solid rate measurements. The decay of the pressure drop between pressure taps 23 and 25 is recorded and taken to evaluate the solid rate. The procedures are explained in the next chapter.

3.2 DATA ACQUISITION OF BASIC PRESSURE READINGS

One of the main errors encountered in determining the time-mean pressure in a fast fluidized bed results from the pronounced pressure fluctuations in the bed. When using U-tube manometers, the evaluation of such a mean value can only be practically accomplished by averaging the absolute maxima and minima obtained for a more or less arbitrary time interval, as was done by Yerushalmi et al. (1974 - 1978), Avidan(1980), Meller(1984) and Shao(1986). This is one reason why pressure transducers were introduced for all pressures measured in the fluidized bed equipment. The piezo pressure transducer used could be installed in the immediate neighborhood of the pressure taps since an output signal of 1 - 5 volts is obtained. The transducer can therefore be wired directly to the remote data aquisition system without significant losses in the transmitting cables. In comparison to the arrangement for U-tube manometers, no filter element is introduced between the

fluidized bed and the pressure transducer. A constant air backflow through the pressure tap prevents the solid from entering the transducer tube without further complications. A common power supply of 12 volts is built into a switchboard near the fluid bed, from where the signals are transmitted to a remote real time computer system.

This system consists of an Intel 86/300 personal computer, upgraded with two analog-to-digital converters for a total of 32 analog channels (Intel board iSBC 311) and a communication slave processor (Intel board iSBX 544). For the data base management an Intel 286/310 with expanded storage capabilities (60 MByte) was added. The iRMX real time operating system was used in both computers.

A number of program libraries were developed and program packages written that allow both an online and offline measurement capability of the pressure readings with the use of a multitask executive. High-level graphics developed proved useful to an efficient data management.

To determine the overall conditions of the fluidization system the mean values for all pressures were determined from 256 readings taken over an interval of ca. 2 min. The values for the solid recirculation rate were determined by analysing the changes in the differential pressure between taps 23 and 25 through the data aquisition system. With the butterfly valve in the storage bed closed, the decay of the pressure drop can be analyzed by means of linear regression

(Gaussian least-square-method). The evaluation of the solid rate assumes thereby that the bed is in steady fluidized conditions and that therefore the pressure drop between the two pressure taps is solely determined by the weight of the fluidized solid. Friction losses of solid and gas at the wall as also any acceleration effects of the solid at the entrance of the standpipe are neglected since their sum amount to far less than 1% of the average pressure drop in the bed.

The procedure is carried out in the following way: 10 readings of the pressure difference are taken as long as the butterfly valve is open (normal conditions) and averaged to get the starting value. Thereafter, the valve is closed, while the data aquisition reads the pressure difference in time intervals of 300 msec. The actual time series measurement is triggered when the value measured is 15 mbar below the starting value to eliminate distrubances that might occur by closing the butterfly valve. The reading is finished when a pressure difference of 40 mbar below the starting value is recognized. The slope obtained from these data by linear regression is converted into a value for the solid rate. This procedure is necessary since the pressure difference often exhibits strong fluctuations. The solid rates thereby obtained for consecutive measurements lie for most cases within an error range of 5% or less.

3.3 TIME SERIES MEASUREMENTS FOR PRESSURE FLUCTUATIONS

For a detailed time series analysis of the pressure readings, a program package was developed for online FFT analysis, either in a one or two-channel mode. The program creates output files consisting of

1) The time series itself (optional)
2) The pressure probability function(s)
3) The power spectra
4) The auto- or cross-correlation (1-channel or two-channel mode, resp.)

The window taken can be varied between 64 and 8192 data points. The minimum time interval possible is 1 msec, corresponding to the largest detectable frequency of 500 Hz. The FFT algorithm used is of a decimation-in-frequency type (Paul, 1982) and a Hanning window is used for the power spectra (Hewlett-Packard Firmware).

For a verification of this program package and also for finding evidence that frequencies in the range of the maximum frequency of 500 Hz can be detected with the hardware set-up, a pressure signal at a frequency of ca. 110 Hz was introduced at the end of the transfer line. This was done by focusing an airjet which was interrupted by the blades of a rotating fan (fan speed ca. 1760 rpm, four blades) on the end of the transfer line. The resulting pressure probability functions and the power spectra for

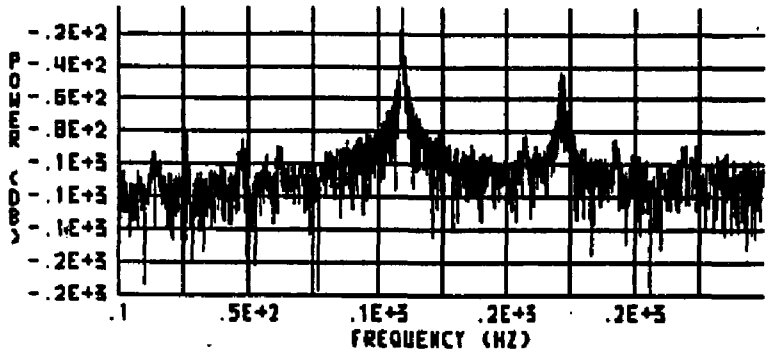

Fig. 13 Power sprectum of a 110 Hz pressure signal (Fan-test arrangement), window of 8192 data points

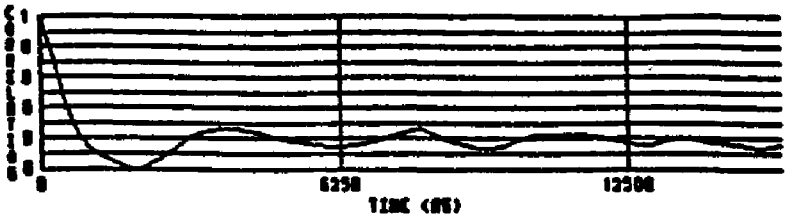

Fig. 14 Auto correlation function of a gauge pressure signal in a slugging fluidized bed

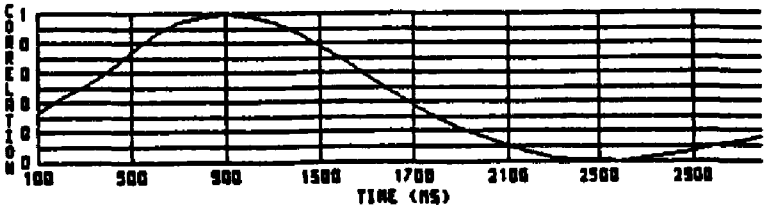

Fig. 15 Cross correlation function of gauge pressure signals in a slugging fluidized bed

this test arrangement are presented in Figure 13 for a window consisting out of 8192 data points. The additional frequency encountered at ca. 170 Hz seems to be a result of the rectangular shape of the input signal (simulated on/off switch).

Since the actual readings in the fast fluidized bed are taken in a far larger time interval, in the range of 100 msec, it can be assumed that damping and signal interference within the transfer lines (time constant of less than 3 msec) and the pressure transducers will not effect the time series measurements.

The output of the correlation functions was checked by a two-channel measurement of pressure readings within a slugging bed to determine the delay time between the signals with the highest probability. A similar measurement analysis was used by Wisecarver et al.(1985) for a slugging fluidized bed and Sitnai et al.(1982) for bubble parameter determination in a bubbling fluidized bed. In Figure 14 and 15 the auto- and cross-correlation functions for the pressure readings at tap 4 and simultaneous readings on pressure taps 5 and 7 are presented. The auto correlation function suggests a main period of oscillation of ca. 4.0 sec, corresponding to 0.25 Hz. The cross correlation function in Figure 15 shows a delay time of maximum probability of ca. 0.9 sec. Knowing that pressure taps 5 and 7 are 0.92 m apart, a slug velocity of 1.02 m/sec can be

calculated which is in good agreement with the observed slug velocity in the transparent column of ca. 1 m/sec and a theoretical evaluation of the slug rising velocity of Ub = 1.08 m/s obtained through the correlation suggested by Matsen (1973) using Ug = 0.65 m/s, Umf = 0.0009 m/s:

(1) $Ub = 0.35 * SQRT(g*Dt) + (Ug - Umf)$

with: Ub = slug rise velocity
Ug = superficial gasvelocity
Umf = superficial gas velocity at
minimum fluidization conditions

4 EXPERIMENTAL RESULTS

During the course of this study the pressure signals in the fast fludized bed system were analyzed for more than 200 individual conditions. A list of the experimental runs can be found in Appendix A. Since such a detailed experimental analysis was chosen, all runs were made with a single solid, a zeolite fluid cat-cracking catalyst, HFZ-33 (Engelhard). The solid has a mean particle size of 59 microns and an apparent density of 1460 kg/m3. It is essentially identical for fluidization characteristics with the catalyst HFZ-20, used by Avidan(1980), Meller(1984) and Shao(1986).

Summarizing the general behavior of the fast fluidized flow a priori it was found that a typical profile for the void fraction over the height of the column is obtained as is shown in Figure 16. The void fraction - simply obtained by the time-mean pressure gradient - was used as a general measure to describe the overall flow pattern. Following Figure 16, fast fluidized flow typically exhibits two regions of nearly constant void fraction, divided by a transition zone, equivalent to the bed surface in a bubbling, slugging or turbulent fluidized bed. It is however much more unclear and difficult to define. It is further understood, that there are additional effects observable near the entrance and exit zones of the fluidizing column. Hence, the void fraction profile will always start with the first differential pressure reading

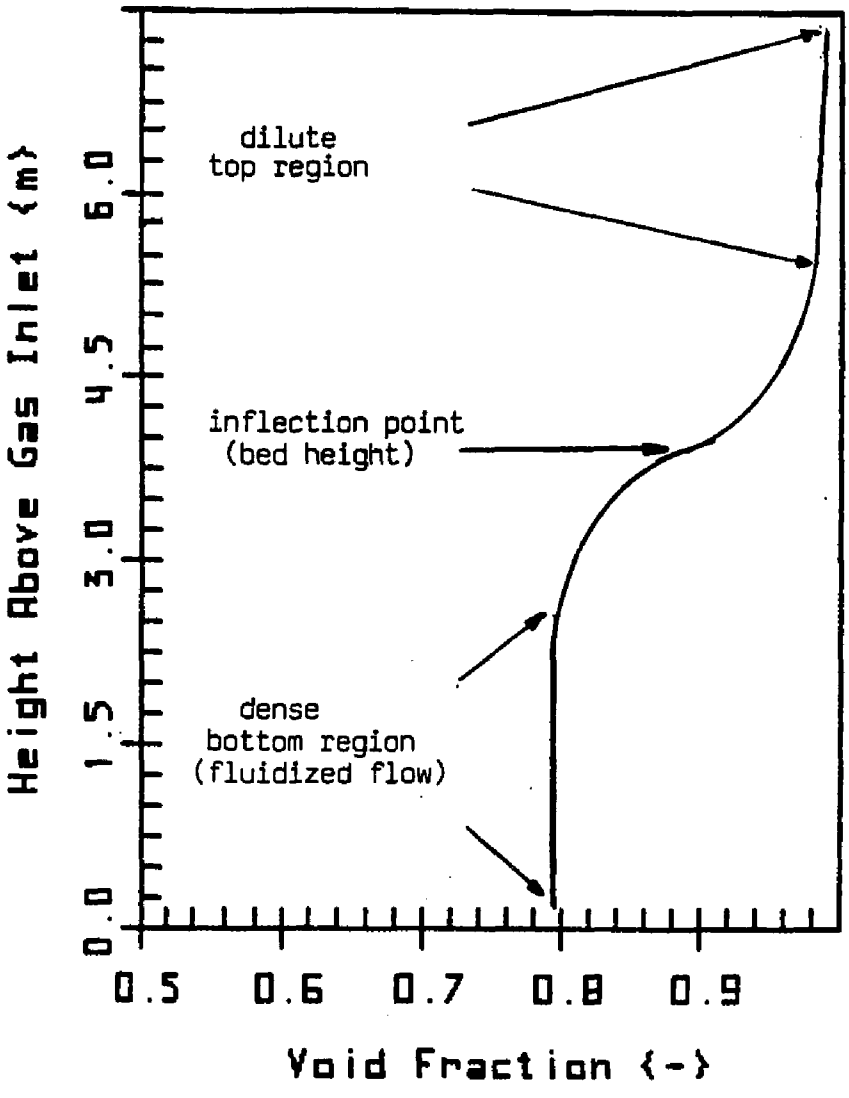

Fig. 16 Typical void fraction profile in a fast fluidized bed

above the entrance zone and will end ca. 0.5 m below the exit section of the fluid bed. This is in contrast to data presented by Meller(1984) and Shao(1986).

Nearly constant void fractions throughout the denser and dilute regions have been pointed out by Li and Kwauk (1980). In this study the above condition was taken as a working definition for fast fluidized flow which later becomes part of a general definition for fast fluidization.

4.1 TIME-AVERAGED VOID FRACTIONS IN THE TOP AND BOTTOM SECTION OF THE FAST FLUIDIZED BED

Before going into a detailed analysis of the pressure readings in a high velocity fluidized bed a number of general, qualitative and quantitative observations of the measured pressure fluctuations need to be noted. The pressure differentials in the bed can be reported in the form of the corresponding value for the crosssectional mean of the void fraction. To use this measure as the void fraction, it is assumed that friction losses and acceleration effects are neglectible.

In Figure 17 - 20 the 95% confidence interval for the mean and the values for the absolute minimum and maximum of the void fraction over the height are represented together with the mean for different superficial gas velocities. The individual data points are connected by straight lines. The scatter of data is mainly due to the slightly different

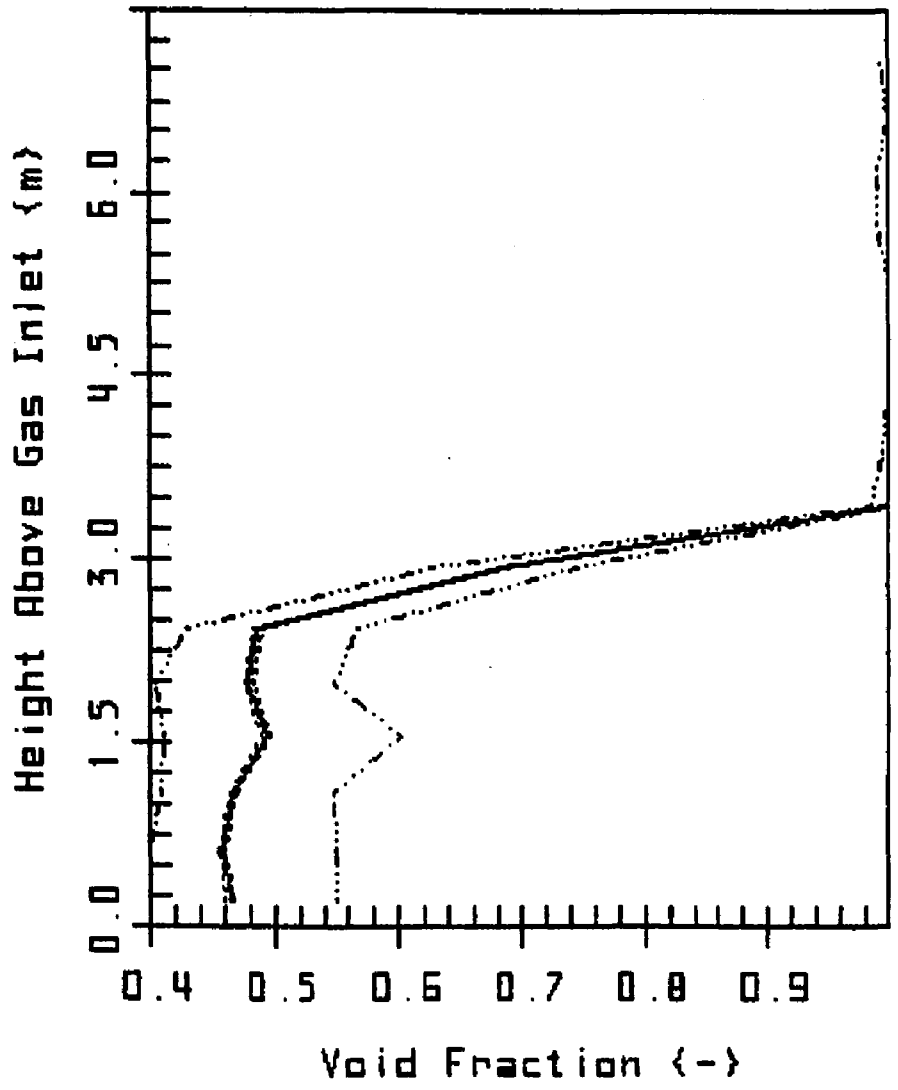

Fig. 17 Void fraction profile of a bubbling fluidized bed (Ug = 0.03 m/s), data points connected by straight lines
(— · · — · · · absolute mimima/maxima)
(- - - - - - - - 95% confidence interval)
(———————— Mean)

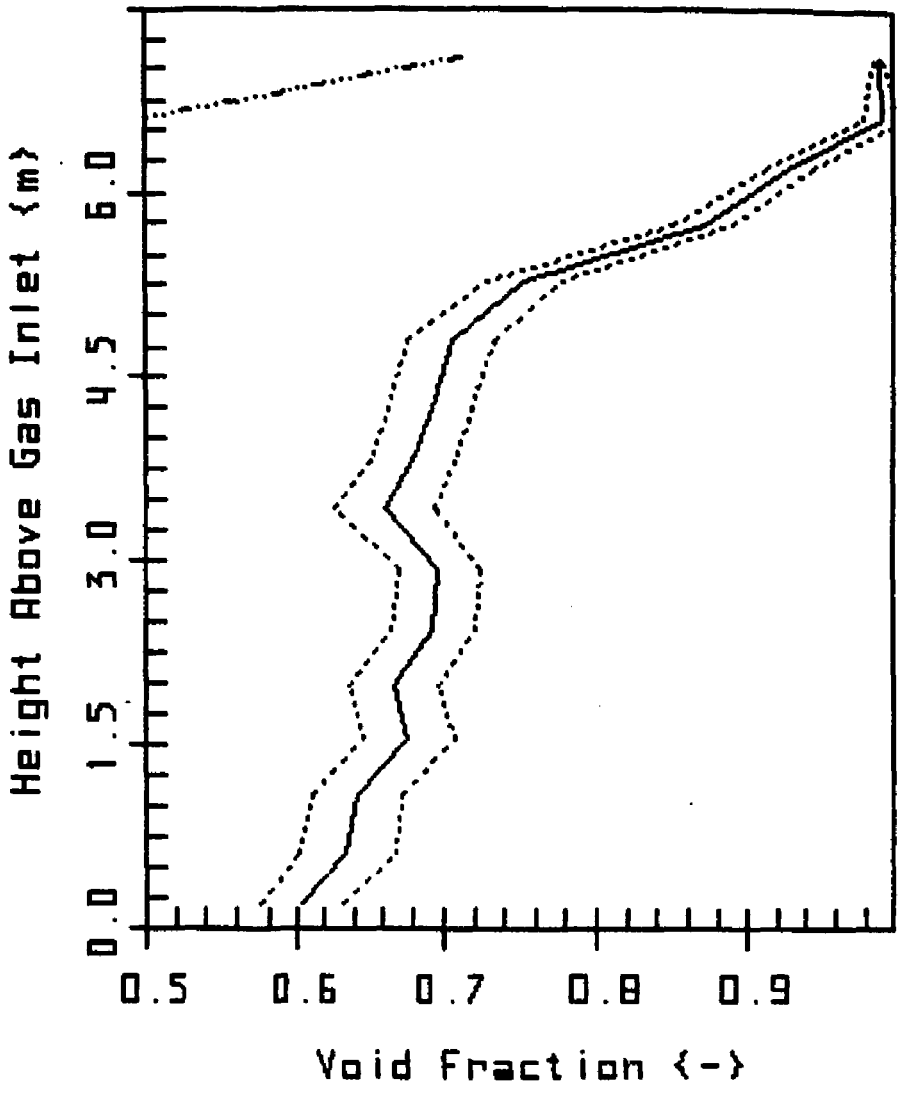

Fig. 18 Void fraction profile of a slugging fluidized bed (Ug = 0.7 m/s), data points connected by straight lines
(— · · — · · absolute mimima/maxima)
(- - - - - - - - 95% confidence interval)
(———— Mean)

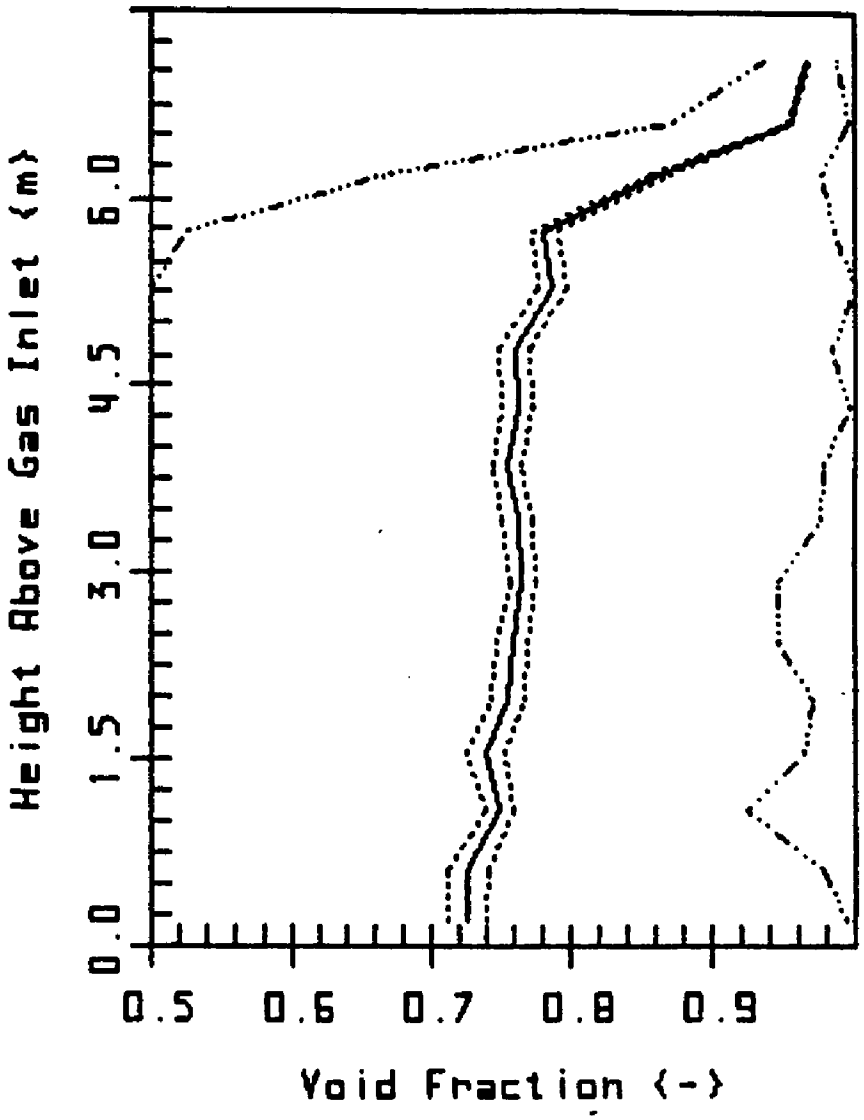

Fig. 19 Void fraction profile in a high velocity fluidized bed (Ug = 1.5 m/s), data points connected by straight lines
(—··—·— absolute mimima/maxima)
(--------- 95% confidence interval)
(———————— Mean)

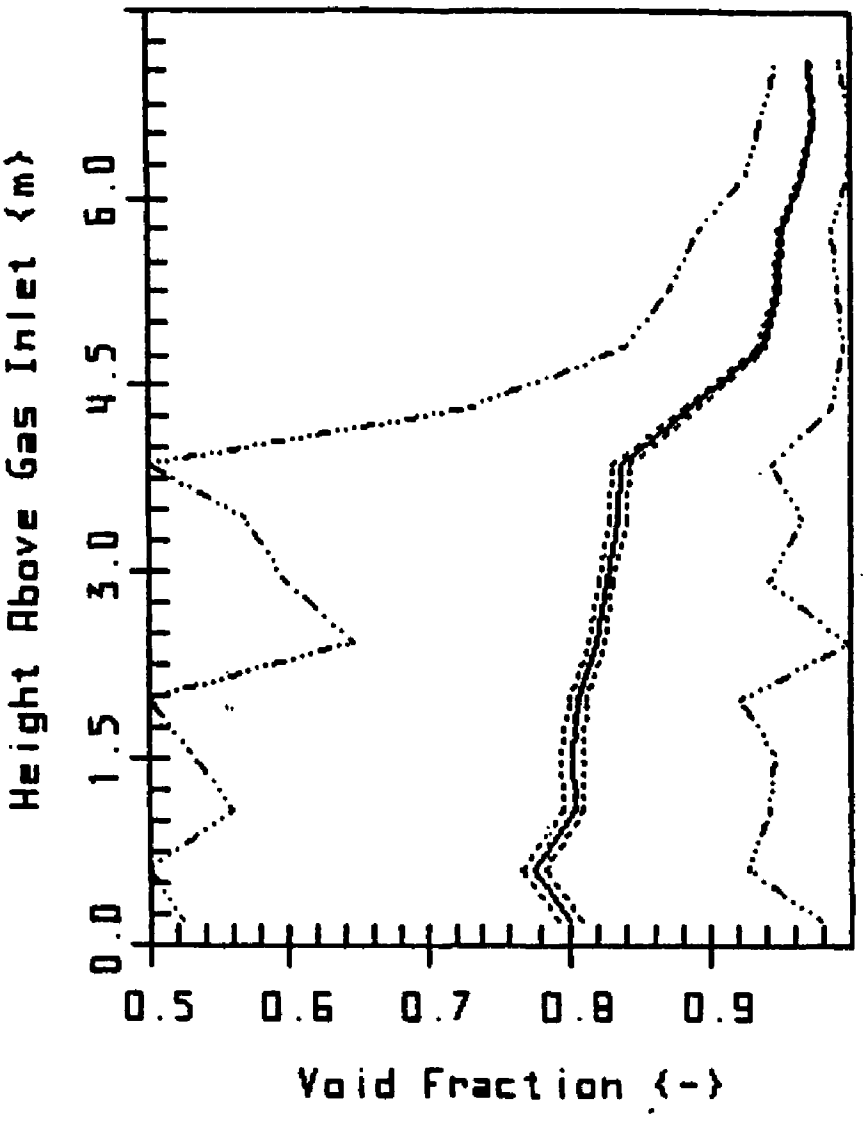

Fig. 20 Void fraction profile in a fluidized bed (Ug = 1.5 m/s, Gs = 133 kg/m2s), data points connected by straight lines
(—·····—·····— absolute mimima/maxima)
(-------- 95% confidence interval)
(———————— Mean)

geometry of each pressure tap and could not be eliminated even with very careful measurement procedures. For the purpose of comparision both bubbling (Figure 17) and slugging fluidized beds (Figure 18) are included. In the bubbling fluidized bed the difference between the minimum and maximum void fraction is only ca. 0.15 below the bed heigth of ca. 2.5 m. The individual values in both slugging and high velocity fluidized beds (Figures 18 - 20) spread over the entire possible range (0.4 to 1.0). The confidence interval for the mean is small, hence reproducability of data within a small error interval is guarantied. Comparing further the different plots it can be concluded that at very low gas velocities the relative as well as the absolute magnitude of fluctuations are small. They have their peak values in the slugging regime and decrease with further increase of gas velocity. Furthermore, the magnitude of the mean pressure gradient decreases sharply in the top region of the bed. The quantitative aspects of these phenomena will be discussed in the following paragraphs.

The probability density functions (PDF's) for various heights are given in Figures 21 - 26. Differential pressure readings were chosen since they show only those fluctuations that occur within the differential height in contrast to those of gauge pressure signals.

In Figures 21 - 23 the first four differential pressure

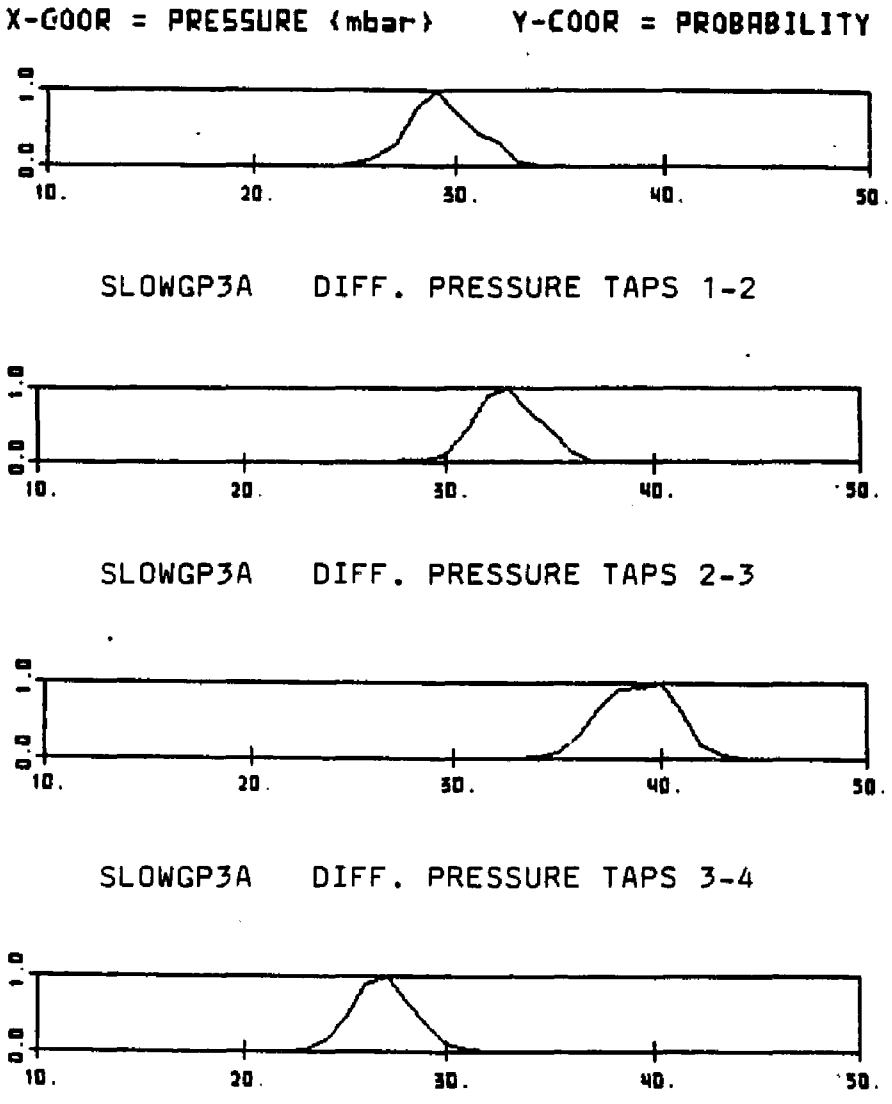

Fig. 21 Probability density functions of differential pressures in a bubbling fluidized bed (Ug = 0.03 m/s)

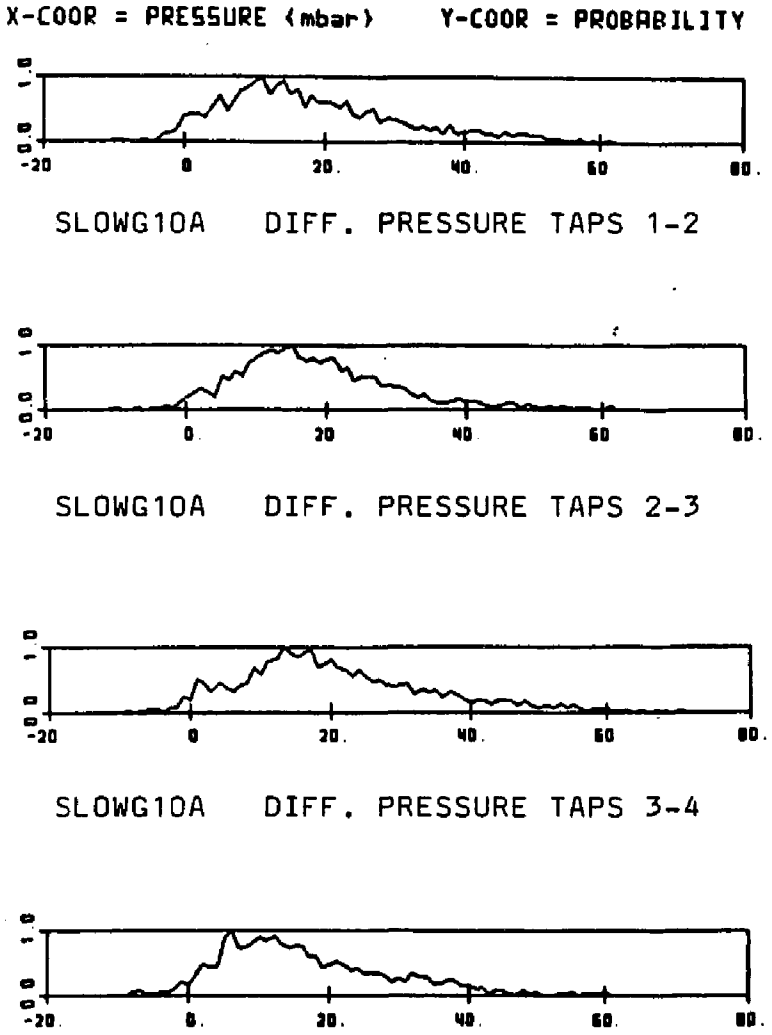

Fig. 22 Probability density functions of differential pressures in a slugging fluidized bed (Ug = 1.0 m/s)

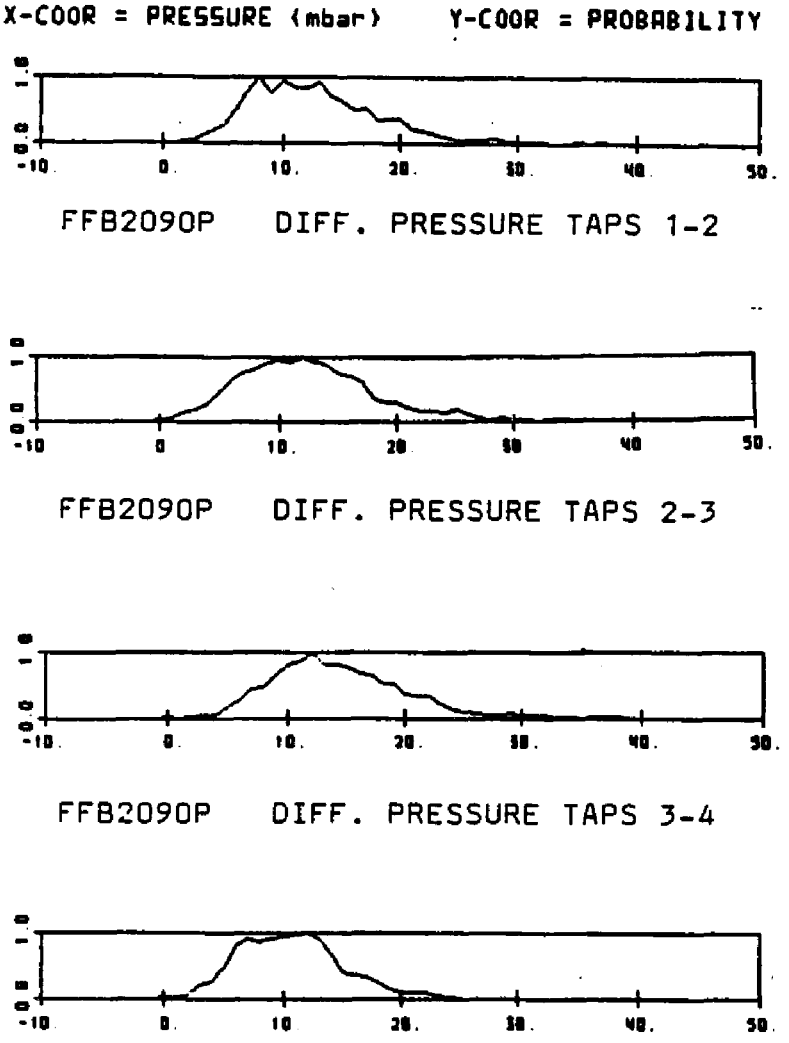

Fig. 23 Probability density functions of differential pressures in a high velocity fluidized bed (Ug = 2.0 m/s, Gs = 88 kg/m2s)

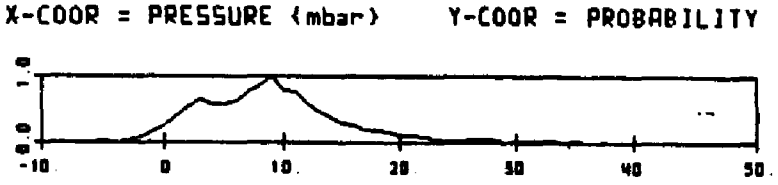

SLOWG10A DIFF. PRESSURE TAPS 12-13

SLOWG10A DIFF. PRESSURE TAPS 13-14

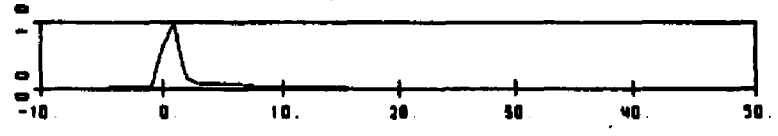

SLOWG10A DIFF. PRESSURE TAPS 14-15

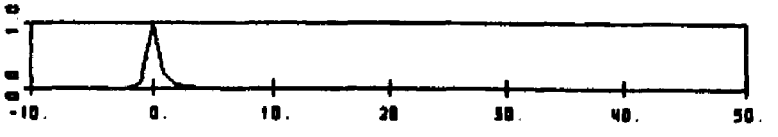

SLOWG10A DIFF. PRESSURE TAPS 15-16

Fig. 24 Probability density functions of differential pressures in the top section of a slugging fluidized bed (Ug = 1.0 m/s)

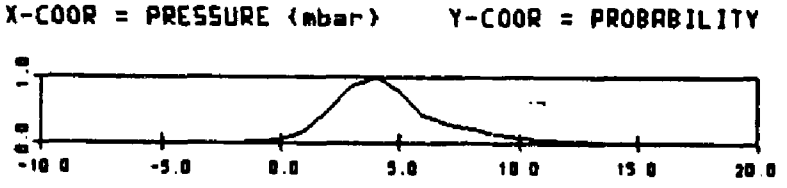

FFB2090P DIFF. PRESSURE TAPS 12-13

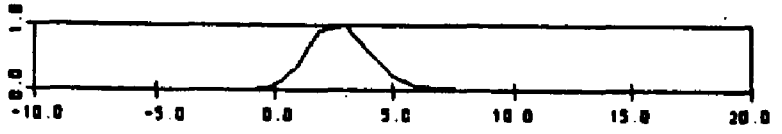

FFB2090P DIFF. PRESSURE TAPS 13-14

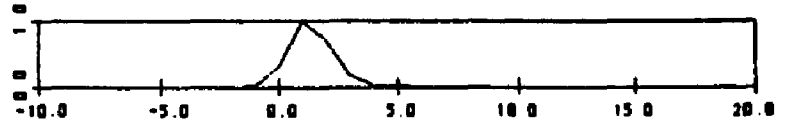

FFB2090P DIFF. PRESSURE TAPS 14-15

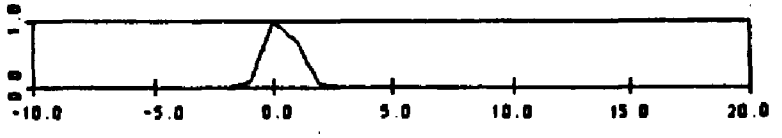

FFB2090P DIFF. PRESSURE TAPS 15-16

Fig. 25 Probability density functions of differential pressures in the top section of a high velocity fluidized bed (Ug = 2.0 m/s, Gs = 88 kg/m2s)

readings at the bottom of the fluidization column are given for different gas velocities. Figure 21 details pressure fluctuations within a bubbling fluidized bed, whereas Figures 22 and 23 correspond to the slugging and fast fluidized regime, resp.. In all cases all differentials lie within the densely fluidized region of the bed. Figures 24 - 25 represent the last four pressure differentials at the top of the bed for the slugging and fast fluidized bed, only partly representing the dense fluidized flow. The corresponding differential lengths are not equal which explains the variations in the location of the PDF maxima. The differential lengths are listed in Appendix B.

From these figures it can be seen that the PDF's in both the slugging and fast fluidized bed are asymmetric in the region of low void fraction at the bottom of the bed and reach a more or less symmetric shape as we move up the column height into the dilute region. It is understood that the length of the dense section in the bed varies and with it the height at which the PDF's become symmetrical. For bubbling fluidized beds such asymmetry is not exhibited.

It can be concluded that the shape of fast bed pressure signals has some similarity to that of a slugging fluidized bed. The asymmetry of the PDF's that can be found in the fast fluidized bed obviously is a result of instabilities with some similar characteristics to those found in a slugging fluidized bed.

It seems necessary to know the functionality of such an asymmetry with the height in the bed. In Figures 26 and 27 the difference between the mean and median values in the PDF's is plotted over the bed height for data obtained on a fast fluidized bed for two different gas velocities (2.0, 5.0 m/s) and various solid rates. The vertical bar in these plots indicates the bed height as found by examining the mean void fraction profile. Figure 28 represents a similar plot for the difference between the minmax-average (average between the absolute minimum and absolute maximum value) and the mean for similar runs. Both the difference between mean and median as well as the difference between the minmax-average and the mean indicate a clearly skewed PDF within the dense fluidized regions.

Skewed PDF's of differential pressure readings are obtained in slugging as well as in high velocity fluidized beds and are therefore not a unique feature of the slugging fluidized bed. It should also be noted that besides a smaller magnitude of the skewness parameters, no clear distinction between the PDF's in the slugging fluidized beds and those in the fast fluidization regime can be seen.

Although a wide scatter of data is evident, the general behavior becomes clear: As we move up the column height, the values seem to decrease slightly with height until the bed height is reached and then they decrease sharply to a value around zero. Above the bed height the values fluctuate

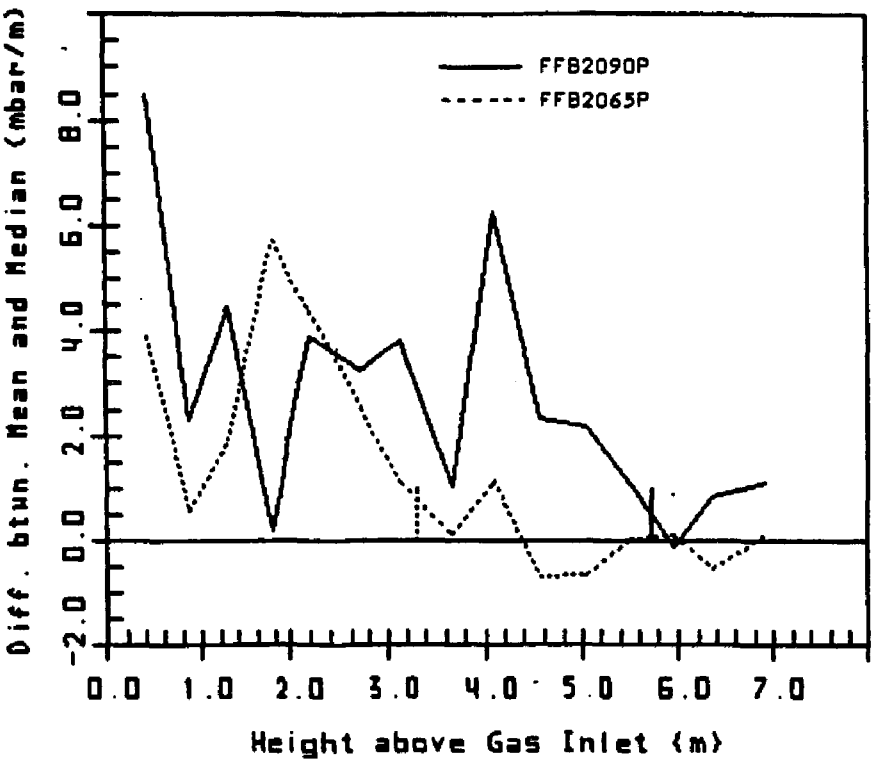

Fig. 26 Difference between the mean and median of the differential pressure readings along the height in a high velocity fluidized bed
(FFB2090P, Ug = 2.0 m/s, Gs = 88 kg/m2s)
(FFB2065P, Ug = 2.0 m/s, Gs = 67 kg/m2s)

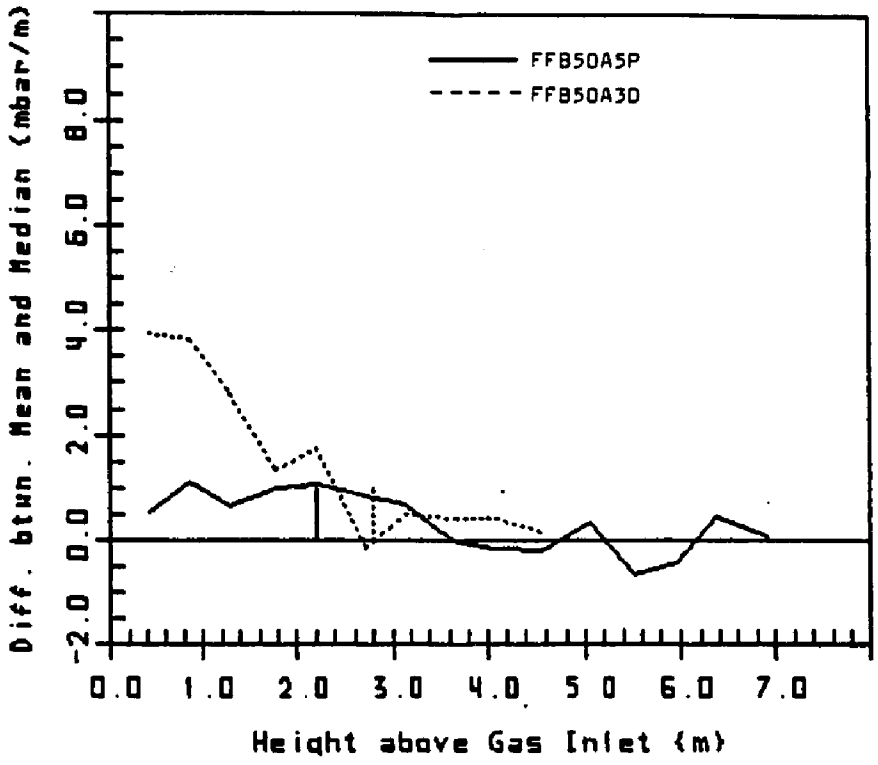

Fig. 27 Difference between the mean and median of the differential pressure readings along the height in a high velocity fluidized bed
(FFB50A5P, Ug = 5.0 m/s, Gs = 150 kg/m2s)
(FFB50A3D, Ug = 5.0 m/s, Gs = 132 kg/m2s)

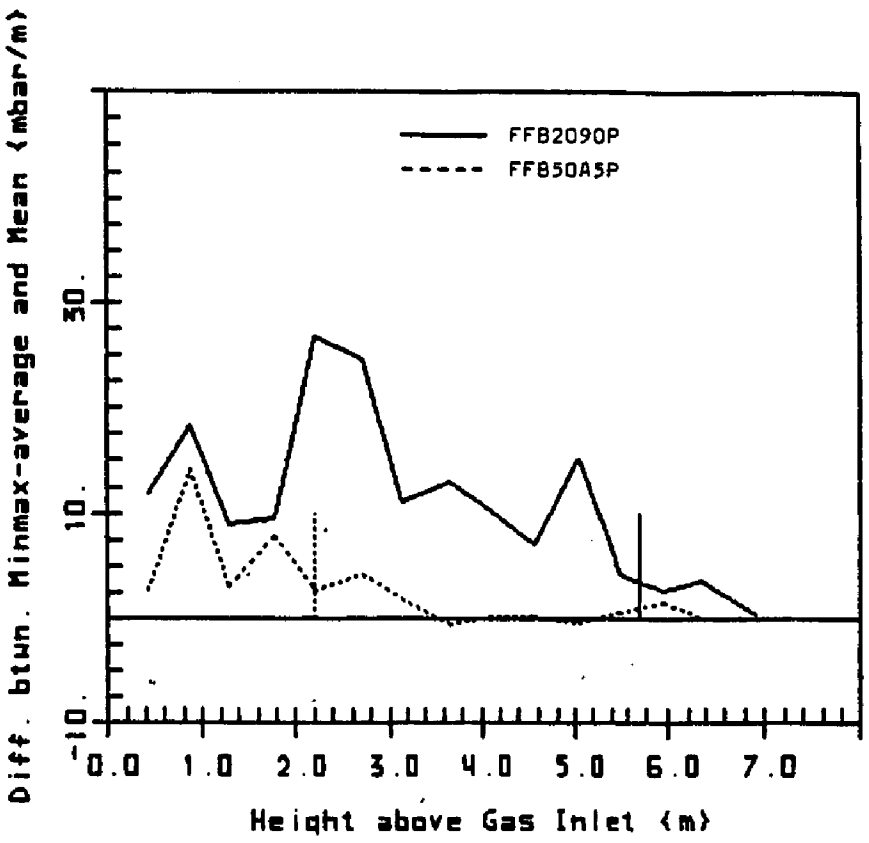

Fig. 28 Difference between the minmax-average and the median of the differential pressure readings along the height in a high velocity fluidized bed
(FFB2090P, Ug = 2.0 m/s, Gs = 88 kg/m2s)
(FFB50A5P, Ug = 5.0 m/s, Gs = 150 kg/m2s)

around the zero value. This is true for both the difference between mean and median as well as for the difference between mean and the minmax-average and is generally true for all the runs made in the slugging and high velocity fluidized regime.

4.1.1. THE VOID FRACTION IN THE BOTTOM REGION OF A FAST FLUDIZED BED.

It was stated already that the void fraction in the two main sections of the fast fluidized bed can be taken as essentially constant over the section height. This however is still to be shown. Due to the asymmetric pressure probability function a number of possible methods to determine a characteristic void fraction can be formulated.

In the following three different values will be compared which are obtained from the PDF's of the pressure gradient in the fluid bed:

1) The median,
2) The mean,
3) The minmax-average.

In Figures 29 - 30 the void fractions in the bed calculated on the basis of the above 3 different values for the differential pressures are plotted in each graph. From right to left these are median, mean and minmax-average. This is true for all runs since the asymmetry is always

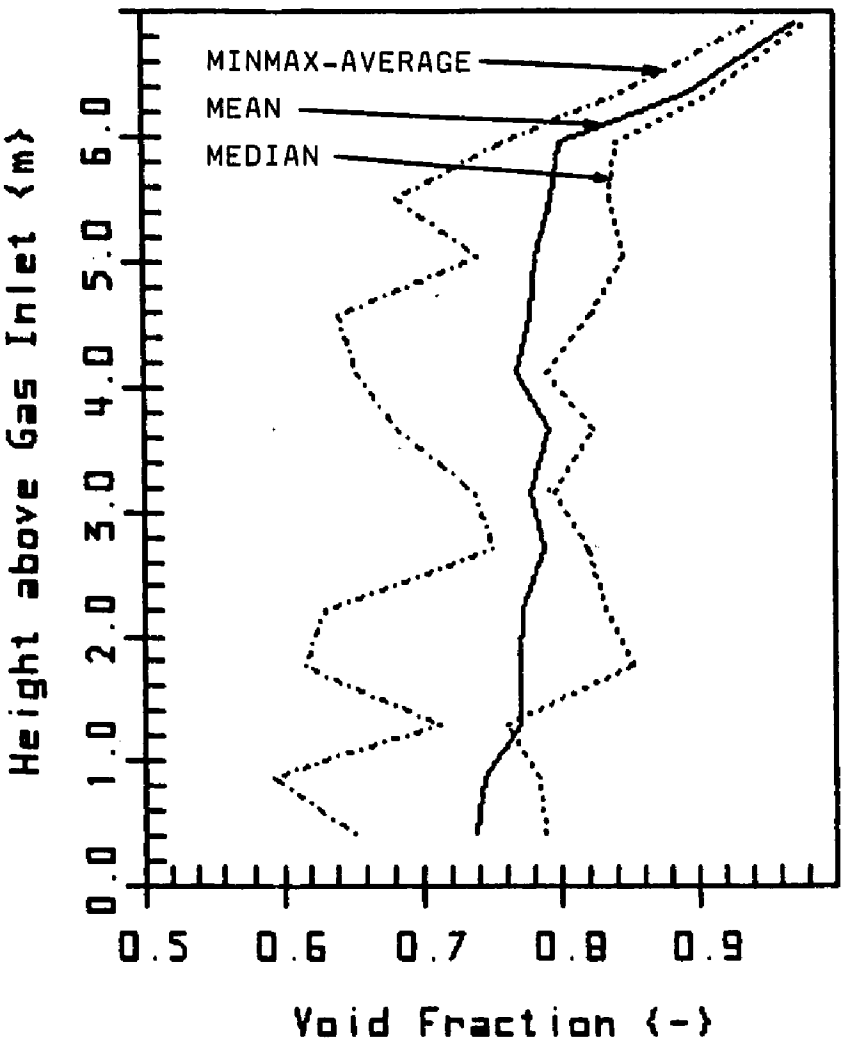

Fig. 29 Void fraction profile in a fast fluidized bed, with values obtained by three different methods, data points connected by straight lines (SLOWG15A, Ug = 1.5 m/s, Gs = 65 kg/m2s)

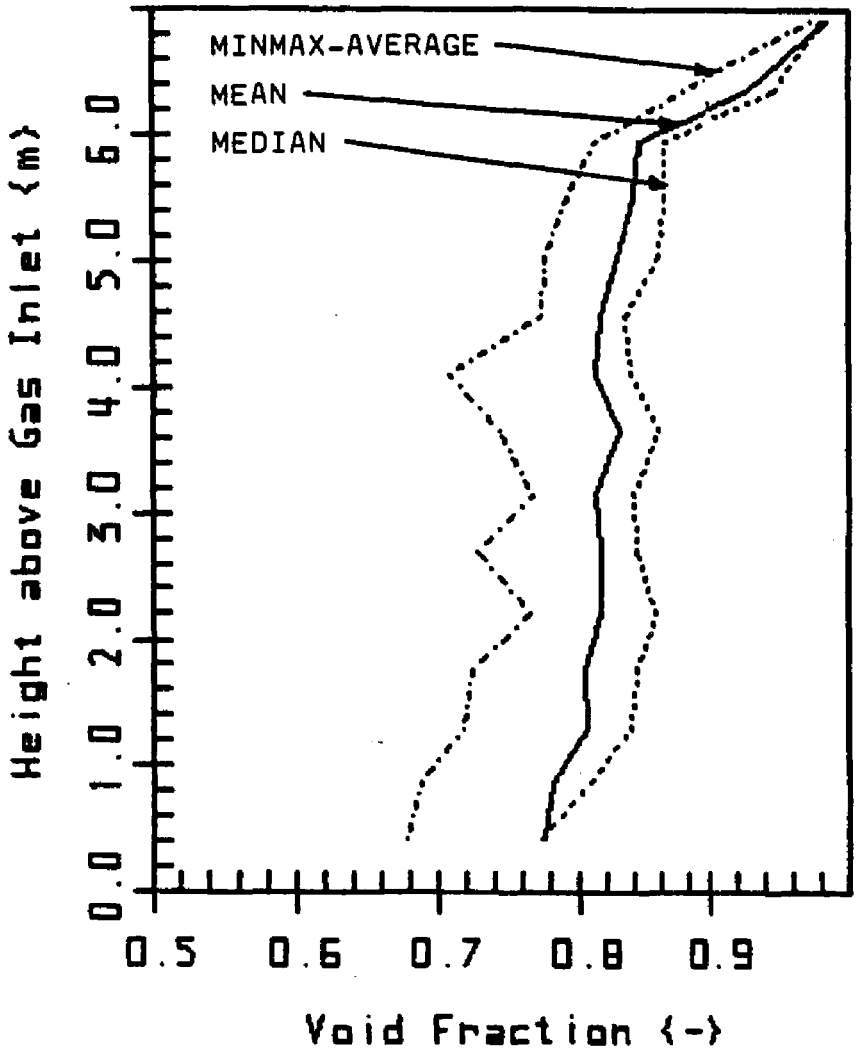

Fig. 30 Void fraction profile in a fast fluidized bed, with values obtained by three different methods, data points connected by straight lines (FFB25FFA, Ug = 2.5 m/s, Gs = 83 kg/m2s)

found to be stronger for higher pressure gradients in fast fluidized beds. Starting with Figure 29 representing a flow with 1.5 m/s gas velocity and 65 kg/m2s solid rate it is shown clearly that it is essential to know which of the definitions is used. Furthermore, it seems that the tendency of increasing void fraction with increasing height within the bottom section is more pronounced when using the minmax-average and diminishingly small when using the mean and median values.

The same plot is shown in Figure 30 for the conditions of 2.0 m/s gas velocity and ca. 115 kg/m2s solid rate. Here the different results lie closer together and it seems again that both mean and median are constant through the entire bottom region. This conclusion holds for the entire set of fast fluidization experiments undertaken. It is therefore concluded that only when using the mean or median of the PDF's, the void fraction obtained within the bottom region of the fast fluidized bed is essentially constant with height.

For a more quantitative picture all the runs that exhibited a bed height of at least 2.9 m, representing a variety of different flow conditions, solid inventories and entrance configurations, were examined. All three values for the pressure gradients within the bottom regions were averaged and a skewness parameter plotted against the gas velocity. In Figure 31 the difference between mean and

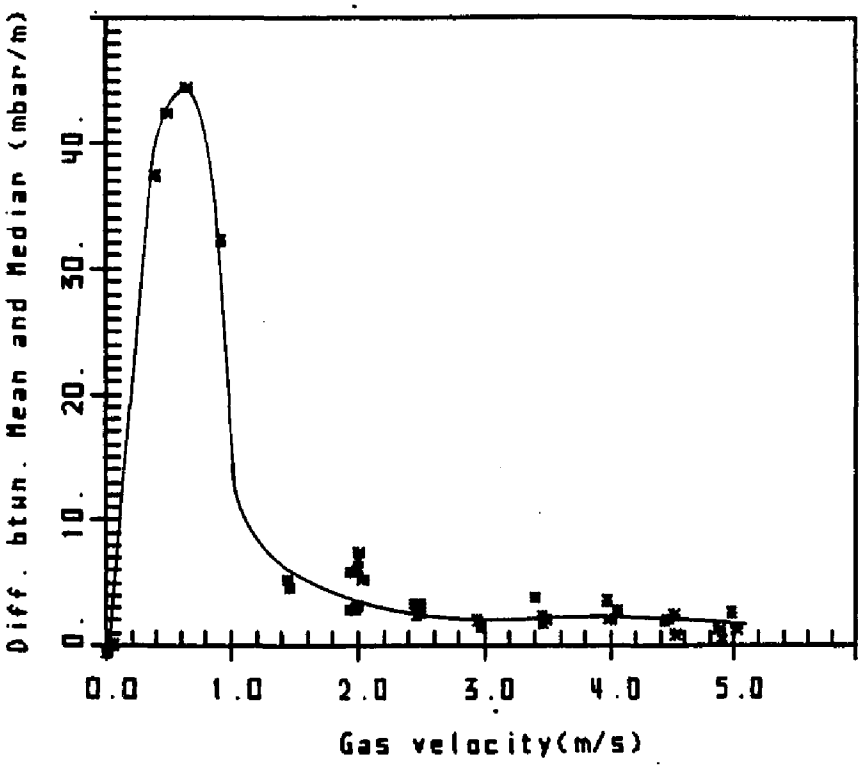

Fig. 31 Mean difference between the mean and median of the differential pressure readings in the dense fluidized region as a function of gas velocity

median for the pressure gradient is plotted against the superficial gas velocity in the bed is shown. Variations within one gas velocity (for Ug > 1.5 m/s) are due to varying solid rates, with higher values resulting from higher solid rates. Some scatter due to measurement errors are also present. The data exhibit a clear maximum in the slugging regime at Ug = 0.7 m/s and then decrease monotonically throughout the total range of gas velocities in the high velocity fluidized regime. If the plot is expanded for the data in the high velocity fluidization regime (Ug > 1.0 m/s), as shown in Figure 32, one might suggest that a clear decay in the skewness of the PDF's exists far beyond the slugging regime (0.3 m/s < Ug < 1.0 m/s) and that the skewness levels off at a gas velocity ca. 3.0 m/s.

To evaluate the magnitude of the pressure fluctuations the standard deviation of the PDF's are plotted against gas velocity (Figure 33). A picture similar to those Figures 31 and 32 is obtained. Once again, the values increase with increasing gas velocity up to a peak value in the slugging fluidization regime. Thereafter, the standard deviation decreases and levels off once again at a gas velocity of about 3.0 m/s. Identical behavior is given for the difference between the absolute maximum and minimum plotted against the gas velocity (Figure 34). A related plot was presented first by Yerushalmi and Cankurt (1978) for discussion of transition from slugging to turbulent

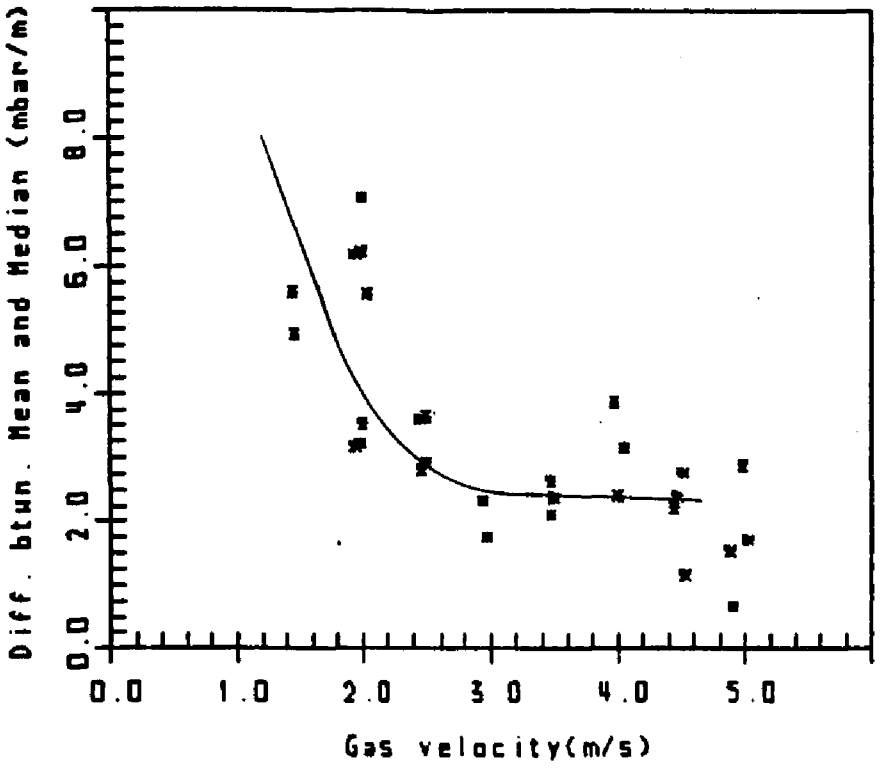

Fig. 32 Mean difference between the mean and median of the differential pressure readings in the dense fluidized region as a function of gas velocity (range of high velocity fluidized beds)

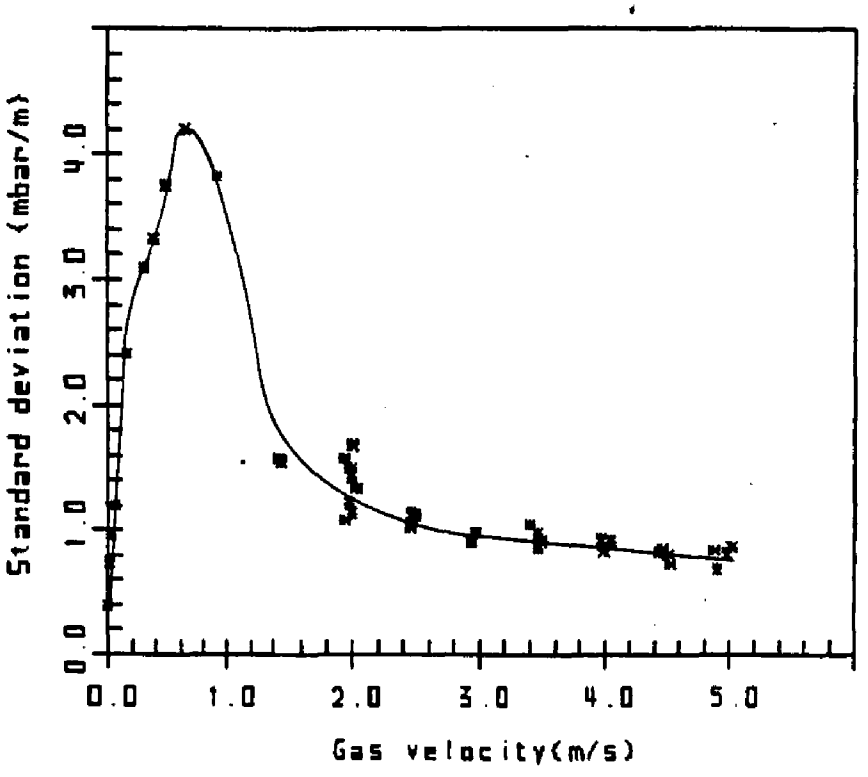

Fig. 33 Mean standard deviation of the differential pressure readings in the dense fluidized region as a function of gas velocity

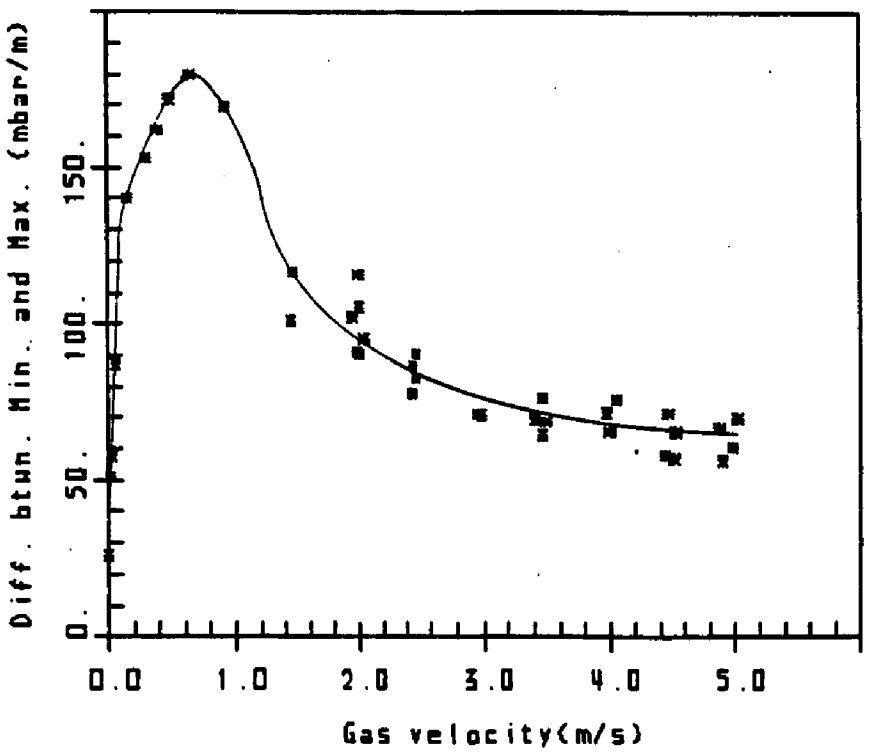

Fig. 34 Mean difference between the minmax-average and the median of the differential pressure readings in the dense fluidized region as a function of gas velocity

fluidization. Figure 34 will be discussed in more detail in Chapter 4.4.

It has already been shown that in the fast fluidization regime the void fraction based on the mean or median of the pressure gradient is essentially constant over the bed height. Therefore it seems reasonable to attribute one void fraction of the dense region to a set of flow parameters. Figure 35 shows such values for the different methods applied. The graph gives a surprising result: Whereas the values based on the minmax-average show a clear tendency towards an increase in the bottom region void fraction with gas velocity, the values based on the mean and median seem to be fairly constant over the velocity range of the fast fluidization experiments (1.5 - 5.0 m/s). For the solid rates used in the experiments the values are scattered over the range from 75% to 85%. When looking at the data for the remaining fluidization regimes we find the following tendencies: The minmax-average results in void fractions of around 50% and lower for the bubbling and slugging regime. Meanwhile, the median values show a clear peak in the slugging regime indicating once again the strongly asymmetric PDF's in the slugging regime. The mean values however represent a smooth curve over the entire gas velocity range. The void fraction seems to reach asymptotically a final value at high gas velocities of about 82% for the given data set.

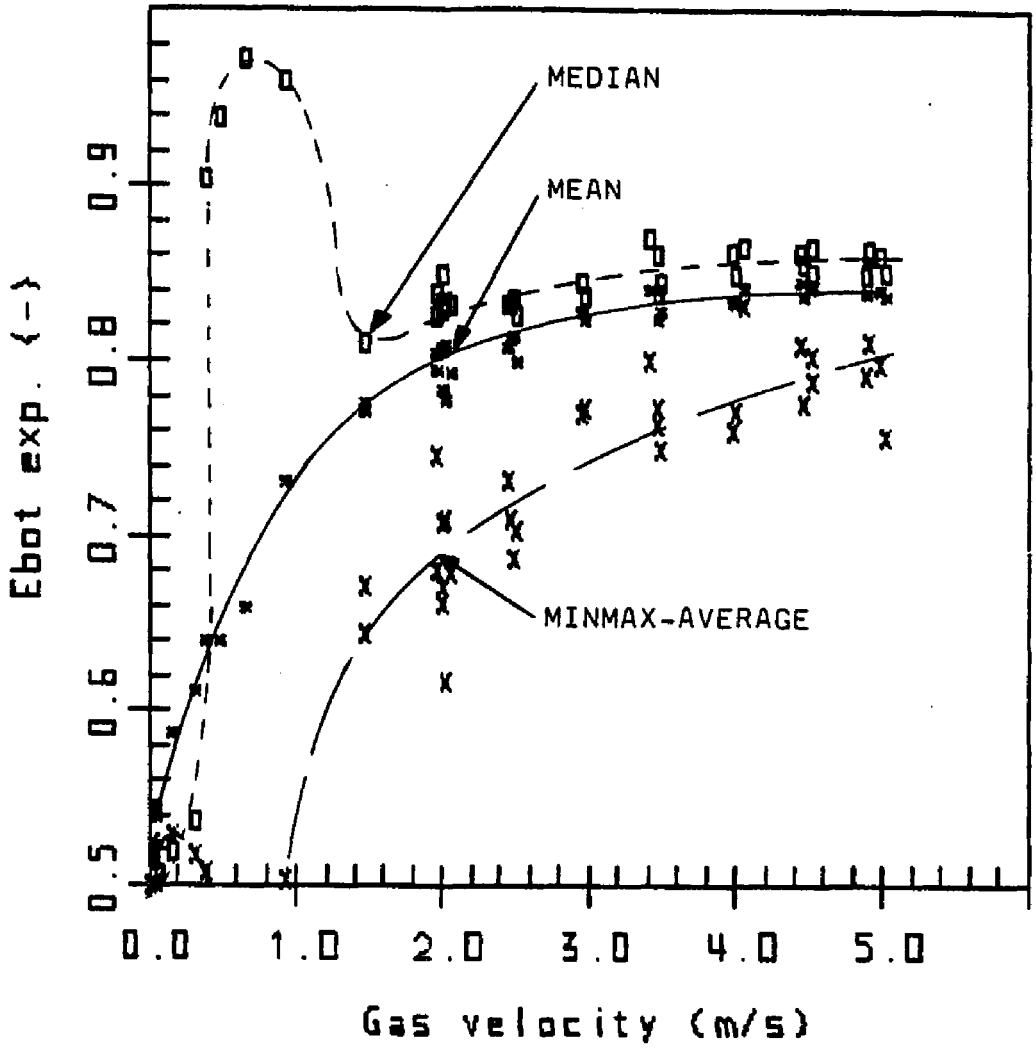

Fig. 35 Mean void fraction in the dense bottom region of gas fluidized beds as a function of the gas velocity, values obtained by three different methods
(0 - median values)
(* - mean values)
(X - minmax - average)

The influence of the gas velocity on the mean void fraction is clear for gas velocities, whereas for solid rates (Figure 36) such influence is harder to discern. But it shows clearly on the other hand the large differences between the values taken from the minmax-average and mean. It should be noted that the tendency to higher values for higher solid rates is partly due to the fact that higher solid rates are obtained at higher gas velocities. Therefore, any tendency shown is also a result of correspondingly higher gas velocities. Keeping the gas velocity constant and only varying the solid rates over a wider range and still maintaining a high solid hold-up in the bed is not possible due to restrictions of the flow and system design. Hence, a complete exploration of this behavior was not possible.

These results are particularly interesting, since the majority of data given in the literature were taken by averaging the absolute minimum and maximum pressure reading on a U-tube manometer. Although the response time of a U-tube manometer is much larger than that of the pressure transducers, the error made by such a measurement will be in principle the same, most likely only smaller in magnitude. This could, in particular, be the case for data reported by Kwauk et al.(1985) on which a correlation was based to evaluate the void fraction in the dense region. The correlation depicts a clear dependence of the mean void fraction on the superficial gas velocity as well as a slight

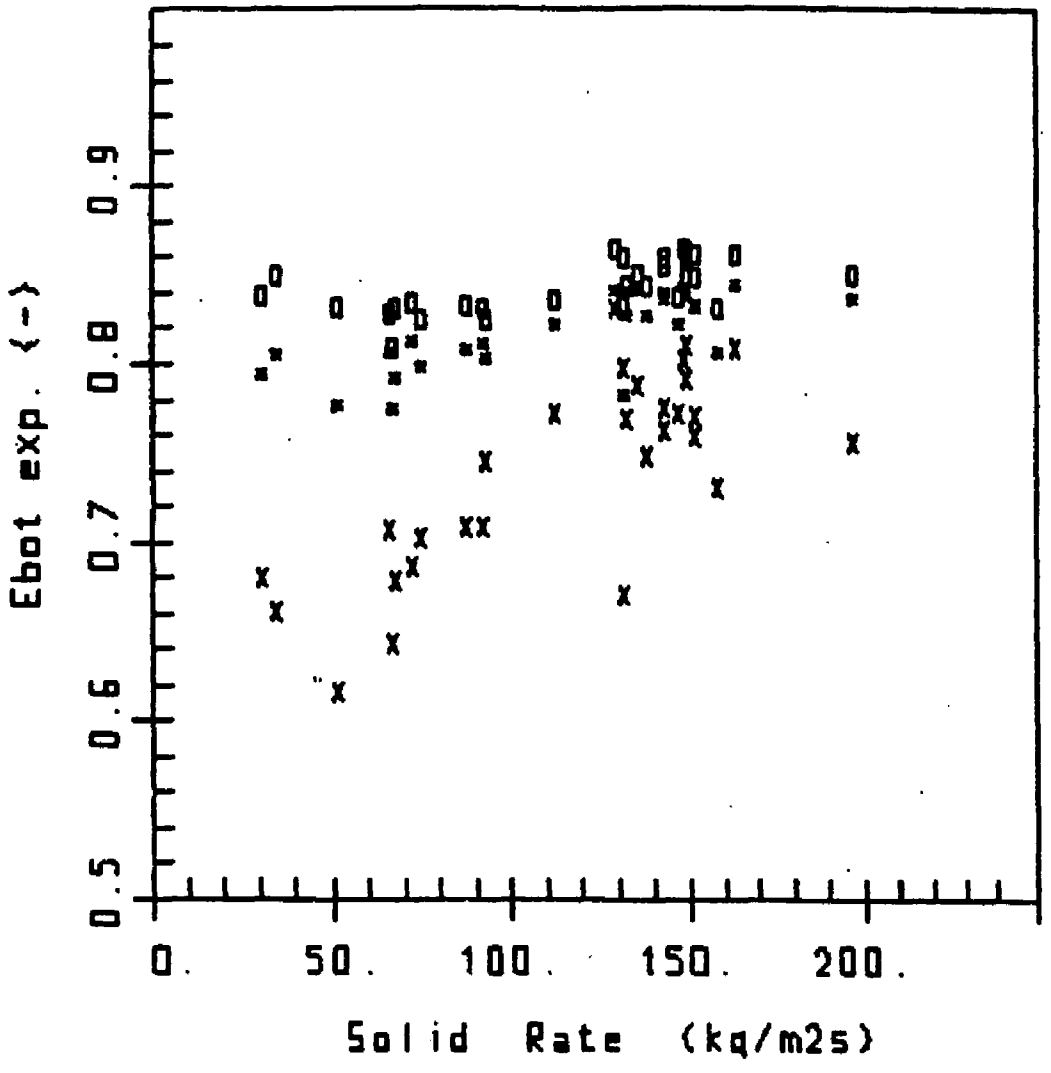

Fig. 36 Mean void fraction in the dense bottom region of gas fluidized beds as a function of the solid rate, values obtained by three different methods
(0 - median values)
(* - mean values)
(X - minmax - average)

dependence on the solid rate which can also be said for the data in this investigation. If indeed Kwauk's data were actually based on the minmax-average, any correlation based on them would also include effects of the asymmetry of the pressure fluctuations. Therefore Kwauk's correration was compared with the present data. The correlation is given through the following equations:

(2) $$1 - Ebot = 0.2513 * ((18*REs + + 2.7 * REs**1.687)/AR)**(-0.4037)$$

with:

(3) $$REs = dp*rof/mu * (Ug - Us (Ebot/(1-Ebot))$$

(4) $$AR = dp**3*rof*g*(ros-rof)/mu**2$$

and: ros = density of solid,
rof = density of gas,
mu = kin. viscosity of gas,
dp = mean particle size,
g = gravity

The results are given in Figure 37 parallel with values for Ebot on the basis of the mean pressure gradients. The correlation does indeed depict a similar function of Ebot on the gas velocity. Nevertheless, the values obtained are ca. 5% higher than the actual experimental data and the slope at higher gas velocities is larger than the data indicate it should be.

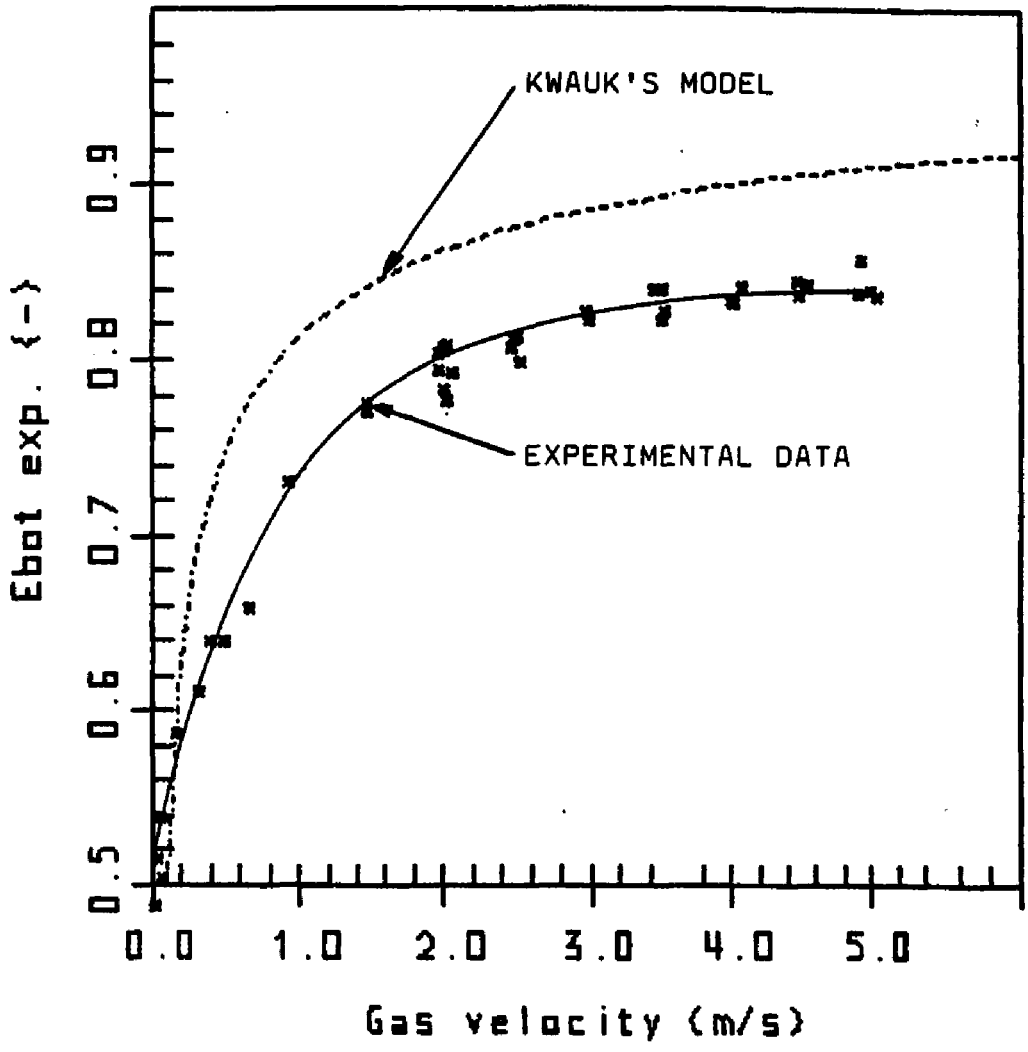

Fig. 37 Mean void fraction in the dense bottom region of gas fluidized beds as a function of the gas velocity. Mean values compared with model by Kwauk (eq. (2) - (4))

The evidence of an essentially constant mean value for the void fraction at higher gas velocities is hard to explain. It seems that a flow pattern is established in the high velocity regime with a preferred void fraction or solid hold-up and that instabilities result in the system exhibiting fluctuations. With respect to the essentially constant void fraction in the densely fluidized region the fast fluidized flow also shows many similarities to the flow in bubbling and turbulent fludized beds.

4.1.2. THE VOID FRACTION IN THE TOP REGION OF THE FAST FLUIDIZED BED

As already mentioned, the pressure fluctuations in the top region of the fast fluidized bed are different from those in the bottom region. In particular they show no pronounced asymmetry in the pressure probability functions and are much smaller in magnitude. In Figures 38 a void fraction profile in the bed is presented showing the values obtained from the median, mean and minmax-average. In this case the gas velocity is around 5.0 m/s and solid rate is ca. 130 kg/m2s. The plot is chosen out of the variety of profiles available because it exhibits a long section of the top region. It becomes clear that there is no significant difference between the three different values within the dilute top region in the fluidization column. This once again emphasises that the pressure signals follow a symmetric pressure probability function. This of course

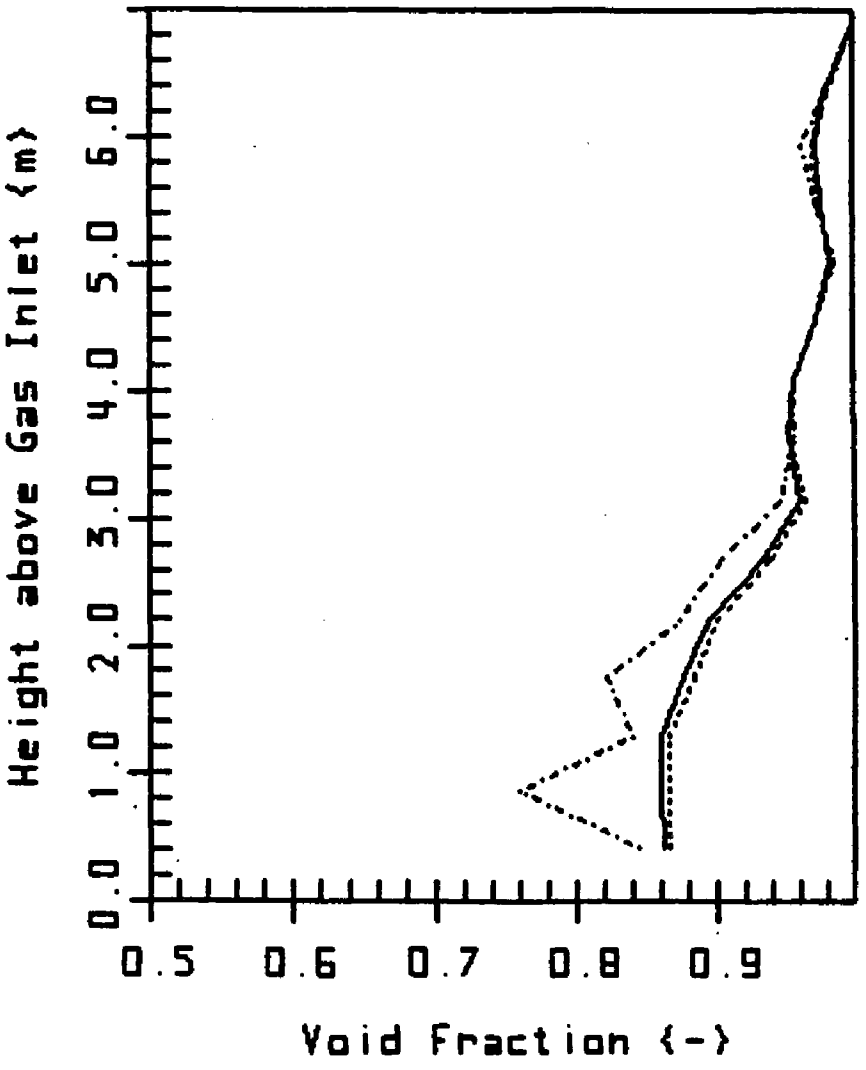

Fig. 38 Void fraction profile in a fast fluidized bed, with values obtained by three different methods, data points connected by straight lines (FFB50A3D, Ug = 5.0 m/s, Gs = 132 kg/m2s)

simplifies the procedure for evaluating an appropriate void fraction for the top region in the fast fluidized bed.

As was found true already above for the bottom region, the void fraction in the top region, after a strong decay in the transition zone shows only a slight trend to higher values for increasing height. For further considerations the void fractions found in the top regions will therefore be summarized by a mean value.

The values obtained, in contrast to those in the bottom region, are clearly dependent on both flow parameters, gas velocity and solid rate. In a first attempt to discribe the void fraction as a function of these parameters, particulate, dispersed flow is assumed, choosing a uniform slip velocity between particle and gas.

With this assumption, the one-dimensional slip velocity can be found through a continuity equation:

(5) $Usl = Ug/E - Us/(1-E)$;

with: E = crosssectional mean void fraction
Us = superficial solid velocity for the theoretical value for E = 0.0
Ug = superficial gas velocity (E = 1.0)
Usl = slip velocity between gas and solid particle

Rearranging this equation, the void fraction Etop in the top dilute region of the fast bed is given for a given set

of Us and Ug:

(6) Etop = 1/2*Usl * ((Ug+Us+Usl)-SQRT((Ug+Us+Usl)**2 - 4*Usl*Ug)) ;

Experimental and calculated results are compared in Figure 39, wherein the slip velocity is set equal to the free fall velocity of the mean particle. The graph shows that all calculated values are higher than the theory would predict, with most calculated points ca. 0.8% higher than the identity line. This result could be caused by different factors: at first, the flow in the column is not undisturbed, as is assumed for the use of the free fall velocity as a slip velocity. Second, the existence of particle aggregates cannot be neglected which would result in a much higher slip velocity. Matsen (1982) proposed for such a dilute 2-phase gas-solid flow an empirical correlation that would predict a much higher slip velocity:

(7) Usl = 10.8 * Ut * (1 - E)**0.239

The results are presented in Figure 40. The plot resembles very much the one shown in Figure 39. The data points are closer to the identity line for this case, but most of the calculated points still lie ca. 0.8% above the identity line. It should be noted that the equation given results for void fractions between 0.95 to 0.99 in values of ca. 3 - 5 times the free fall velocity of the mean particle. The apparent slip velocity even in this dilute

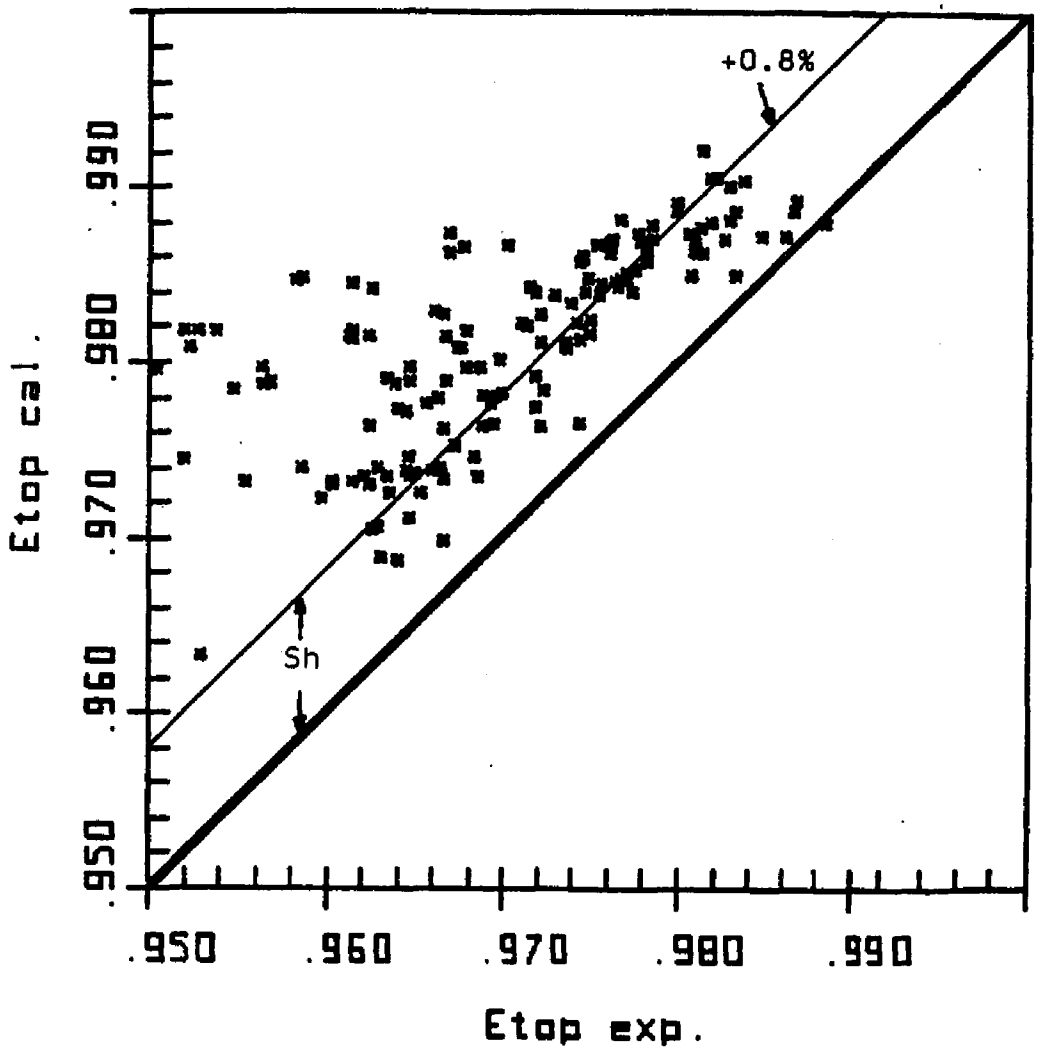

Fig. 39 Mean void fraction in the top dilute region of at fast fluidization, experimental data compared with calculated data (eq. (6))

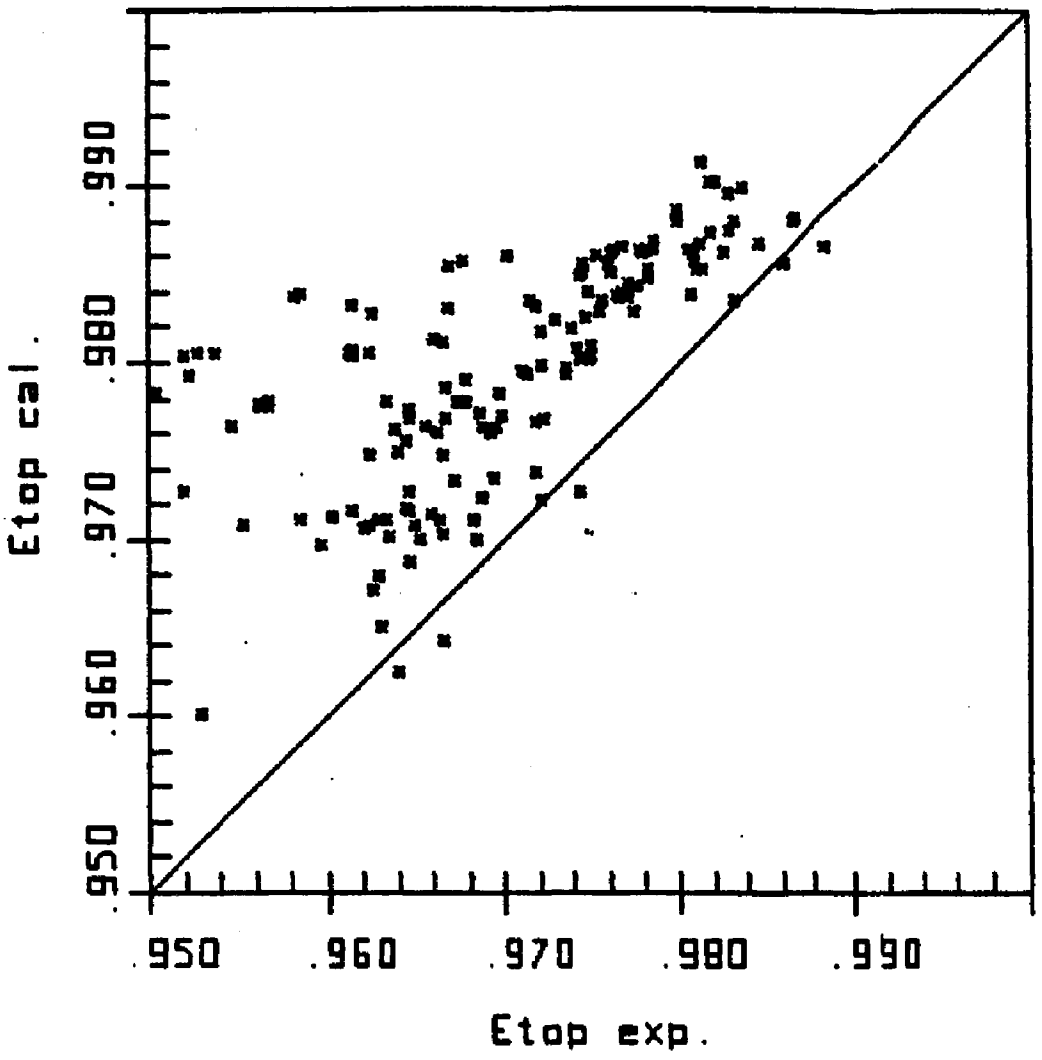

Fig. 40 Mean void fraction in the top dilute region of at fast fluidization, experimental data compared with calculated data (eq. (6) and (7))

region is much higher. Applying a particulate flow model that would fit for the experimental data would result in slip velocities that are without any physical meaning.

It can be argued that the data would fit a modified particulate flow model if one would agree that additional solid is kept within the column in a form of a relatively stagnant wall zone. With this consideration an additional solid hold-up of ca. 0.8% volume fraction in the column would rectify the fit of at least most of the data. With this the exact value for the slip velocity chosen (Figure 39) would not be so critical. This would result in the following equation:

(8) Etop = 1/2*Usl * ((Ug+Us+Usl)-SQRT((Ug+Us+Usl)**2 - 4*Usl*Ug)) - Sh ;

with: Sh = volume fraction of additional solid holdup

Such an assumption is not made without considering the results of the radial solid concentration as measured by Weinstein et al.(1984,1985) and Hartge et al.(1985). Both depict additional solid near the wall of the fluidizing column even in the very dilute flow in the top region of the bed. Figure 41 shows such a radial profile in the top region of a fluidized bed as measured by Shao(1986) for the same solid and in the identical equipment used in the present investigation. With this in mind, one must clearly take such an additional solid hold-up into consideration.

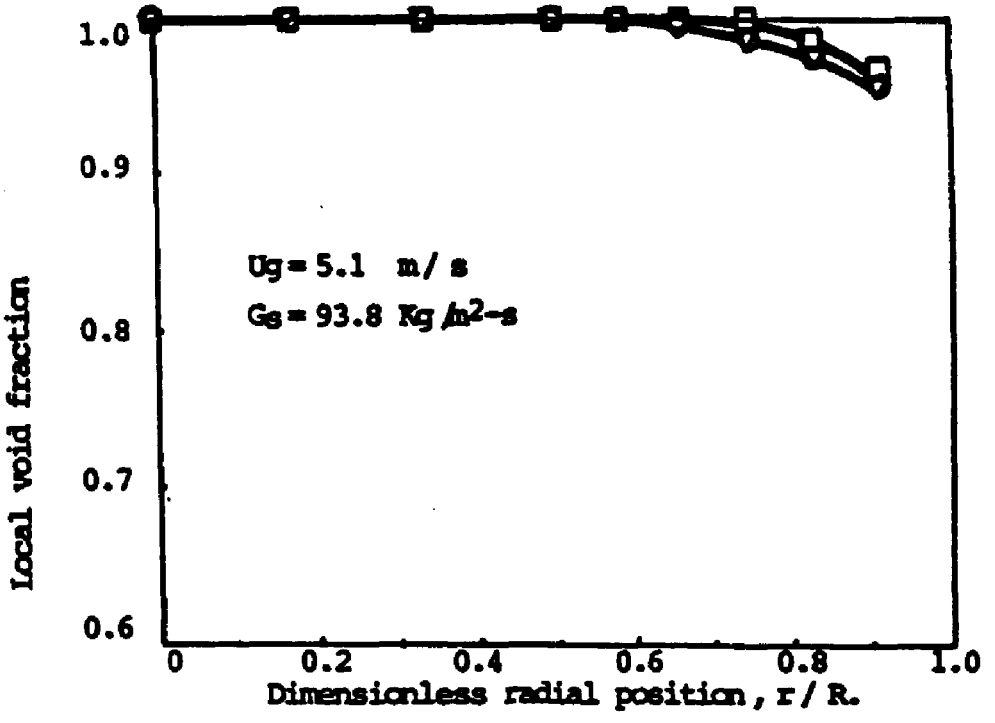

Fig. 41 Radial voidage distribution in the dilute top region of a fast fluidized bed (Shao, 1986)

How much solid in fact is accumulated near the wall will obviously vary with flow conditions. Hence, it is not surprising, that the deviations from equation (8) are evident. However, a limit to a minimum solid hold-up seems to exist which for the data presented is around 0.5%. Further conclusions will only be possible with accurate results of the radial solid distribution and radial profile of the gas velocity.

In addition an empirical correlation proposed by Kwauk (1985), which does not take the above mentioned effect into account, was checked with these experimental data for the purpose of completeness. The correlation is defined as follows:

(9) $$1 - Etop = 0.05547 * ((18*REs + + 2.7 * REs**1.687)/AR)**(-0.6222)$$

with:

(10) $$REs = dp*rof/mu * (Ug - Us (Etop/(1-Etop))$$

(11) $$AR = dp**3*rof*g*(ros-rof)/mu**2$$

and: ros = density of solid,
rof = density of gas,
mu = kin. viscosity of gas,
dp = mean particle size,
g = gravity

Figure 42 shows the results of such a comparison. The

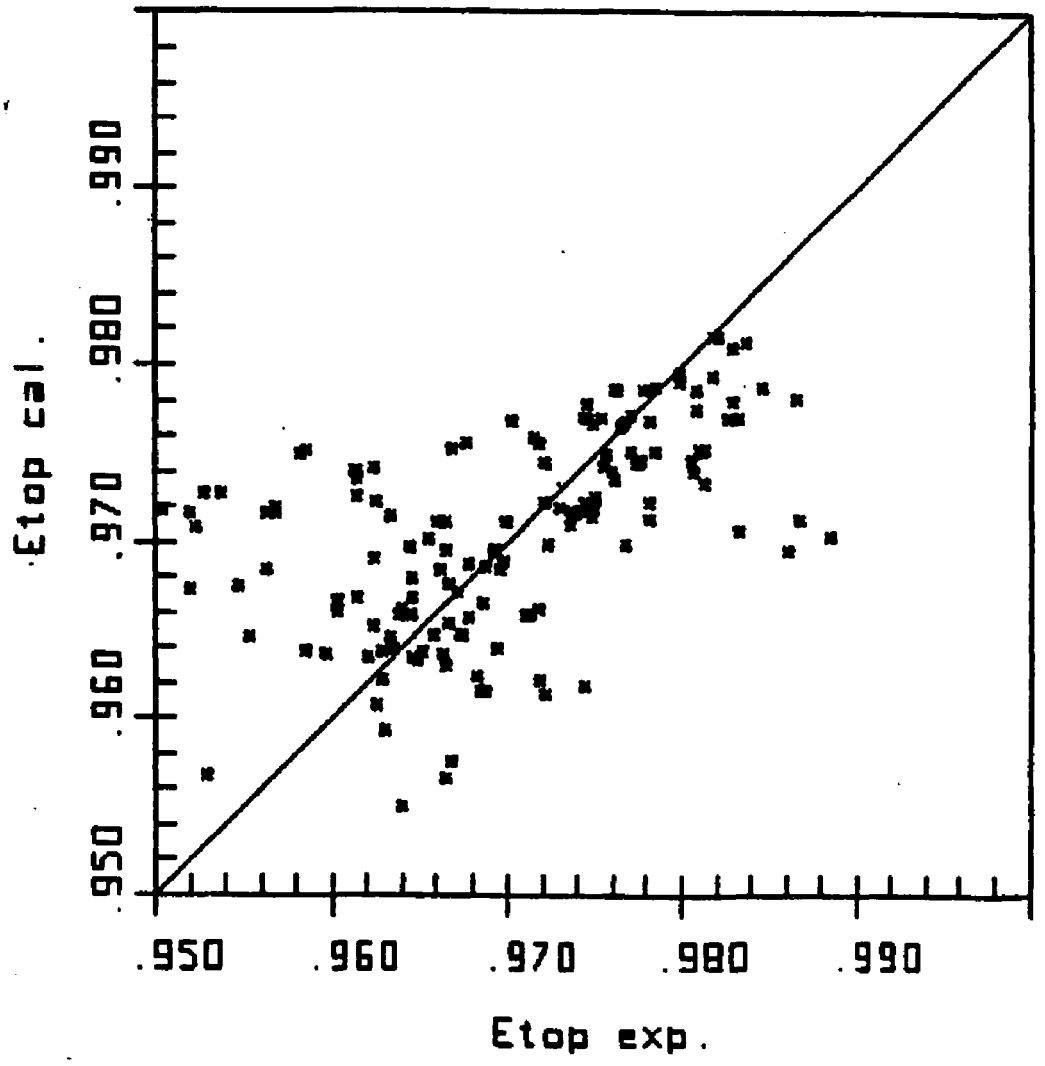

Fig. 42 Mean void fraction in the top dilute region of at fast fluidization, experimental data compared with calculated data from model by Kwauk et al. (eq. (9) - (11))

data are grouped quite arbitrarily around the identity line, but the correlation gives a good estimate considering the empirical character of the equations. On the other hand, one should consider that the correlation is not based on a physical picture of the flow in the top region of the fast fluidized bed. Also, this correlation is for data taken in column of approximately the same diameter so that any effects of column diameter on the magnitude of the additional wall region hold-up is not evident.

4.2 VARIATIONS OF THE BED HEIGHT IN A FAST FLUIDIZED BED

In 1983 Weinstein et al. made known the importance of the properties of the downcomer in a fast fluidized bed unit on the solid hold-up in the fast bed. There the main concern was the total solid inventory. Since it was found earlier in this work that a fast fluidized bed consists mainly of two distinct regions with constant mean void fractions, it seems reasonable to introduce an additional parameter describing the solid hold-up in the bed. This parameter has already been defined above. In analogy to the bubbling fluidized bed, it is the 'bed height' of a fast fluidized bed referred to the height of the fluidization column, at which the void fraction profile decays sharply. More precisely, this is where the average between the two void fractions in top and bottom parts is reached. Knowing the three variables, Etop, Ebot and the bed height the solid

hold-up is sufficiently well defined.

Weinstein et al.(1983), Kwauk(1985), Rhodes and Geldart(1986) concluded for the solid hold-up that it will be set by the conditions in the recirculation leg. More precisely said, the solid hold-up in the fast fluidized bed will increase until the pressure balance between downcomer and fast bed is achieved. Kwauk and Rhodes and Geldart used such a pressure balance in connection with the assumption that the entire downcomer operates in the bubbling regime and therefore has a constant pressure drop per unit length. Such a pressure balance obviously exists, assuming that the downcomer indeed is in fully fluidized conditions and solid velocities in the standpipe are resonably small so as not to effect the pressure drop in the standpipe significantly.

In the following the gauge pressures in the fluidization system are represented for different positions parallel to the corresponding void fraction profiles in the fast fluidized section (Figures 43-48). For the reader, these positions will be explained in detail and should be compared when necessary with the scheme of the equipment shown in Figure 12:

Label A: The lowest point in the system, bottom of U-bend

Label B: Position just below the control valve for solid rate

Label C: Position just above the control valve

Label D: Position just above the distributor plate in the

storage bed

Label E: Position within the storage bed - in most cases above the fluid bed surface

Label F: Position at the top of the bed, whereat lower pressure corresponds to the downcomer, higher value to the fast bed column; the difference is the the sum of the pressure drops in the exit section of the bed and the primary cyclone

The connection between Level F and Level A finally represents the pressure drop across the entire fast bed.

In Figure 43 are shown the system pressure balance for superficial gas velocities of 1.0, 2.0 and 3.0 m/s with the system operating with an unrestricted standpipe (control valve fully open). It shows that the solid in the downcomer is in fact fluidized as seen on the constant slope over the entire solid holding leg. If however, the gas velocities are increased and with this the solid recirculation rates, the picture becomes quite different (Figure 44). In particular the pressure in the lowest section between Levels A and B reverses leaving the highest pressure at a position just below the solid control valve. This is obviously a result of acceleration effects that are evident already at the gas inlet which is located near Level A. On the other hand, the pressure drop in the exit section of the bed - the difference between the two pressures at Level F increases to

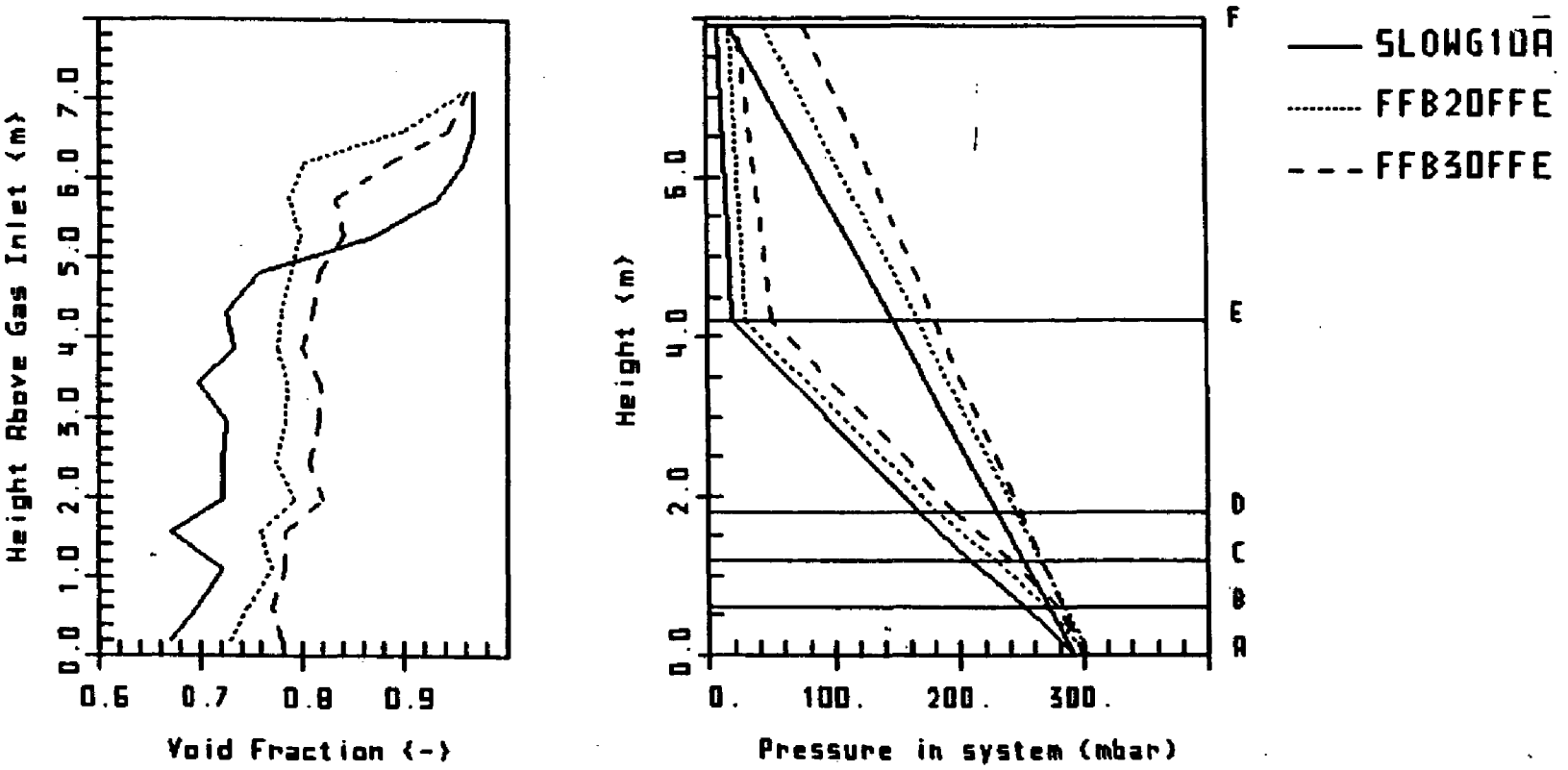

Fig. 43 Void fraction profile and pressure distribution in system, solid control valve fully open,
data points connected by straight lines
(SLOWG10A, Ug = 1.0 m/s)
(FFB20FFE, Ug = 2.0 m/s)
(FFB30FFE, Ug = 3.0 m/s)

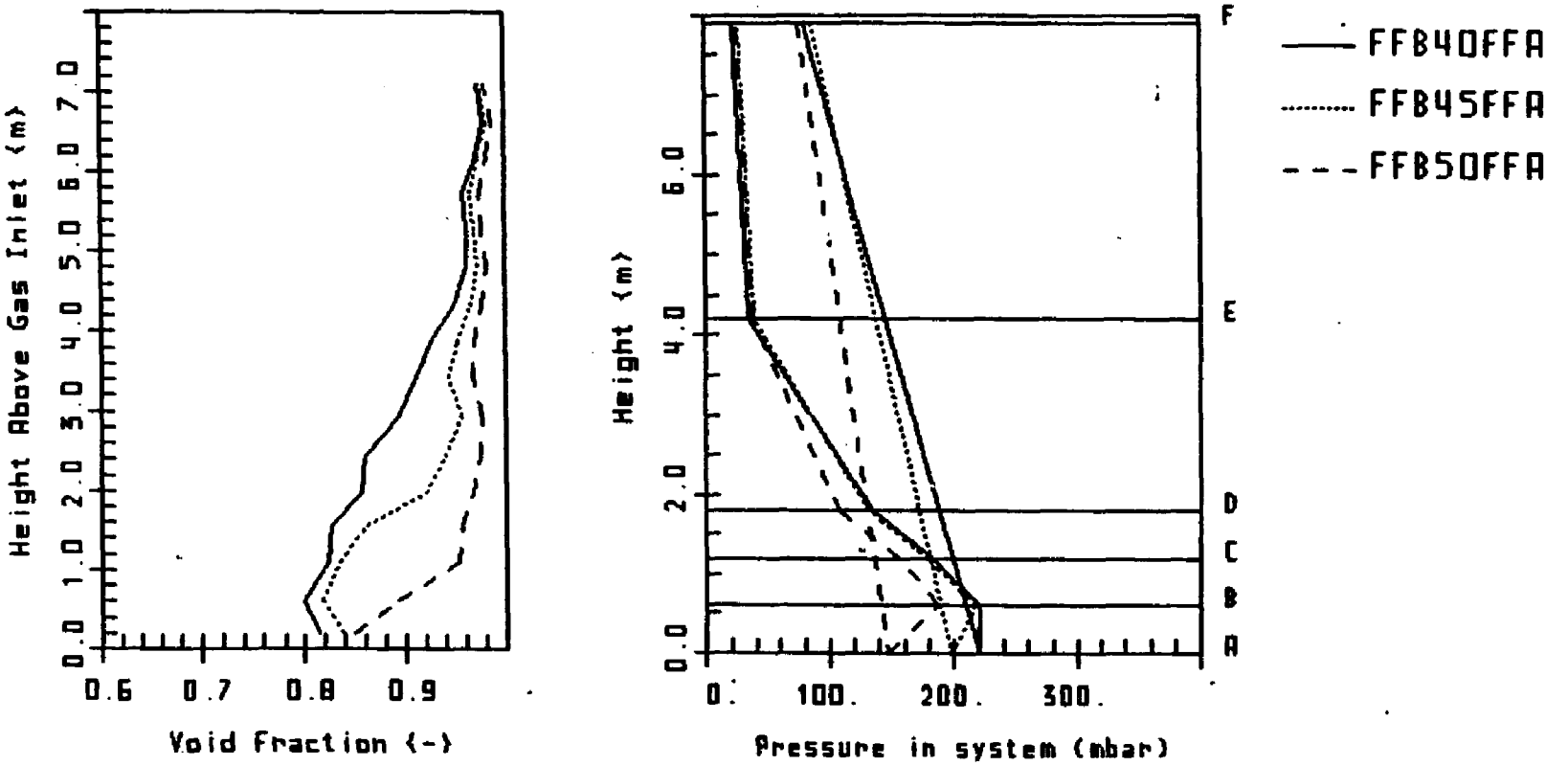

Fig. 44 Void fraction profile and pressure distribution in system, solid control valve fully open,
data points connected by straight lines
(FFB40FFA, Ug = 4.0 m/s)
(FFB45FFA, Ug = 4.5 m/s)
(FFB50FFA, Ug = 5.0 m/s)

a large value. Both effects subtract from the total pressure drop for the remaining pressure drop over the fast bed column and clearly increase with gas velocity. Therefore it is understood, that the bed height in the fast bed will under certain conditions reach zero not because of certain flow conditions, but only because of equipment related constraints.

This is important to mention, since over the last decade a number of generalized fluidization diagrams have been presented that include a so-called transport velocity, at which no fast fluidization phenomena can be obtained (Avidan, 1980, Li et al., 1982). In other words, the mean void fraction over the total bed is equal to the one in a pneumatic transport line. With the use of the above mentioned results, this simply means that the bed height reaches zero height and the entire bed consists only of the top region with void fractions comparable to those of dilute phase pneumatic transport. Considering the constraints given by each individual experimental set-up, such a transport velocity might in certain cases only represent the velocity at which the sum of the pressure drop in the exit of the fast bed and the pressure drop across the gas inlet section begins to balance the solid head in the downcomer.

A completely different condition is given when the solid circulation is controlled by the butterfly valve located in the standpipe (Figures 45 - 48). Due to an additional

pressure drop across the control valve, the maximum pressure in the system is now located just above the valve (Level C). In such a case, the theory does not hold anymore that the solid hold-up in the fast bed is determined by the pressure drop in the downcomer. Certainly, the overall pressure drop on both sides of the system is equal, but the solid hold-up no longer increases in the fast bed until the maximum possible pressure drop of the downcomer, the case where the downcomer is completely fluidized, is reached. The part below the solid control valve remains in all cases observed practically free of solid, leaving both pressures at Level B and A equal.

In Figure 45 the results are presented for superficial gas velocities in the fast bed at 2.0, 2.5 and 3.0 m/s, with the solid rate, the total solid inventory and the nozzle configuration at the entrance kept constant. The bed height obviously decreases dramatically over such a small range in gas velocities. Looking at the system pressures, one can see that the pressure drop over the Level B to C changes dramatically. Wheras at 2.0 m/s the maximum pressure still lies below the solid control valve, this is no more true for higher gas velocities.

Similar results are obtained, if the solid rate is changed from 90 to 110 and 130 kg/m2s with all other parameters again kept constant (Figure 46). The bed height increases with increasing solid rate and the system adapts

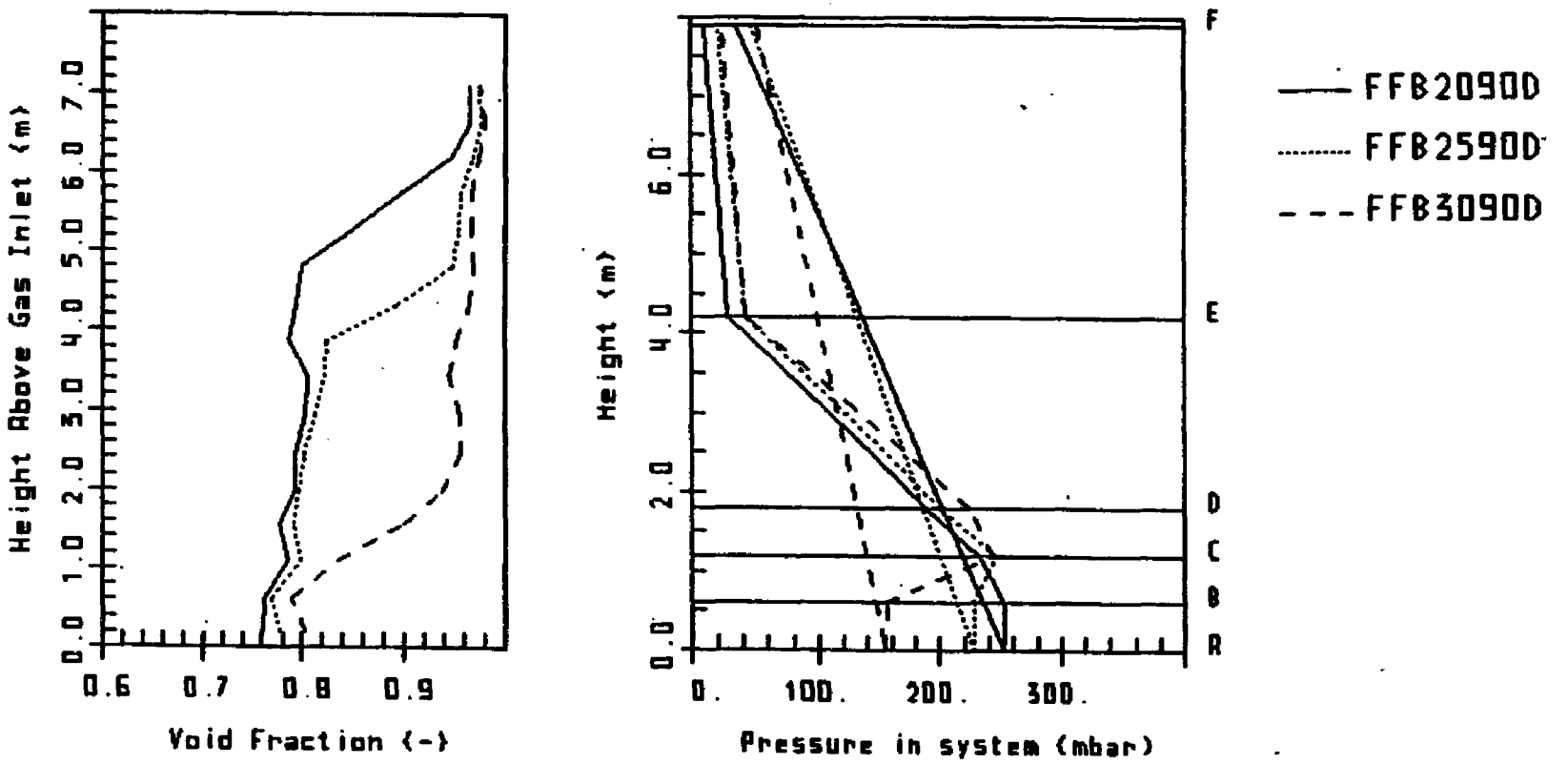

Fig. 45 Void fraction profile and pressure distribution in system for varying gas velocities, data points connected by straight lines (FFB2090D, Ug = 2.0 m/s, Gs = 94 kg/m2s) (FFB2590D, Ug = 2.5 m/s, Gs = 93 kg/m2s) (FFB3090D, Ug = 3.0 m/s, Gs = 89 kg/m2s)

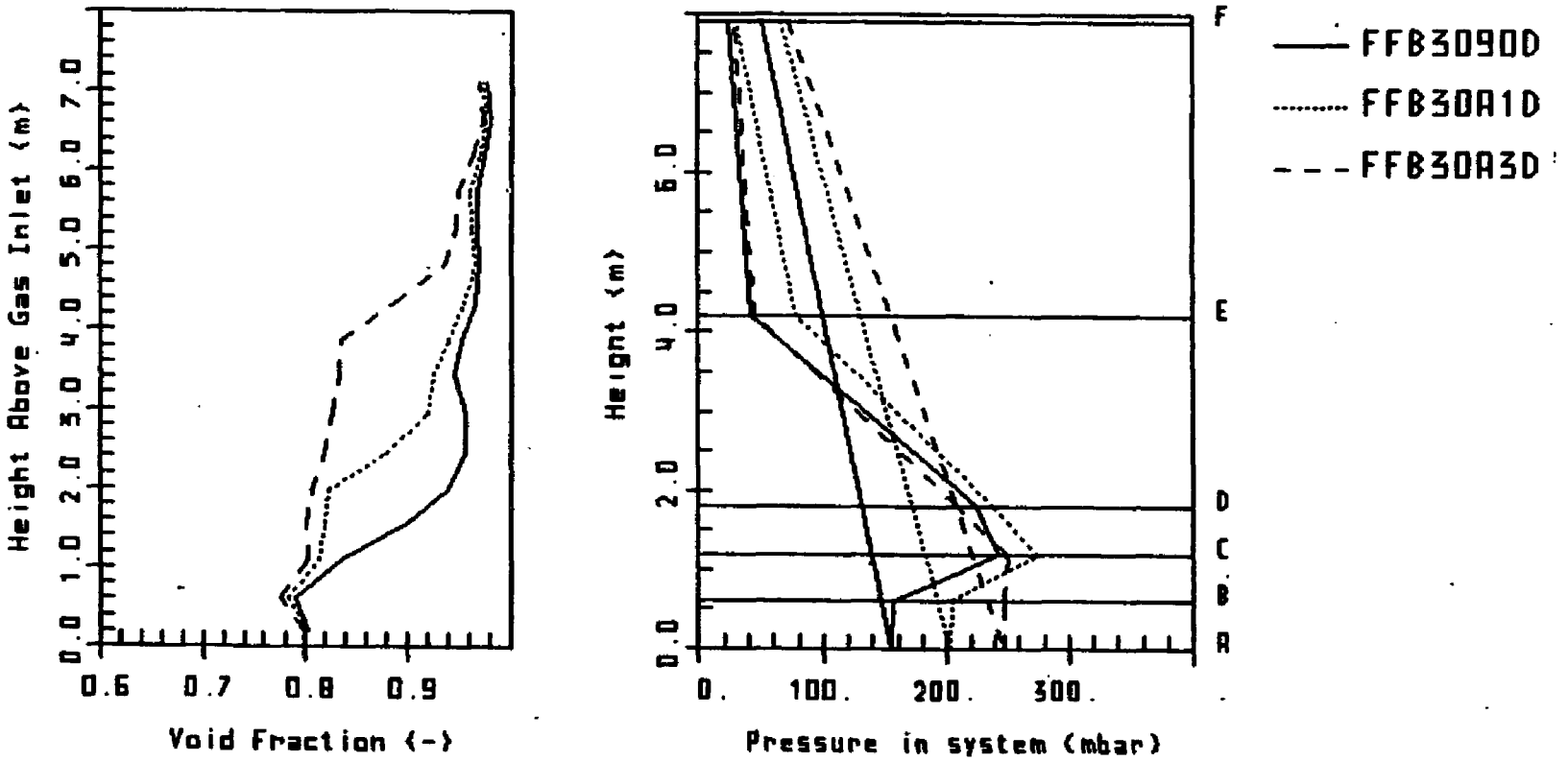

Fig. 46 Void fraction profile and pressure distribution in system for varying solid rates, data points connected by straight lines
(FFB3090D, Ug = 3.0 m/s, Gs = 89 kg/m2s)
(FFB30A1D, Ug = 3.0 m/s, Gs = 113 kg/m2s)
(FFB30A3D, Ug = 3.0 m/s, Gs = 133 kg/m2s)

once again to the pressure balance by ajusting the pressure over the solid valve. In both cases presented, the pressures at Levels A and B are almost identical, which means that solid is falling in free fall from the control valve to the U-bend section. Under these conditions it can be assumed that the conditions at the entrance of the bed are more or less independent of the pressure profile in the downcomer.

With this in mind, it is interesting to determine whether or not the bed height could be influenced by simply changing the nozzle arrangement for the air inlet at the bottom of the fast fluidized bed. Gas velocity and solid rate were kept constant and the incoming air partly introduced at the pair of nozzles positioned upstream (N3). The results for 0%, 20% and 40% air introduced at nozzle N3 (Figure 12) are given in Figure 47. The solid hold-up first decreases at the 20% split and then increases clearly at 40%. For the system pressures this means that the pressure drop changes between Levels B and C.

From this it is suggested that the very conditions at the air inlet also influence the bed height, unless the bed height is restricted by a maximum pressure drop across the downcomer. These conditions, however, are hard to quantify. This is in particular shown in Figure 48 where the only parameter varied is the total solid hold-up in the system. One would expect that when using a restricted standpipe such

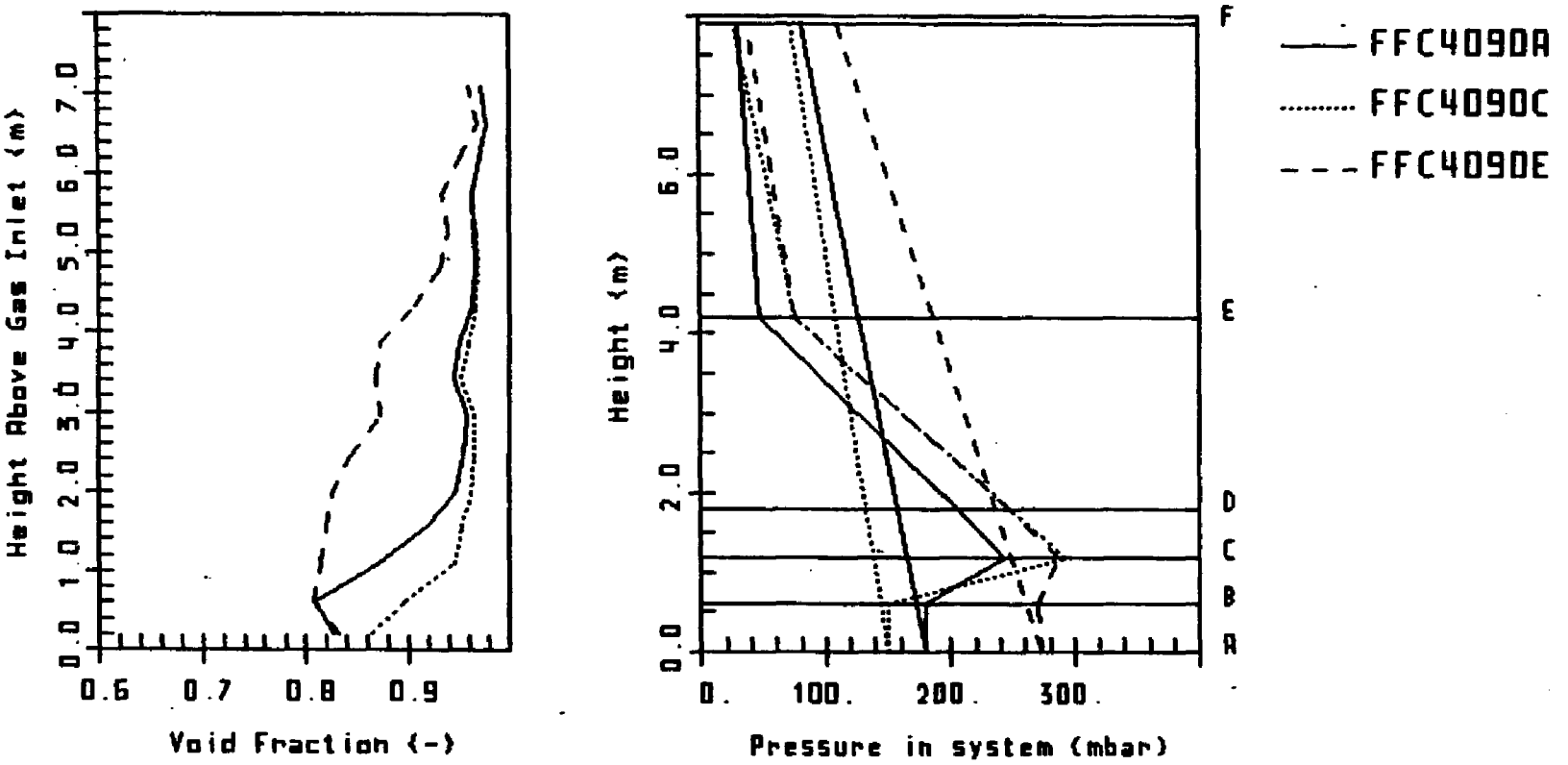

Fig. 47 Void fraction profile and pressure distribution in system for varying entrance conditions, data points connected by straight lines (Ug = ca. 4.0 m/s, Gs = ca. 90 kg/m2s) (FFC4090A, 0% of air at nozzle N3) (FFC4090C, 20% of air at nozzle N3) (FFC4090E, 40% of air at nozzle N3)

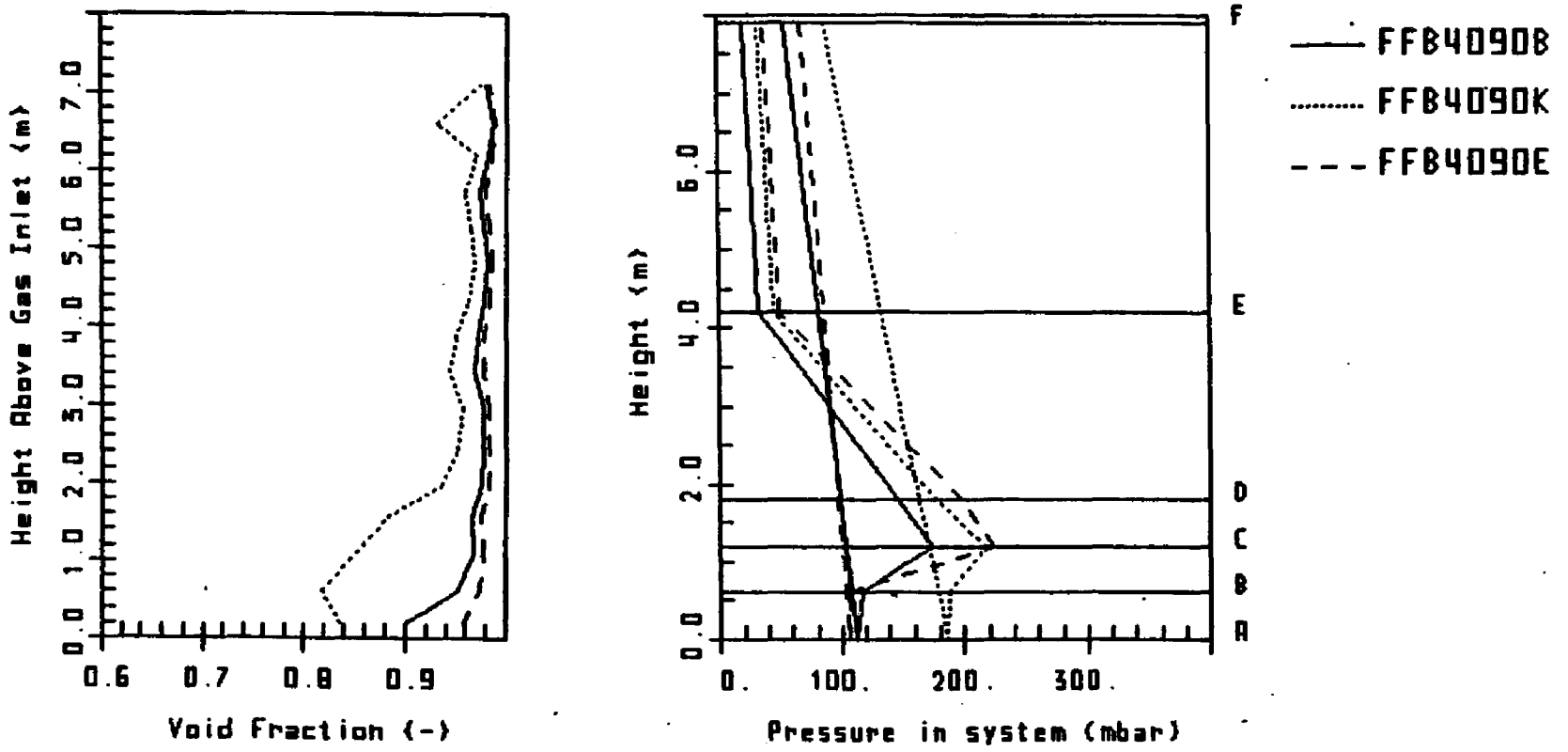

Fig. 48 Void fraction profile and pressure distribution in system for varying solid inventory in system, data points connected by straight lines
(Ug = ca. 4.0 m/s, Gs = ca. 90 kg/m2s)
(FFC4090B, 70 in. of solid in storage)
(FFC4090K, 90 in. of solid in storage)
(FFC4090E, 115 in. of solid in storage)

a change in conditions would not effect the void fraction profile. Nevertheless, the total solid inventory in the system clearly affects the flow in the fast bed, but no clear dependence of the inflection point on the solid inventory can be observed. The highest inflection point is obtained at a medium value for the solid inventory. No clear conlusions on this effect can be drawn. It might be possible that the ability of the recirculation leg to respond to the inherent pressure fluctuations in the system will also determine the total solid hold-up.

It becomes clear that the bed height is not unique for a given set of the flow parameters, gas velocity and solid rate, and can be ajusted within certain limits by changing the flow conditions at the entrance of the fast bed. Such a procedure could be helpful in controlling fast fluidized bed reactors.

4.3 FFT ANAYSIS OF PRESSURE SIGNALS IN THE FAST FLUIDIZED BED

In Chapter 4.1 it was shown that strong asymmetric pressure fluctuations are one dominant characteristic of the 2-phase flow in the dense section of the fast fluidized bed. Therefore the pressure signals of both gauge pressures and differential pressures, predominantly in the dense region of the bed, were analyzed by a Fourier transform algorithm to determine the power spectrum, auto- and cross-correlation

functions.

4.3.1 PREDOMINANT FREQUENCIES OF PRESSURE SIGNALS

In Figure 49 typical power spectra for gauge pressure signals are presented. In these cases a fluid bed at 4.0 m/s superficial gas velocity was chosen with varying solid rate (110, 130 and 190 kg/m2s). The bottom plot represents - in contrast to the others - a condition with non-restricted standpipe.

Unfortunately the power spectra deliver only vague information about predominant frequencies. This is patrially a result of the nature of the FFT analysis, which results in clearly defined peaks in the power spectra, only if the oscillations are clearly periodic. This is not necessarily the case for the pressure signals of a fast fluidized bed. Also, one has to realize that fluctuations, whether periodic or not are evident throughout the system. They clearly influence the overall pressure reading, i.e. the gauge pressures, at different positions in the bed from where they originated. The gauge pressure signals are therefore an overlay of a number of fluctuations - whether they occur in the fast bed side or in the downcomer.

Figure 50 tries to clarify such a statement. Four auto-correlation functions are presented, which result from gauge pressure signals at:

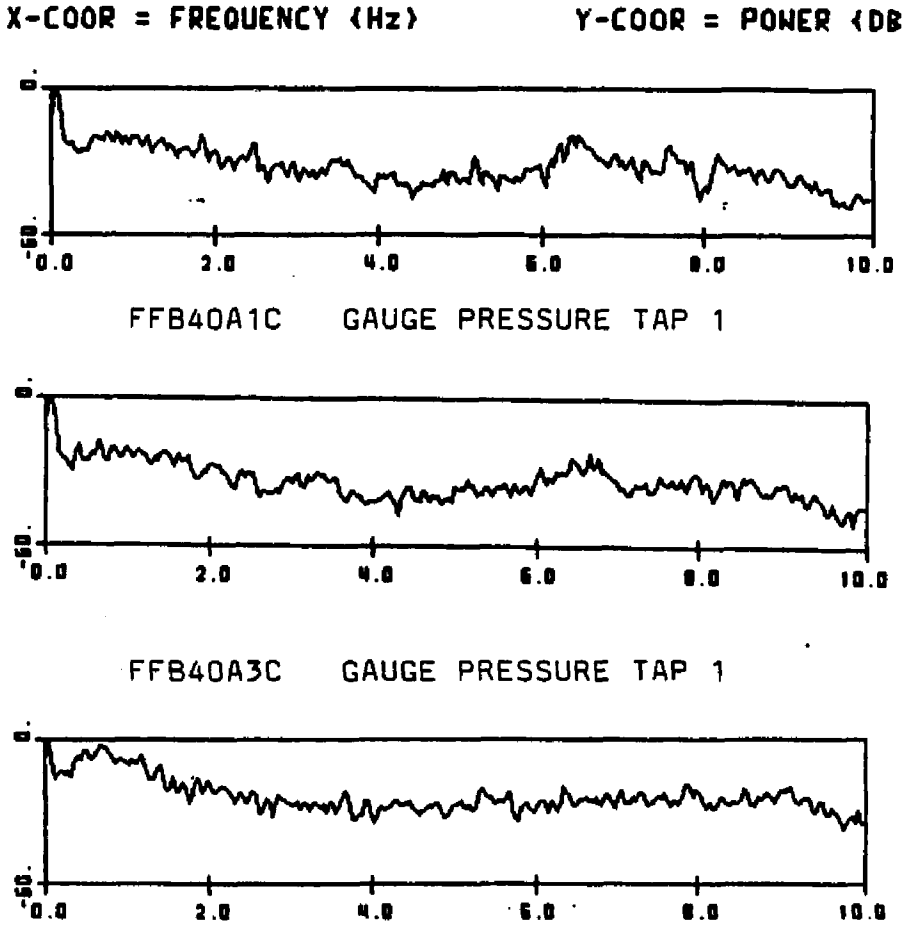

Fig. 49 Power spectra of gauge pressure signals in a fast fluidized bed at pressure tap 1
(FFB40A1C, Ug = 4.0 m/s, Gs = 110 kg/m2s)
(FFB40A3C, Ug = 4.0 m/s, Gs = 130 kg/m2s)
(FFC40FFE, Ug = 4.0 m/s, Gs = 190 kg/m2s)

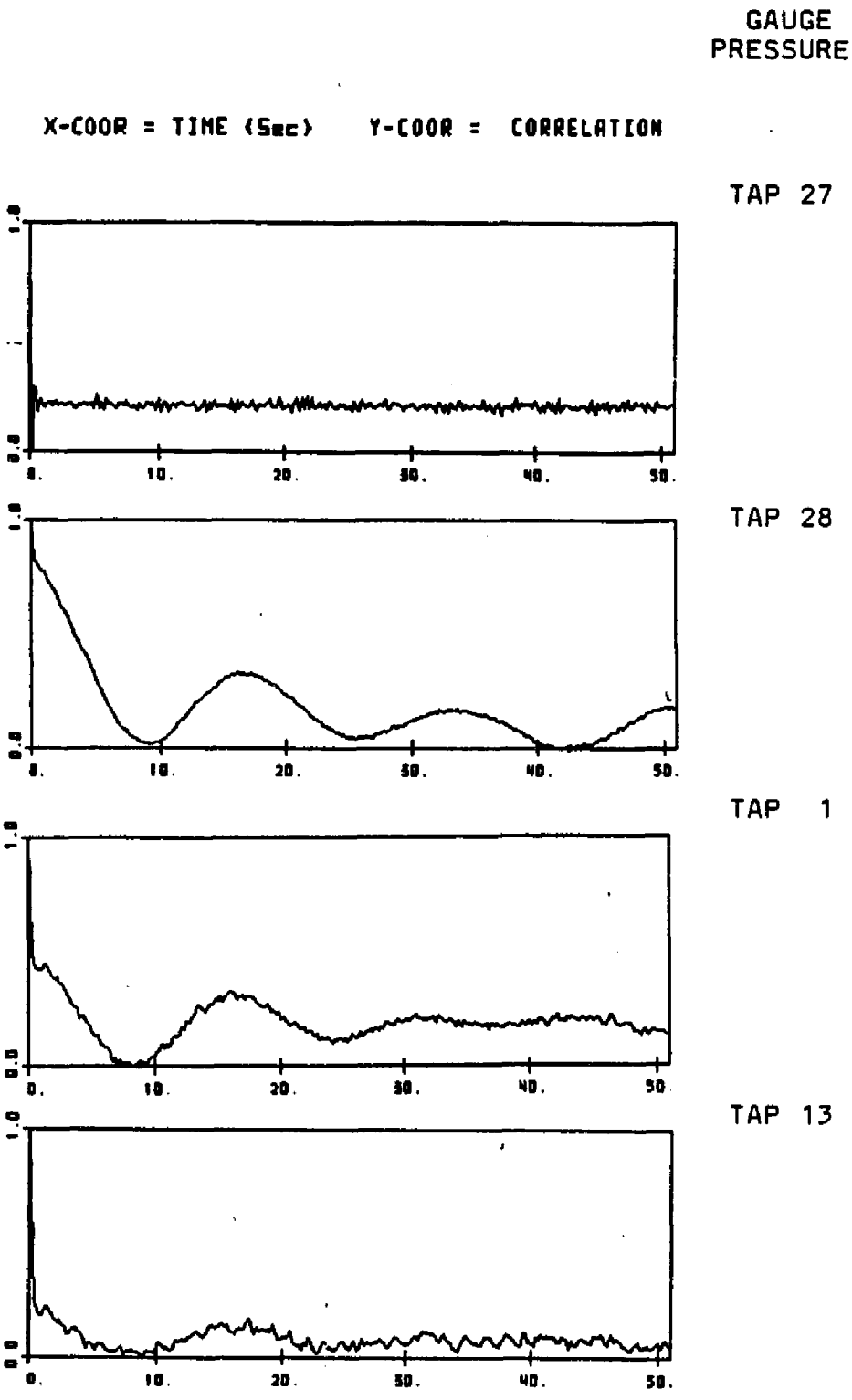

Fig. 50 Auto correlation functions of gauge pressure signals at different location within the system (FFB35FFD, Ug = 3.5 m/s, Gs = 143 kg/m2s)

1) position just below the solid control valve (Tap 27)

2) position at the air inlet (Tap 28)

3) position just above the air inlet (Tap 1)

4) position in the top dilute region (Tap 13)

A gas velocity of 3.5 m/s was used and the solid control valve was fully open, resulting in a solid rate of ca. 140 kg/m2s. The graphs depict in a very clear way a pressure fluctuation originating at the air inlet and being transmitted upward to the top of the bed. On the other hand, the oscillation is obviously damped out in the first correlation function presented, a result of the large solid hold-up in the standpipe. The frequency, taken from the wave length of the auto correlation function, can be estimated to be ca. 0.06 Hz. A clearly periodic signal as such is only evident under very certain conditions Nevertheless, this example shows how fluctuations can be transmitted throughout the bed and that very low frequencies in the pressure signals are possible.

The influence of fluctuations originating at positions outside a certain measurement volume can be eliminated by measuring the differential pressure between two pressure taps at different positions in the fast bed. Since the main purpose is to determine predominant frequencies that are characteristic to the flow, such an approach will indeed determine only frequencies that originate from the flow between the pressure taps.

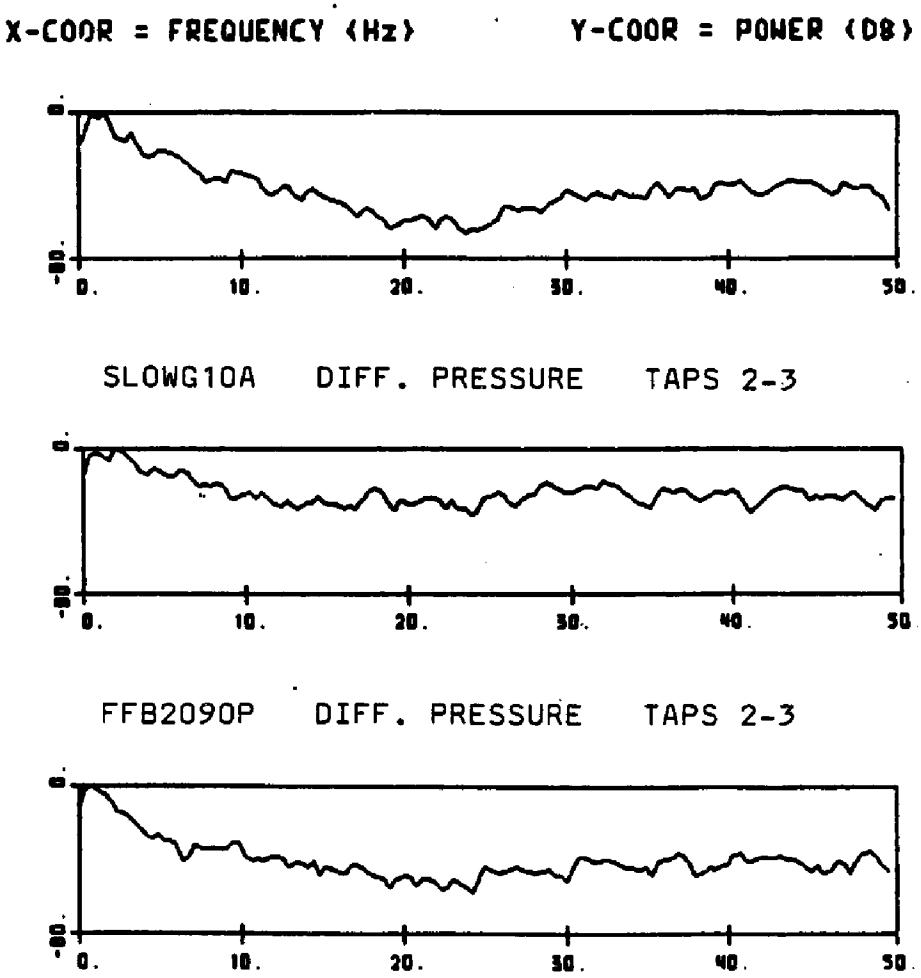

Fig. 51 Power spectra of differential pressure signals in a fast fluidized bed at pressure between taps 2 and 3
(SLOWG10A, Ug = 1.0 m/s, Gs = 0 kg/m2s)
(FFB2090P, Ug = 2.0 m/s, Gs = 88 kg/m2s)
(FFC4090P, Ug = 4.0 m/s, Gs = 93 kg/m2s)

In Figure 51 three power spectra are given that were taken over the identical differential height in the fast bed for three different gas velocities. The top plot corresponds to a turbulent fluidized bed with 1.0 m/s gas velocity. The remaining two plots are for 2.0 and 4.0 m/s gas velocity, resp.. In the latter two cases the solid recirculation is held constant at 90 kg/m2s. In all three cases the predominant frequencies lie in the range between 0.25 and 2.0 Hz. This is true for all runs made. The value range - even if further data are examined - is independent of all flow conditions.

4.3.2 WAVE SPEED IN FAST FLUIDIZED FLOW

It is interesting to examine whether or not the analysis of correlation functions of two pressure signals gives a picture of the structure of the flow in the turbulent and fast fluidized bed in analogy to bubbling and slugging fluidized beds (Sitnai et al., 1982, Wisecarver et al., 1985). Once again the gauge pressure signals proved not to be useful for such analysis, but the result using differential pressure signals are of value.

Figure 52 shows the typical cross correlation functions that were obtained in the dense region of the bed for increasing heights. In this case the superficial gas velocity was 3.0 m/s and a solid rate set to 130 kg/m2s. All plots show a clear maximum around 300 milliseconds.

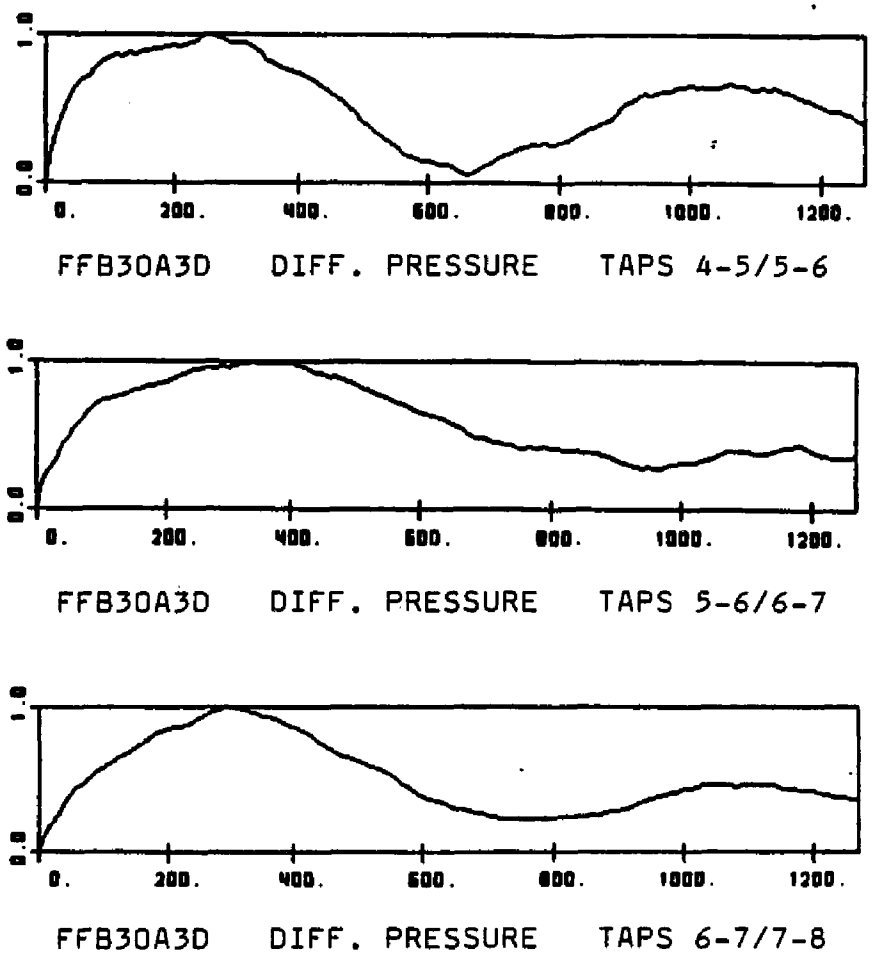

Fig. 52 Cross correlation function of differential pressure signals in a fast fluidized bed at different heights within the dense region (FFB30A3D, Ug = 3.0 m/s, Gs = 133 kg/m2s)

Variations in the localtion of the maximum are mainly due to the varying differential lengths between the pressure taps. The resulting signal speed amounts for all presented cross-correlation functions to ca. 1.5 m/s.

The results for an identical analysis in the dilute top region of the bed are shown in Figure 53. The three correlation functions given are representative for all measurements taken. In this case, they correspond to the same run as Figure 51. The signal delay time, the value at which the cross correlation function exhibits its maximum lies around 50 ms. In some cases this maximum even reaches the zero value. This means obviously that no clear signal delay time can be detected. In this case it is no more appropriate to associate a signal speed to the corresponding maximum of the cross-correlation function.

An interpretation of such a signal speed between two ajacent pressure differentials is given with Figure 54. Suppose an agglomerate of solid is moving upward within the fluid bed, causing an additional pressure drop within the corresponding section. If the next section is reached, the same signal peak is generated in the second differential pressure signal. In this case, one has to assume that the agglomerate still exists as more or less the same entity. With this, a signal delay time corresponding to the speed of the agglomerate will result in a maximum of the cross correlation function. It is questionable as to what form

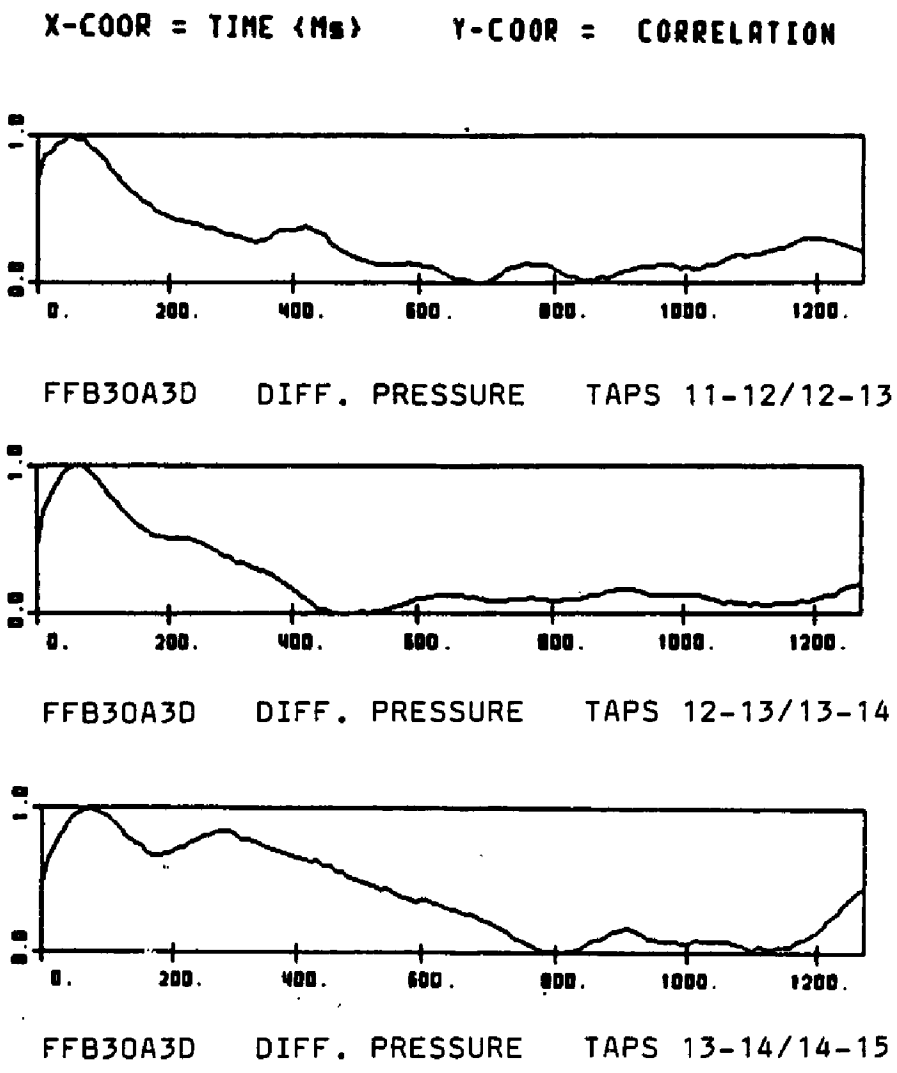

Fig. 53 Cross correlation function of differential pressure signals in a fast fluidized bed at different heights within the dilute region (FFB30A3D, Ug = 3.0 m/s, Gs = 133 kg/m2s)

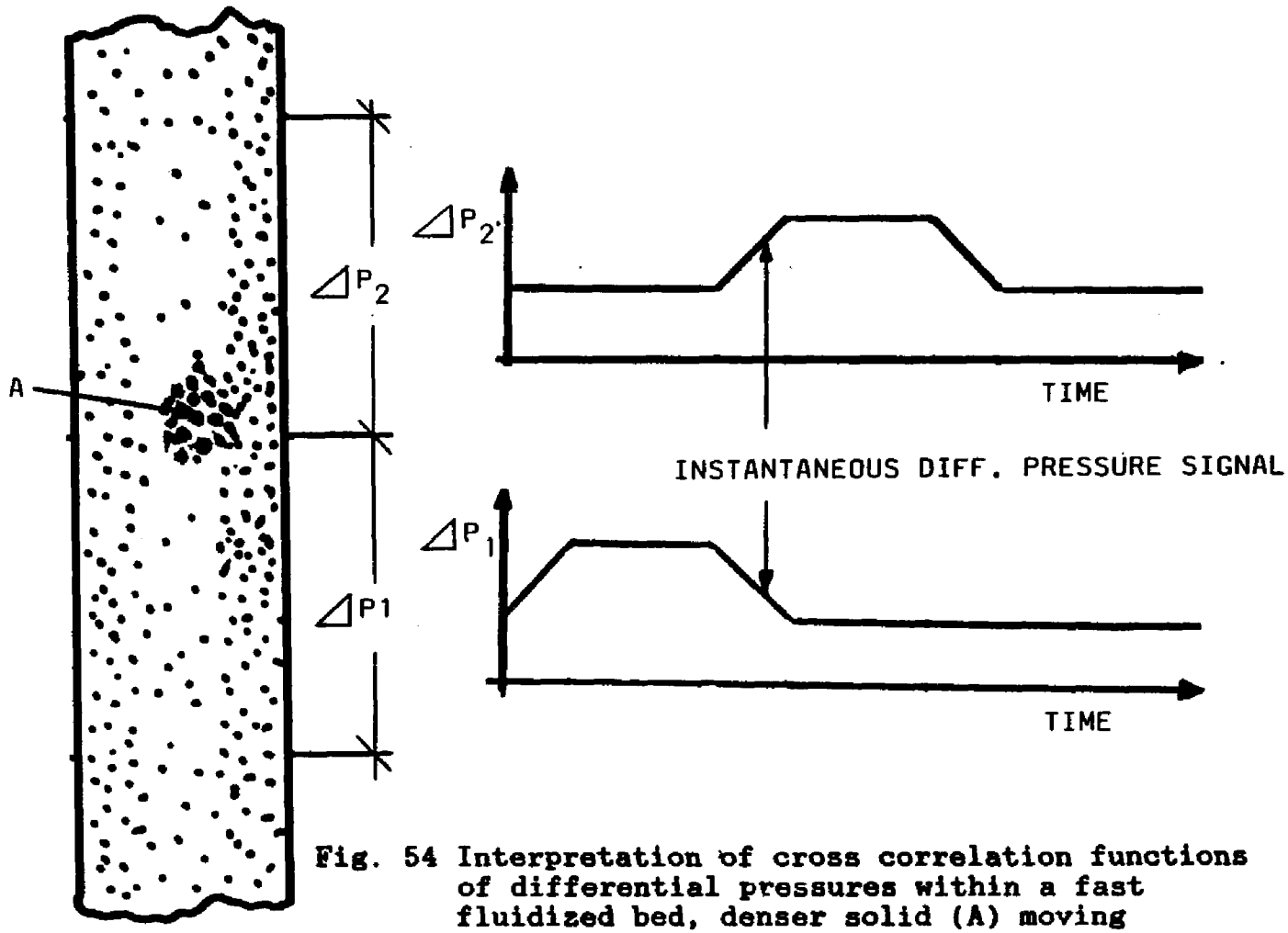

Fig. 54 Interpretation of cross correlation functions of differential pressures within a fast fluidized bed, denser solid (A) moving upward

such additional solid has as it moves upward, but the following results suggests that the form itself seems to be very stable.

Figures 55 - 57 show cross correlation functions obtained in the fast fluidized bed at a gas velocity of 2.0 m/s with unrestricted standpipe (solid rate = 130 kg/m2s). Starting with the first, second and third pressure differential respectively (Figure 55 - 57), the distance between the correlated pressure differentials is increased from ca. 0.45 to 1.5, 2.2 upto ca. 3.2 m. Within deviations of up to 20% the corresponding signal speed that results for all the data is an average of 1.5 m/s. This suggests that at least the majority of disturbances measured are stable throughout the dense region up to the transition region, where it disappears. Since clusters or solid agglomerates would seem not to have such stability, this signal speed is in the following referred to as an internal wave speed in the dense fluid bed.

It is surprising also that the wave speed obtained is not a function of height within the dense region of the bed. Wave speeds for different flow conditions as a function of the height are presented in Figure 58. The two different plots correspond to gas velocities of 2.0 and 3.0 m/s. The bed height as determined from the void fraction profile is indicated by a corresponding vertical line at the bottom of the graph. In both cases the wave speed is practically

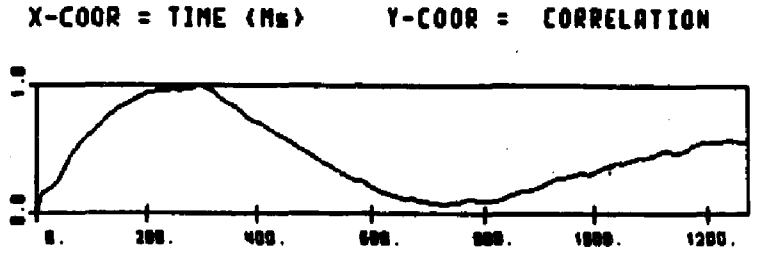

SPC20FFA DIFF. PRESSURE TAPS 1-2/2-3

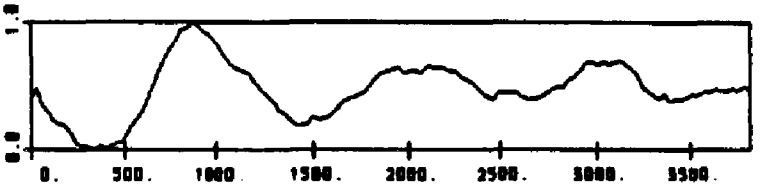

SPC20FFA DIFF. PRESSURE TAPS 1-2/4-5

SPC20FFA DIFF. PRESSURE TAPS 1-2/6-7

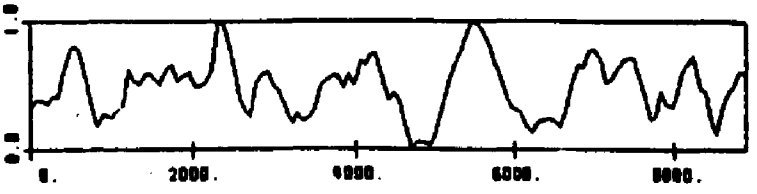

SPC20FFA DIFF. PRESSURE TAPS 1-2/8-9

Fig. 55 Cross correlation function of differential pressure signals in a fast fluidized bed over different heights within the dense region, first pressure differential over taps 1 and 2 (SPC20FFA, Ug = 2.0 m/s, Gs = 108 kg/m2s)

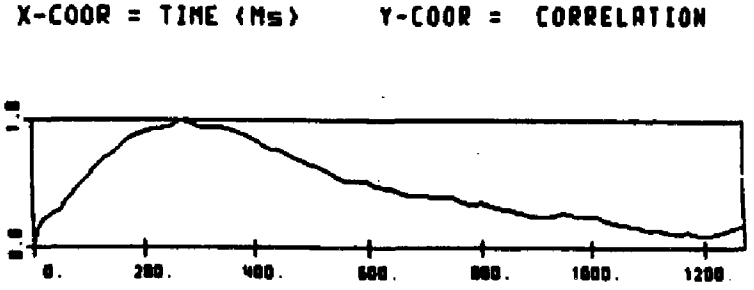

SPC20FFC DIFF. PRESSURE TAPS 2-3/3-4

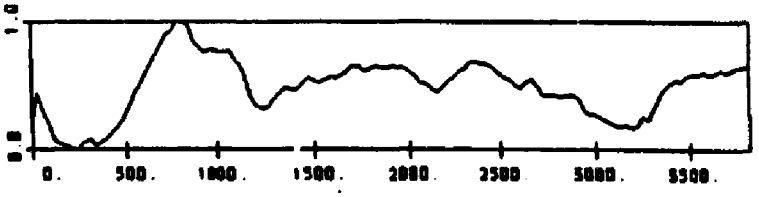

SPC20FFC DIFF. PRESSURE TAPS 2-3/5-6

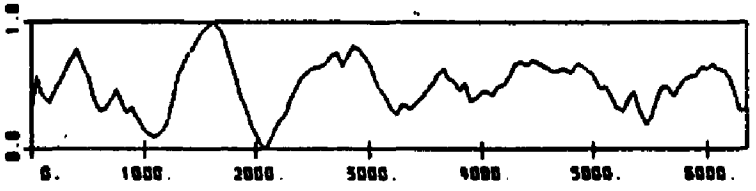

SPC20FFC DIFF. PRESSURE TAPS 2-3/7-8

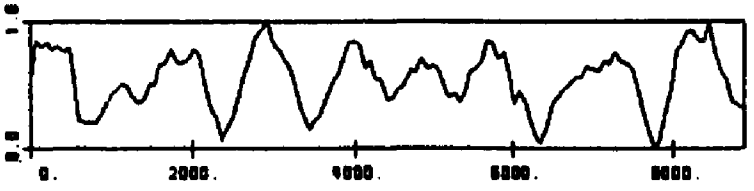

SPC20FFC DIFF. PRESSURE TAPS 2-3/9-10

Fig. 56 Cross correlation function of differential pressure signals in a fast fluidized bed over different heights within the dense region, first pressure differential over taps 2 and 3 (SPC20FFC, Ug = 2.0 m/s, Gs = 131 kg/m2s)

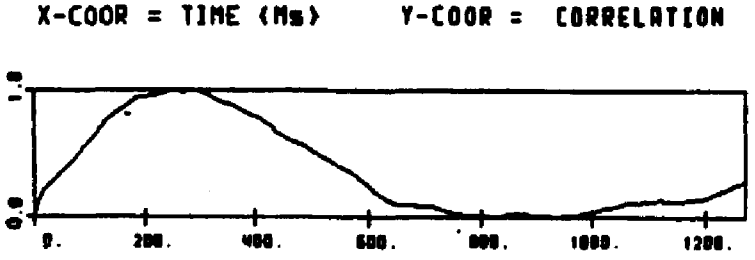

SPC20FFC DIFF. PRESSURE TAPS 3-4/4-5

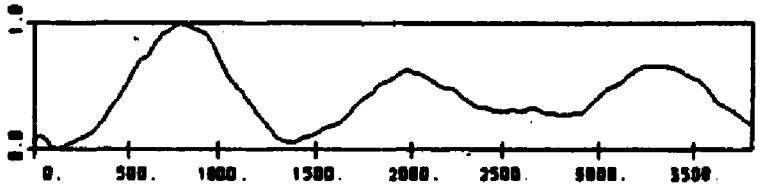

SPC20FFC DIFF. PRESSURE TAPS 3-4/6-7

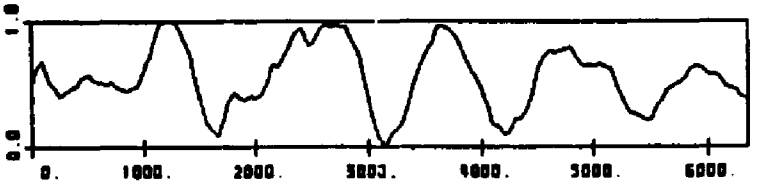

SPC20FFC DIFF. PRESSURE TAPS 3-4/8-9

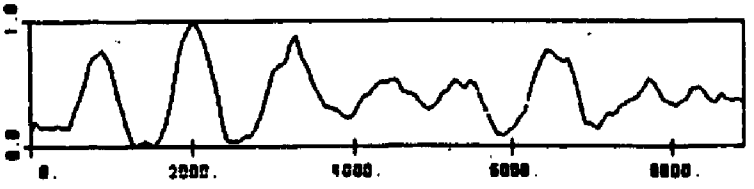

SPC20FFC DIFF. PRESSURE TAPS 3-4/10-11

Fig. 57 Cross correlation function of differential pressure signals in a fast fluidized bed over different heigths within the dense region, first pressure differential over taps 3 and 4 (SPC20FFC, Ug = 2.0 m/s, Gs = 131 kg/m2s)

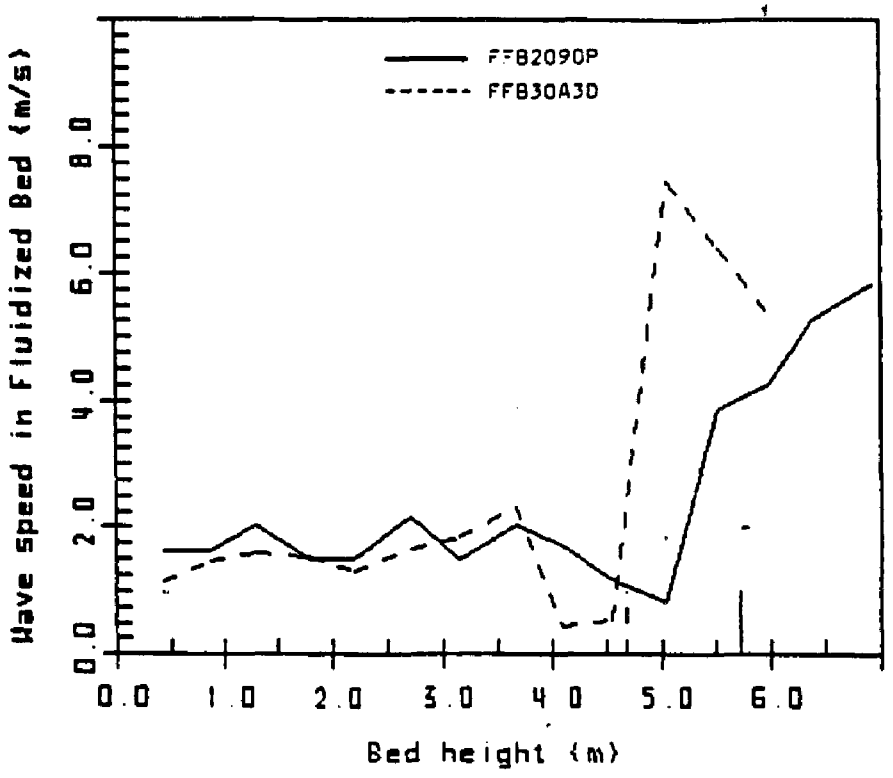

Fig. 58 Wave speed in two fast fluidized beds as a function of height
(FFB2090P, Ug = 2.0 m/s, Gs = 88 kg/m2s)
(FFB30A3D, Ug = 3.0 m/s, Gs = 133 kg/m2s)

constant over the height and clearly changes around the bed surface. As was mentioned, results for the wave speed above this point are without clear meaning. Once again this result also holds over the entire spectrum of gas velocities and solid rates, even in slugging and turbulent fluidized beds.

Since the wave speed does not change over the entire dense region of the bed one can attribute a mean wave speed in the bed to certain flow conditions. This is similar in approach to that taken for the void fractions in top and bottom region. In Figure 59 the resulting mean wave speed for the total number of runs available is presented as a function of the superficial gas velocity. At gas velocities between 0.01 and 0.30 m/s the wave speed corresponds to the mean bubble velocity of the bubbling fluidized bed. Meanwhile, between 0.30 and 0.90 m/s the value represents the speed of the rising slug in the slugging fluidized bed. Turbulent and fast fluidized flow in our equipment exhibit a fairly constant wave speed. Only above 4.0 m/s does the wave speed increase over 2.0 m/s and the data scatter widely.

Also plotted is the slug velocity (Matsen, 1973) which is given through equation (1) in Chapter 3.3. The experimental results in the slugging regime (0.3 m/s < Ug < 1.0 m/s) fit quite well the theoretical line. The values are generally higher than equation (1) would predict. This

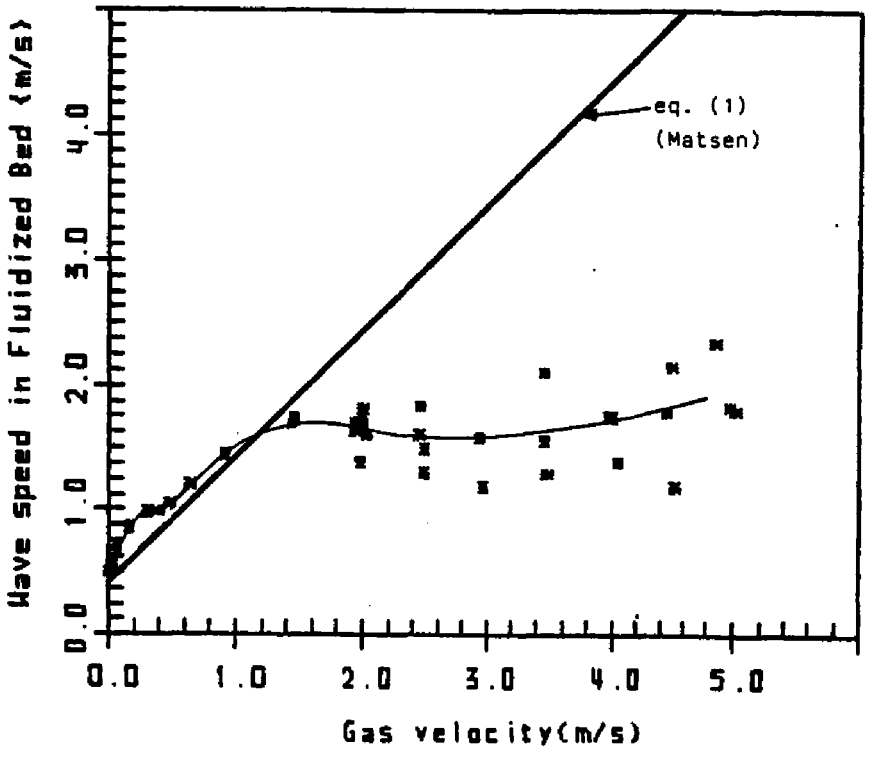

Fig. 59 Wave speed in the dense fluidized regions in various fluidized beds as a function of gas velocitiy, with theoretical slug velocity by Matsen (eq. (1))

is however not surprising, especially since the slugs observed are not necessarily axisymmetric. In cases like this it is suggested to increase the constant by 0.35 in equation (1) which would move the straight line to higher values for the wave speed (Hikita et al., 1983).

Looking more generally at the wave speed as a function of gas velocity it can be seen in Figure 59 that at a certain gas velocity the wave speed in the bed levels off. Within this data set this is at a gas velocity of ca. 1.5 m/s. The fact that such a wave speed exists at all adds to the evidence that the hydrodynamic structure within turbulent and fast fluidized beds has similarities to that in slugging fluidized beds.

Together with results for the mean void fraction, one can conclude that the flow in the dense region of the fast fluidized bed shows very similar properties over a wide span of flow parameters. No differences between turbulent and fast fluidized beds can be seen in the dense fluidized region of the bed even with X-ray flow visualization (Shao, 1986).

4.4 DISCUSSION OF EXPERIMENTAL RESULTS

The data presented raise the question whether or not fluidization regimes, as used presently, are properly defined to describe the different fluidized flow patterns. The dense bottom region in the fast fluidized bed is found

to be, as already mentioned, comparable to the fluidized section of a turbulent fluidized bed. This fluidized flow in the fast fluidized bed shows also a number of similarities to the flow in bubbling or slugging fluidized beds.

The above-mentioned regimes of fluidization are defined by Yerushalmi and Cankurt(1979). They described the transition between slugging and turbulent fluidized flow by the velocity Uc at which the relative pressure fluctuations level off after passing through a maximum in the slugging regime. Two plots that allow such a characterization are given in Figures 60 and 61 which are similar to Figure 33 and 34, resp.. In this case, however, the values are normalized by the mean pressure gradient, as was done in the above mentioned paper. The scattering of the data makes it hard to define an exact transition in both plots, but indicate that such a significant decay in the relative fluctuations, although fuzzy, exists.

The transition between the turbulent and fast fluidization regimes occurs over a relatively small gas velocity range during which the solid carry-over in the bed increases dramatically with increasing gas velocity. The existence of such a transition velocity range can also be seen for the data available, but it is clear that such a transition is not accompanied by a qualitative change in the pressure signals or in the flow structure as observed by

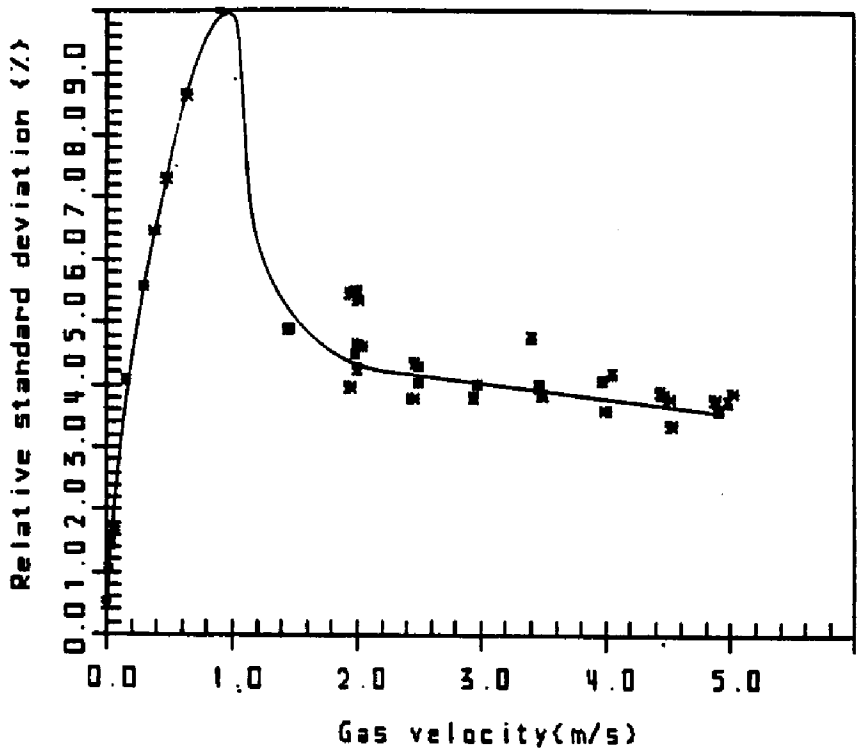

Fig. 60 Standard deviation of differential pressure signals within the dense fluidized region, normalized by the mean pressure difference

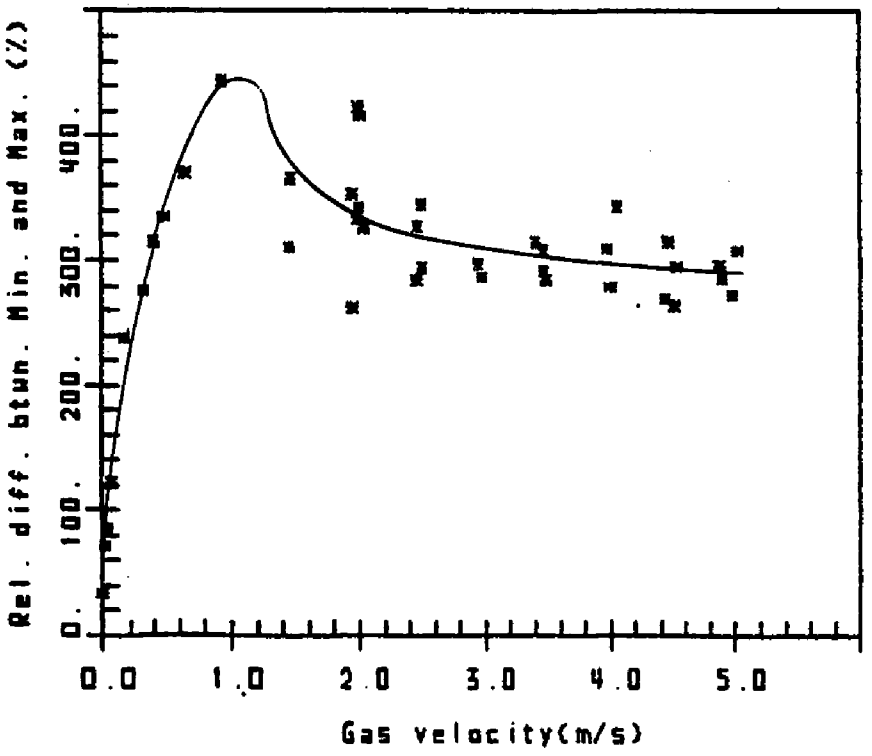

Fig. 61 Difference between the absolute minimum and maximum of differential pressure signals within the dense fluidized region, normalized by the mean pressure difference

X-ray visualization (Shao, 1986). However the magnitude of the pressure fluctuations clearly becomes smaller with gas velocity.

With this, one can conclude that both transition velocities as defined by Yerushalmi do not describe a clear change of the dense fluidized flow itself, but only describe some observable side effects. In terms of Uk these are special features of a slugging fluidized bed which are only evident at small bed diameters. Also Uk is then clearly a function of the bed diameter. In terms of Utr it really refers to the property of the flow in the upper dilute region of the bed which does not necessarily affect the fluidized flow in the dense bed.

Although both transitions unquestionably exist, the main flow characteristics which have been measured to date within the fluidized regions do not point them out. In Figure 62 the mean void fraction in the dense fludized region is again given as a function of the gas velocity. In this figure, one possible construction is given for the transition velocity dividing two newly defined fluidization classifications: Low and high velocity fluidization. High velocity fluidized beds will therefore be characterized by a relatively constant void fraction (in the dense region) over the gas velocity. Meanwhile low velocity fluidized beds, i.e. bubbling and slugging fluidized beds, show a strong increase of such void fraction with gas velocity. As one

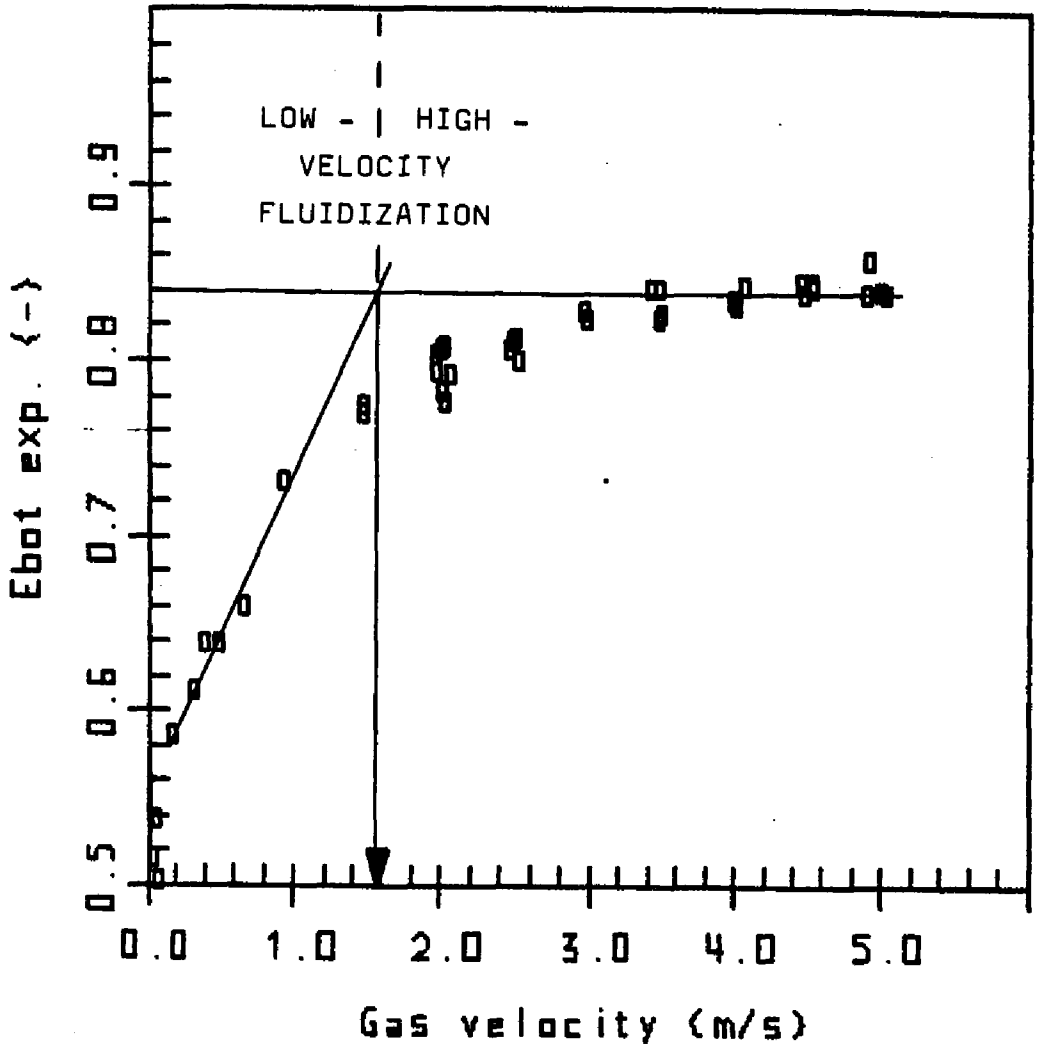

Fig. 62 Construction of transition velocity deviding low and high velocity fluidization on the basis of the mean void fraction in the dense fluidized region

possibility it is suggested to determine the transition velocity as the velocity at which the linear bed expansion curve of slugging or bubbling fluidized beds intersects the mean void fraction line of high velocity fluidization.

In a similar construction, found in Figure 63, the transition velocity is obtained by the intersection between the linear function of the slug rise velocity and the mean wave speed in high velocity fluidized beds. With the present experimental data this velocity corresponds obviously to the above mentioned transition velocity Uk between slugging and turbulent fluidized beds. As it was mentioned before, the wave speed is essentially constant for all gas velocities (and solid rates) within the turbulent and fast fluidization regimes (high velocity fluidization). Such a transition, however, might prove to be useful also in cases where no slugging phenomena can be observed. Instead of a linear function of the slug rising velocity a correlation for bubble velocities could be applied and the transition velocity be found again by the intersection between this function and the relatively constant wave speed of the high velocity fluidized beds.

The usefulness of both definitions is still to be shown. However, with the present data base such transition velocities between low and high velocity fluidized beds seem more appropriate if one considers the actual flow in the dense fluidized region of the bed. Low velocity fluidized

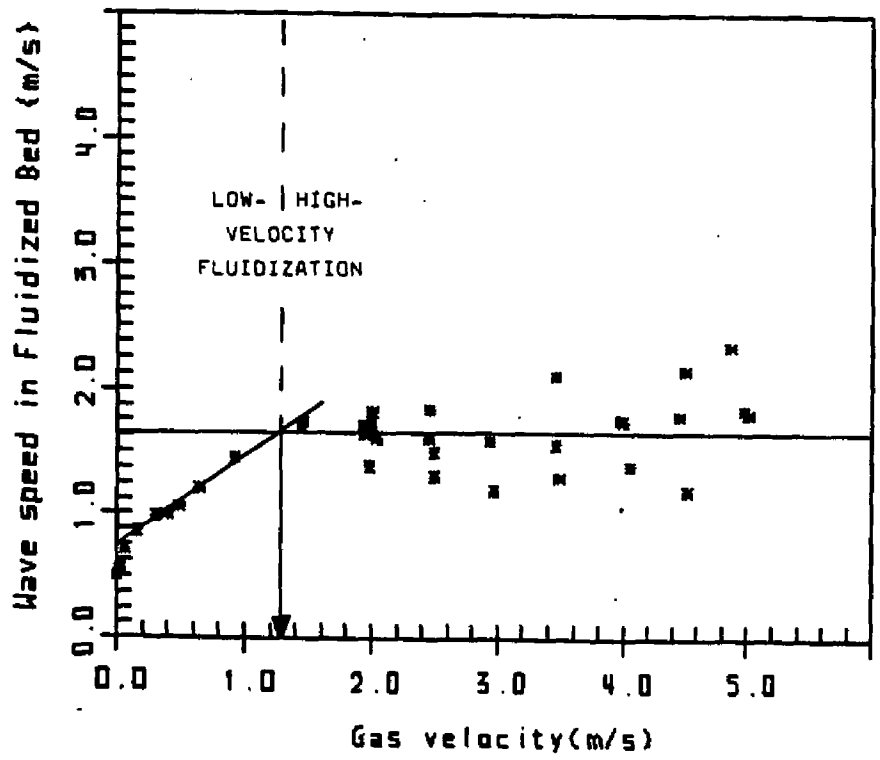

Fig. 63 Construction of transition velocity deviding low and high velocity fluidization on the basis of the mean wave speed in the dense fluidized region

beds are therefore characterized by a clear increase in the mean bed void fraction with a gas velocity. But this void fraction is more or less constant for high velocity fluidized beds. On the other hand the upward velocity of 'instabilities' in low velocity fluidized beds (bubbles or slugs) increases clearly with increasing gas velocity. But it should be noted that such a flow characteristic appears once again as constant within the gas velocity range of high velocity fluidized beds investigated herein. In all cases the solid rate is a parameter that does not clearly affect the void fraction or the wave speed in both fluidization classes. Since the transition between the two newly defined fluidization classes is not sharp, it is not expected that the transition velocities obtained from Figures 62 and 63 will be identical. The question as to which of the two methods will be best applicable needs to be shown in future studies. It also needs to be shown to what extent the diameter of the fluidization column and the characteristics of the solid influence the dependencies depicted in Figures 62 and 63.

In contrast to the transition between low and high velocity fluidized beds no information is available for any transition to a dilute phase flow. Certainly, one can obtain such a flow at any gas velocity by adjusting the bed height as was mentioned in Chapter 4.2. On the other hand, however, a dense phase region can also be obtained. Neither with the present data nor with literature data can such an

ultimate velocity be observed for the existence of high velocity fluidized flow. The transition velocity Upt, as mentioned in the paper by Yerushalmi and Cankurt does not at all relate to such a velocity. This characteristic velocity was obtained from data at a fixed location within the fluidization column. It relates mainly to the fact that the bed height or inflection point in the fast fluidized bed is dependent on the various flow and equipment related parameters and moved up and down past their fixed location unobserved by the investigators. It needs to be further noted that at high gas velocities no dense fluidized flow pattern can be observed simply because the pressure drops in the entrance and exit sections of the fluidization column are already in balance with the maximum pressure drop in the downcomer of the equipment (see Chapter 4.2). Both effects must not be mistaken as transition to another flow classification beyond high velocity fluidization.

With the above, the class of high velocity fluidized beds obviously exhibits a unique flow pattern. Whereas in bubbling or slugging fluidized beds the physical picture of the flow is well understood, a proper model representation for high velocity fluidized beds is yet to be established.

From previous investigations, as mentioned in Section 2.2.1, it can be concluded that the majority of solid particles over the crosssectional area can be found in a dense layer near the wall of the column. The corresponding

void fraction at the wall reaches even on a time averaged basis a value around that of minimum fluidization (ca. 0.50). It was also mentioned in the same chapter that the corresponding solid velocity in this layer is very small and exhibits mostly negative values on a time averaged basis.

With the present results the physical picture of the flow in high velocity fluidized beds must therefore include the following three regions over the crosssection:

1) Stagnant or downflowing solid in a compact form very near the wall
2) Upward moving solid with an average velocity (wave speed) fairly independent of the gas-velocity and solid rate which balances to a large extend the down flow of solid in the region 1 above
3) A dilute gas-solid core flow preferentially moving in the center of the fast fluidization column, at least for column diameters comparable to the one present in that investigation.

The form in which solid under 2) would travel upward is is not clear, however it is suggested that clusters independently suspended in a dilute flow are not a possible interpretation since such a cluster would most likely not be preserved over the entire dense flow region as pointed out earlier. On the other hand such clusters would also show a velocity very much dependent on the gas velocity since it seems unreasonable that the slip velocity betweeen gas and

cluster would increase due to chages in the cluster size in exactly the same proportion that the gas velocity increases. It is therefore suggested that the solid under 2) is moving between the dense wall region and the dilute core in the form of a wave.

With this model is seems more obvious why the magnitude and assymetry of the pressure fluctuations, the mean void fraction of the flow and the wave speed in the high-velocity fluidized bed are only a weak function of the gas velocity and solid rate. The differential pressure and its fluctuations are determined overwhelmingly by the properties of the dense annulus region, which is composed of partly stagnant or downflowing solid and solid rolling along it upward in form of waves (1) and 2)). The properties of this wall region only are therefore quite independent of the flow parameters. It seems very likely that a fluid dynamic stability analysis will lead to further insights into the flow. It needs to be noted further that the dense region in large scale fluidized beds might also be found in other regions other than wall regions. However, evidence for such dense regions not ajacent to the wall could not be found in laboratory investigations on a fast fluidized bed of 0.40 inside diameter (Hartge et al., 1985).

5. CONCLUSIONS

A number of significant conclusions can be drawn from the results presented in this work. In most cases these will revise present concepts describing the behavior of fast fluidized beds:

1) Typical fast fluidization can be described as a dense fluidized flow of solid at the bottom of the fluidization column with similarities to bubbling and turbulent fluidized beds. Strong pressure fluctuations are encountered within the dense fluidized region. For the differential pressure readings show asymmetric probability density functions. Void fraction calculations based on differential pressure measurements made with manometers are distorted. This is probably true for a majority of data in the literature where the average between absolute minimum and maximum of differential pressure readings was used. Time-mean measurements result in void fractions essentially constant over the entire length of the dense fluidized region. These mean void fractions are a very weak function of both the gas velocity and solid rate over the entire high velocity fluidization regime.

2) A dilute 2-phase flow exists at the top of the dense fluidized region with properties similar to those of pneumatic transport lines. The mean void fraction of the flow can be expressed by a particulate flow model with uniform slip velocities between solid particles and gas

taking into account additional solid hold-up in the wall region. The value for this hold-up varies with superficial gas velocity and solid rate in a range between 0.5% and 3%. With a value of 0.8% the model fits the majority of data.

3) The two flow regions in a fast fluidized bed are connected via a transition zone resembling the bed surface in turbulent fluidization. The transition in terms of the bed void fraction is much smoother. The position of this transition zone (bed height) of the fast fluidized bed is clearly dependent on the flow conditions at the bottom of the bed. Although both gas velocity and solid rate clearly affect the bed height, it is suspected that they equally affect the flow conditions at the gas inlet. Because of this, no conclusions can be drawn on whether or not the entrance flow conditions alone determine the bed height of a fast fludized bed. The bed height is limited by the maximum possible pressure drop over the recirculation leg only in cases where a unrestricted standpipe is used.

4) Upward travelling instabilities were detected within the fluidized region similar to those of slugging fluidized beds, but the magnitude of the fluctuations is much smaller. The instabilities seem to be stable over the entire length of the dense fluidized region. A corresponding wave speed is detected as constant over the total length of the fluidized region. Its value averages around 1.6 m/s for a wide range of superficial gas velocities (1.5 - 5.0 m/s).

5) Summarizing the results it can be concluded that solid is present in the dense fluidized region of a high velocity fluidized bed in at least three different forms:

i) Dipersed dilutely in the upward flowing gas

ii) Stagnant or down-flowing very near the wall at a void fraction close to minimum fluidization conditions

iii) Travelling upward in the form of denser packed solid aggregates with a constant average velocity between the two above regions in form of a solid wave.

6) Two classifications for fluidized beds are suggested: Low and high velocity fluidized beds. In low velocity fluidized beds the mean void fraction as well as the velocity of upward traveling instabilities (bubbles, slugs) is clearly a function of the superficial gas velocity. High velocity fluidized beds do not show any clear influence of the superficial gas velocity on the flow condition. In particular, the wave speed in the bed (velocity of instabilities) as also the mean void fraction are essentially constant over the entire range of gas velocity and solid rates.

APPENDIX A

SUMMARY OF EXPERIMENTAL DATA

DATA BASE

SUMMARY OF EXPERIMENTAL DATA

DATA BASE

Name of Experiment	Flow parameter			Entrance condition flow rates in			Experiments			
	Invt. (in.)	Ug (m/s)	Gs (kg/m2s)	N1 (cfm)	N2 (cfm)	N3 (cfm)	SCAN	#1	#2	#3
SLOWGP3A	100.00	0.03	0.0	0.0	00.0	1.0	Y	C	U	-
SLOWGP3B	100.00	0.03	0.0	0.0	00.0	1.0	N	-	-	-
SLOWGP5A	100.00	0.05	0.0	0.0	00.0	1.7	Y	C	U	-
SLOWGP5B	100.00	0.05	0.0	0.0	00.0	1.7	N	-	-	-
SLOWGP7A	100.00	0.07	0.0	0.0	00.0	2.3	Y	C	U	-
SLOWGP7B	100.00	0.07	0.0	0.0	00.0	2.3	N	-	-	-
SLOWG01A	100.00	0.10	0.0	0.0	00.0	3.5	Y	C	U	-
SLOWG01B	100.00	0.10	0.0	0.0	00.0	3.5	N	-	-	-
SLOWG02A	100.00	0.19	0.0	0.0	00.0	7.0	Y	B	U	-
SLOWG03A	115.00	0.35	0.0	0.0	00.0	12.0	Y	H	X	-
SLOWG03B	115.00	0.35	0.0	0.0	00.0	12.0	N	-	-	-
SLOWG03C	100.00	0.34	0.0	0.0	00.0	12.0	Y	C	U	-
SLOWG04A	100.00	0.43	0.0	0.0	00.0	13.3	Y	C	U	-
SLOWG05A	115.00	0.52	0.0	0.0	00.0	18.0	Y	H	X	-
SLOWG05B	115.00	0.52	0.0	0.0	00.0	16.0	N	-	-	-
SLOWG05C	100.00	0.51	0.0	0.0	00.0	18.0	Y	C	U	-
SLOWG05D	100.00	0.51	0.0	0.0	00.0	18.0	N	-	-	-
SLOWG07A	115.00	0.69	0.0	0.0	00.0	24.0	Y	H	-	-
SLOWG07B	115.00	0.70	0.0	0.0	00.0	24.0	N	-	-	-
SLOWG07C	100.00	0.68	0.0	0.0	00.0	24.0	Y	C	U	-
SLOWG07D	100.00	0.69	0.0	0.0	00.0	24.0	N	-	-	-
SLOWG10A	115.00	1.01	0.0	0.0	10.0	25.0	Y	H	Y	-
SLOWG10B	115.00	1.02	0.0	0.0	10.0	25.0	N	-	-	-
SLOWG10C	115.00	1.03	0.0	0.0	10.0	25.0	Y	H	Y	-
SLOWG10D	115.00	0.89	0.0	0.0	00.0	30.0	N	-	-	-
SLOWG10E	115.00	0.98	0.0	0.0	00.0	34.0	Y	H	X	-
SLOWG10F	115.00	0.98	0.0	0.0	00.0	34.0	N	-	-	-
SLOWG10G	100.00	0.98	0.0	0.0	00.0	33.0	Y	C	U	-
SLOWG10H	100.00	0.98	0.0	0.0	00.0	33.0	N	-	-	-
SLOWG15A	115.00	1.48	65.88	0.0	22.0	30.0	Y	C	Y	-
SLOWG15B	115.00	1.50	67.32	0.0	40.0	12.0	Y	H	X	-
SLOWG15C	115.00	1.50	64.76	0.0	40.0	12.0	N	-	-	-

SUMMARY OF EXPERIMENTAL DATA

DATA BASE

Name of Experiment	Invt. (in.)	Flow parameter Ug (m/s)	Gs (kg/m2s)	Entrance condition flow rates in N1 (cfm)	N2 (cfm)	N3 (cfm)	Experiments SCAN	#1	#2	#3
FFB2001A	73.25	2.03	35.39	0.0	45.0	23.0	Y	C	Y	-
FFB2020A	68.75	2.08	21.75	0.0	45.0	20.0	Y	6	U	-
FFB2030A	73.25	2.06	29.63	0.0	45.0	20.0	Y	-	-	-
FFB2030C	68.75	1.98	31.97	0.0	45.0	20.0	Y	A	X	-
FFB2050D	117.00	2.04	52.41	0.0	45.0	22.0	Y	A	W	-
FFB2050E	117.00	2.05	51.43	0.0	45.0	22.0	N	-	-	-
FFB2050J	90.00	2.02	53.39	0.0	45.0	25.0	N	-	-	-
FFB2050K	90.00	2.04	54.14	0.0	45.0	25.0	N	-	-	-
FFB2050P	100.00	2.04	49.88	0.0	45.0	20.0	Y	H	X	-
FFB2050Q	100.00	2.04	50.56	0.0	45.0	20.0	N	-	-	-
FFB2065P	100.00	2.03	66.83	0.0	45.0	22.0	Y	H	X	-
FFB2065Q	100.00	2.03	63.25	0.0	45.0	22.0	N	-	-	-
FFB2070D	115.00	2.08	88.80	0.0	45.0	25.0	Y	E	Y	-
FFB2070E	115.00	2.08	88.31	0.0	45.0	25.0	N	-	-	-
FFB2090D	115.00	1.98	94.16	0.0	45.0	22.0	Y	H	Y	-
FFB2090E	115.00	1.97	86.96	0.0	45.0	22.0	N	-	-	-
FFB2090P	100.00	2.04	88.34	0.0	45.0	25.0	Y	H	X	-
FFB2090Q	100.00	2.08	88.39	0.0	45.0	25.0	N	-	-	-
FFB20FFB	73.25	2.05	33.43	0.0	45.0	23.0	N	-	-	-
FFB20FFD (L)	115.00	2.03	114.69	0.0	45.0	25.0	Y	H	Y	-
FFB20FFE	115.00	2.04	132.40	0.0	45.0	25.0	N	-	-	-
FFB20FFJ	90.00	1.96	87.50	0.0	45.0	25.0	N	-	-	-
FFB20FFK	90.00	1.96	94.84	0.0	45.0	25.0	N	-	-	-
FFB20FFP	100.00	2.05	122.00	0.0	45.0	28.0	N	-	-	-
SPC20FFA	115.00	2.00	108.34	0.0	45.0	24.0	Y	*	*	-
SPC20FFB	115.00	1.99	104.86	0.0	45.0	24.0	N	-	-	-
SPC20FFC	115.00	2.01	131.68	0.0	45.0	24.0	Y	*	*	-
SPC20FFD	115.00	2.02	123.17	0.0	45.0	24.0	N	-	-	-
FFB2550A	88.88	2.65	49.34	0.0	55.0	28.0	Y	B	Y	-
FFB2550B	88.88	2.47	47.11	0.0	50.0	28.0	N	-	-	-
FFB2552A	88.88	2.52	52.16	0.0	55.0	28.0	N	-	-	-
FFB2570A (L)	88.88	2.50	70.59	0.0	55.0	28.0	Y	B	Y	-
FFB2570B	88.88	2.53	73.48	0.0	55.0	28.0	N	-	-	-
FFB2570D	115.00	2.53	75.38	0.0	60.0	22.0	Y	7	V	-
FFB2570E	115.00	2.56	72.96	0.0	60.0	22.0	N	-	-	-
FFB2572A	88.88	2.51	71.47	0.0	55.0	28.0	N	-	-	-
FFB2590D	115.00	2.50	93.42	0.0	60.0	23.0	Y	D	Y	-
FFB2590E	115.00	2.48	88.70	0.0	60.0	23.0	N	-	-	-
FFB25FFA	88.88	2.51	82.77	0.0	55.0	30.0	N	-	-	-
FFB25FFD	117.00	2.49	158.39	0.0	60.0	25.0	Y	H	Y	-
FFB25FFE	117.00	2.48	161.53	0.0	60.0	25.0	N	-	-	-
FFB25FFJ	90.00	2.55	297.87	0.0	60.0	28.0	N	-	-	-
FFB25FFK	90.00	2.55	306.73	0.0	60.0	28.0	N	-	-	-

SUMMARY OF EXPERIMENTAL DATA

DATA BASE

Name of Experiment	Flow parameter		Entrance condition flow rates in			Experiments			
	Invt. (in.)	Ug (m/s)	Gs (kg/m2s)	N1 (cfm)	N2 (cfm)	N3 (cfm)	SCAN	#1	#2	#3
FFB3002A	88.88	3.05	96.26	0.0	70.0	30.0	Y	?	?	-
FFB3002B	88.88	2.90	92.80	0.0	70.0	30.0	N	-	-	-
FFB3050D	115.00	3.14	53.67	0.0	70.0	28.0	N	-	-	-
FFB3050E	115.00	3.08	53.59	0.0	70.0	28.0	N	-	-	-
FFB3050J	90.00	3.01	55.61	0.0	65.0	30.0	N	-	-	-
FFB3050K	90.00	2.99	57.12	0.0	65.0	30.0	N	-	-	-
FFB3050M	70.00	3.09	54.24	0.0	70.0	28.0	N	-	-	-
FFB3050N	70.00	3.11	52.71	0.0	70.0	28.0	N	-	-	-
FFB3070D	115.00	3.09	70.05	0.0	70.0	26.0	Y	3	T	-
FFB3070E	115.00	3.08	71.41	0.0	70.0	26.0	N	-	-	-
FFB3070F	115.00	3.04	68.05	0.0	70.0	26.0	N	-	-	-
FFB3070J	90.00	3.10	66.79	0.0	70.0	30.0	N	-	-	-
FFB3070K	90.00	3.06	67.96	0.0	70.0	30.0	N	-	-	-
FFB3070M	70.00	3.10	74.73	0.0	70.0	30.0	N	-	-	-
FFB3070N	70.00	3.10	75.50	0.0	70.0	30.0	N	-	-	-
FFB3090D	115.00	3.01	89.34	0.0	70.0	26.0	Y	7	V	-
FFB3090E	115.00	2.96	87.89	0.0	70.0	26.0	N	-	-	-
FFB3090G	115.00	3.03	84.52	0.0	70.0	32.0	N	-	-	-
FFB3090H	115.00	3.04	88.62	0.0	70.0	32.0	Y	H	Y	-
FFB3090J	90.00	3.00	86.07	0.0	70.0	30.0	N	-	-	-
FFB3090K	90.00	3.00	91.28	0.0	70.0	30.0	N	-	-	-
FFB3090P	100.00	3.07	85.75	0.0	70.0	28.0	Y	H	X	-
FFB3090Q	100.00	3.09	88.49	0.0	70.0	28.0	N	-	-	-
FFB30A1D	115.00	3.00	112.92	0.0	70.0	30.0	Y	B	Y	-
FFB30A1E	115.00	3.02	111.75	0.0	70.0	30.0	N	-	-	-
FFB30A3D	115.00	2.98	133.13	0.0	70.0	30.0	Y	F	Y	-
FFB30A3E	115.00	2.98	125.51	0.0	70.0	30.0	N	-	-	-
FFB30C1A (L)	88.88	3.01	108.65	0.0	70.0	30.0	N	-	-	-
FFB30C1B	88.88	3.00	111.17	0.0	70.0	30.0	N	-	-	-
FFB30C1C	88.88	2.96	111.10	0.0	70.0	30.0	N	-	-	-
FFB30C2A (L)	88.88	2.98	118.37	0.0	70.0	30.0	N	-	-	-
FFB30FFD	115.00	2.93	200.12	0.0	70.0	30.0	N	-	-	-
FFB30FFE	115.00	2.92	185.30	0.0	70.0	30.0	N	-	-	-
FFB30FFJ	90.00	2.95	348.31	0.0	70.0	30.0	N	-	-	-
FFB30FFK	90.00	2.95	370.70	0.0	70.0	30.0	N	-	-	-
FFB30FFM	70.00	2.99	113.77	0.0	70.0	30.0	N	-	-	-
FFB30FFN	70.00	3.00	110.91	0.0	70.0	30.0	N	-	-	-

SUMMARY OF EXPERIMENTAL DATA

DATA BASE

Name of Experiment	Flow parameter		Entrance condition flow rates in			Experiments			
	Invt. (in.)	Ug (m/s)	Gs (kg/m2s)	N1 (cfm)	N2 (cfm)	N3 (cfm)	SCAN	#1	#2	#3
FFB3550A	88.88	3.50	54.85	0.0	85.0	24.0	N	-	-	-
FFB3570D	115.00	3.57	68.47	0.0	80.0	32.0	N	-	-	-
FFB3570E	115.00	3.59	68.83	0.0	80.0	32.0	N	-	-	-
FFB3570F	115.00	3.56	73.17	0.0	80.0	32.0	N	-	-	-
FFB3570J	90.00	3.56	68.85	0.0	80.0	35.0	N	-	-	-
FFB3570K	90.00	3.54	67.89	0.0	80.0	35.0	N	-	-	-
FFB3575A	88.88	3.51	74.17	0.0	85.0	30.0	N	-	-	-
FFB3590A	73.20	3.50	87.64	0.0	82.0	30.0	Y	5	U	-
FFB3590B	73.20	3.51	87.15	0.0	82.0	30.0	N	-	-	-
FFB3590D	115.00	3.52	93.53	0.0	80.0	32.0	Y	4	T	-
FFB3590E	115.00	3.57	92.61	0.0	80.0	32.0	N	-	-	-
FFB3590J	90.00	3.54	91.33	0.0	83.0	35.0	N	-	-	-
FFB3590K	90.00	3.54	96.10	0.0	83.0	35.0	N	-	-	-
FFB35A1A (L)	73.20	3.54	109.50	0.0	85.0	30.0	Y	7	V	-
FFB35A1B	73.20	3.52	110.58	0.0	85.0	30.0	N	-	-	-
FFB35A1D	115.00	3.46	107.27	0.0	80.0	32.0	Y	5	U	-
FFB35A3A	73.50	3.52	138.72	0.0	85.0	32.0	Y	B	X	-
FFB35A3B	73.20	3.51	131.80	0.0	85.0	32.0	N	-	-	-
FFB35A3D	115.00	3.54	136.04	0.0	85.0	31.0	Y	-	S	-
FFB35A3E	115.00	3.50	138.95	0.0	85.0	30.0	N	-	-	-
FFB35C1A	88.88	3.55	110.37	0.0	85.0	30.0	N	-	-	-
FFB35C3A	88.88	3.48	132.09	0.0	85.0	30.0	N	-	-	-
FFB35C6A	88.88	3.52	138.01	0.0	85.0	32.0	N	-	-	-
FFB35FFB	73.50	3.50	147.41	0.0	85.0	32.0	Y	B	X	-
FFB35FFD	115.00	3.50	143.09	0.0	85.0	34.0	Y	H	Y	-
FFB35FFE	115.00	3.52	186.85	0.0	85.0	35.0	N	-	-	-
FFB35FFF	115.00	3.44	215.80	0.0	85.0	33.0	Y	H	Y	-
FFB35FFG	115.00	3.40	185.05	0.0	85.0	32.0	N	-	-	-
FFB35FFJ	90.00	3.45	282.56	0.0	83.0	35.0	N	-	-	-
FFB35FFK	90.00	3.52	281.97	0.0	85.0	35.0	N	-	-	-
SPC35FFA	115.00	3.53	228.39	0.0	68.0	33.0	N	-	-	-

SUMMARY OF EXPERIMENTAL DATA

DATA BASE

Name of Experiment	Invt. (in.)	Flow parameter Ug (m/s)	Gs (kg/m2s)	Entrance condition flow rates in N1 (cfm)	N2 (cfm)	N3 (cfm)	Experiments SCAN	#1	#2	#3
FFB4065P	100.00	4.02	64.00	0.0	90.0	36.0	Y	H	X	-
FFB4065Q	100.00	4.09	67.35	0.0	90.0	36.0	N	-	-	-
FFB4070J	90.00	4.08	75.73	0.0	90.0	42.0	N	-	-	-
FFB4070K	90.00	4.11	76.28	0.0	90.0	42.0	N	-	-	-
FFB4090A	69.50	4.07	92.35	0.0	100.0	30.0	Y	5	U	-
FFB4090B	69.50	4.07	88.96	0.0	100.0	30.0	N	-	-	-
FFB4090D	115.00	4.09	88.31	0.0	95.0	34.0	Y	3	T	-
FFB4090E	115.00	4.09	74.18	0.0	95.0	34.0	N	-	-	-
FFB4090J	90.00	4.01	86.03	0.0	90.0	42.0	N	-	-	-
FFB4090K	90.00	4.00	86.46	0.0	90.0	42.0	N	-	-	-
FFB4090P	100.00	4.00	92.50	0.0	90.0	38.0	Y	H	X	-
FFB40A1A	73.50	4.07	109.05	0.0	100.0	30.0	Y	7	V	-
FFB40A1B	73.50	4.07	111.24	0.0	100.0	30.0	N	-	-	-
FFB40A1D	115.00	4.04	106.76	0.0	95.0	34.0	N	-	-	-
FFB40A1E	115.00	4.04	105.41	0.0	95.0	34.0	Y	3	T	-
FFB40A1J	90.00	4.01	103.52	0.0	92.0	42.0	N	-	-	-
FFB40A1K	90.00	4.04	104.36	0.0	92.0	42.0	N	-	-	-
FFB40A3A	73.50	4.08	129.93	0.0	100.0	33.0	Y	7	V	-
FFB40A3B	73.50	4.08	130.71	0.0	100.0	33.0	N	-	-	-
FFB40A5A	73.50	4.04	152.12	0.0	100.0	33.0	Y	B	X	-
FFB40A5B	73.50	4.04	146.82	0.0	100.0	33.0	N	-	-	-
FFB40C2A	88.88	4.02	123.34	0.0	100.0	30.0	N	-	-	-
FFB40C4A	88.88	4.07	144.70	0.0	100.0	33.0	N	-	-	-
FFB40FFA	73.50	3.98	165.88	0.0	100.0	33.0	N	-	-	-
FFB40FFB	73.50	4.01	152.15	0.0	100.0	33.0	Y	B	X	-
FFB40FFC	73.50	4.01	155.54	0.0	100.0	33.0	N	-	-	-
FFB40FFD	115.00	4.05	216.21	0.0	100.0	38.0	Y	F	Y	-
FFB40FFE	115.00	4.04	189.93	0.0	100.0	38.0	N	-	-	-
FFB40FFJ	90.00	3.99	293.86	0.0	95.0	42.0	N	-	-	-
FFB40FFK	90.00	3.99	289.58	0.0	95.0	42.0	N	-	-	-

SUMMARY OF EXPERIMENTAL DATA

DATA BASE

Name of Experiment	Flow parameter			Entrance condition flow rates in			Experiments			
	Invt. (in.)	Ug (m/s)	Gs (kg/m2s)	N1 (cfm)	N2 (cfm)	N3 (cfm)	SCAN	#1	#2	#3
FFB4570A	62.00	4.53	69.04	0.0	105.0	38.0	N	-	-	-
FFB4570B	62.00	4.51	71.97	0.0	105.0	38.0	N	-	-	-
FFB4590A	62.00	4.53	90.18	0.0	110.0	38.0	Y	S	U	-
FFB4590B	62.00	4.54	90.68	0.0	110.0	38.0	N	-	-	-
FFB4590D	117.00	4.55	91.59	0.0	110.0	35.0	N	-	-	-
FFB4590E	117.00	4.57	86.86	0.0	110.0	35.0	N	-	-	-
FFB45A1A	62.00	4.56	100.69	0.0	110.0	38.0	Y	T	V	-
FFB45A1B	62.00	4.58	103.14	0.0	110.0	38.0	N	-	-	-
FFB45A3D	115.00	4.56	136.10	0.0	120.0	30.0	Y	B	Y	-
FFB45A3E	115.00	4.50	116.52	0.0	120.0	30.0	N	-	-	-
FFB45A5D	115.00	4.54	148.77	0.0	120.0	30.0	Y	C	Y	-
FFB45A5E	115.00	4.55	153.98	0.0	120.0	30.0	N	-	-	-
FFB45FFA	69.50	4.50	143.40	0.0	110.0	38.0	Y	B	X	-
FFB45FFB	62.00	4.53	110.76	0.0	110.0	38.0	N	-	-	-
FFB45FFD	115.00	4.47	172.92	0.0	110.0	40.0	N	-	-	-
FFB45FFE	115.00	4.52	187.17	0.0	120.0	35.0	N	-	-	-
FFB45FFF	116.50	4.47	164.18	0.0	120.0	35.0	Y	H	Y	-
FFB45FFG	116.50	4.54	132.28	0.0	120.0	35.0	N	-	-	-

SUMMARY OF EXPERIMENTAL DATA

DATA BASE

Name of Experiment	Flow parameter			Entrance condition flow rates in			Experiments			
	Invt. (in.)	Ug (m/s)	Gs (kg/m2s)	N1 (cfm)	N2 (cfm)	N3 (cfm)	SCAN	#1	#2	#3
FFB5070A	61.00	5.07	67.04	0.0	110.0	50.0	N	-	-	-
FFB5070B	61.00	5.07	66.73	0.0	110.0	50.0	N	-	-	-
FFB5070M	70.00	5.05	68.33	0.0	115.0	45.0	N	-	-	-
FFB5070N	70.00	5.01	69.58	0.0	115.0	45.0	N	-	-	-
FFB5090A	61.00	4.98	90.58	0.0	110.0	50.0	Y	5	U	-
FFB5090B	61.00	4.98	92.00	0.0	110.0	50.0	N	-	-	-
FFB5090D	115.00	5.03	85.42	0.0	130.0	30.0	N	-	-	-
FFB5090E	115.00	4.94	96.27	0.0	129.0	30.0	N	-	-	-
FFB5090M	70.00	5.06	93.94	0.0	120.0	45.0	N	-	-	-
FFB5090N	70.00	5.06	92.83	0.0	120.0	45.0	N	-	-	-
FFB5090P	100.00	4.95	88.37	0.0	110.0	50.0	Y	G	X	-
FFB5090Q	100.00	5.10	94.56	0.0	110.0	50.0	N	-	-	-
FFB50A1D	115.00	5.09	112.66	0.0	130.0	31.0	Y	4	U	-
FFB50A1E	115.00	4.97	108.65	0.0	130.0	30.0	N	-	-	-
FFB50A3D	115.00	5.02	132.43	0.0	130.0	39.0	Y	C	X	-
FFB50A3E	115.00	5.05	134.70	0.0	130.0	39.0	N	-	-	-
FFB50A5D	115.00	4.91	149.56	0.0	130.0	37.0	Y	C	X	-
FFB50A5E	115.00	4.92	129.90	0.0	130.0	37.0	N	-	-	-
FFB50A5P	100.00	4.93	149.76	0.0	115.0	51.0	Y	G	X	-
FFB50A5Q	100.00	4.96	149.01	0.0	115.0	51.0	N	-	-	-
FFB50FFA	62.00	4.97	108.08	0.0	110.0	50.0	Y	5	U	-
FFB50FFB	61.20	5.04	105.83	0.0	110.0	51.0	N	-	-	-
FFB50FFC	61.20	4.95	107.03	0.0	110.0	50.0	N	-	-	-
FFB50FFD	89.00	5.05	197.37	0.0	130.0	37.0	Y	D	Y	-
FFB50FFE	89.00	5.04	195.32	0.0	130.0	37.0	N	-	-	-
FFB50FFM	70.00	4.95	154.31	0.0	120.0	45.0	N	-	-	-
FFB50FFN	70.00	5.03	172.13	0.0	120.0	45.0	N	-	-	-

APPENDIX B

INFORMATION ON PRESSURE DIFFERENTIALS

INFORMATION ON PRESSURE DIFFERENTIALS

Pressure between taps #	Diff. Length (m)	Corresponding Channel in Date Acquisition
01 - 02	00.400	02
02 - 03	00.435	03
03 - 04	00.521	04
04 - 05	00.391	05
05 - 06	00.445	06
06 - 07	00.473	07
07 - 08	00.572	08
08 - 09	00.394	09
09 - 10	00.464	10
10 - 11	00.476	11
11 - 12	00.467	12
12 - 13	00.483	13
13 - 14	00.445	14
14 - 15	00.451	15
15 - 16	00.356	16
16 - 17	00.638	17

R E F E R E N C E S

Arastroopour, H. and D. Gidaspow (1979), "Vertical Pneumatic Cocveying Using Four Hydrodynamic Models," Ind. Eng. Chem. Fundam., 18, pp. 123 - 130

Arena, U., Cammarato, a. and Pistone, L. (1985), "High Velocity Fluidization Behaviour of Solids in a Laboratory Scale Circulating Bed," Paper presented at the First Int'l. Conference on Circulating Fluidized Beds, Halifax, Canada

Avidan, A.A. (1980), "Bed Expansion and Solid Mixing in High Velocity Fluidized Beds," Ph.D. Thesis, City University of New York

Avidan, A.A. and J. Yerushalmi (1982), "Bed Expansion in High Velocity Fluidization," Pow. Techn., 32, pp. 223 - 232

Batch, J. (1980), "Entwicklungsstand der Wirbelschicht-feuerung", VDI-Berichte 363

Beisswenger, H., Daradimos,G, Janssen, K. and Petersen, V. (1980), "Die Verbrennung ballastreicher, meist schwefelhaltiger Brennstoffe in der zirkulierenden Wirbelschicht" , Aufbereitungs- technik, 12, pp. 616 - 621

Beisswenger, H., Petersen, V. and Plass, L. (1981), "Circulating Fluid Bed Combustion for Energy Production and Process Heat Delivery," Proceeding to the second World Congress of Chem. Engng., Montreal, Canada, vol. 3

Beisswenger, H., Daradimos, G., Janssen, K. and Petersen, V. (1981), "Use of Circulating Fluidized Beds as High Temperature Reactor," Germ. Chem. Engng., 4, pp. 285 - 291

Berker, A. and Tulig, T. J. (1986), "Hydrodynamis of Gas-Solid Flow in a Catalytic Cracker Riser: Implications for Reactor Selectivity Performance," Chem. Eng. Science, 41, pp. 821-827

Brereton, C. and L. Stroemberg (1985), "Some Aspects of the Fluid Dynamic Behavior of Fast fluidized Beds," Paper presented at the First Int'l Conference of Circulating Fluidized Beds, Halifax, Canada

Bitterlich, E. (1980), "Die Wirbelschichttechnologie als Prozess zur umweltfreundlichen Energieerzeugung", VGB Kraftwerkstechnik, 60, pp.373 - 374

Cankurt, N.T. and J. Yerushalmi (1978), "Gas Backmixing in High Velocity Fluidized Beds," in "Fluidization", Davidson J.F and D.L. Kearins, Cambridge Univ. Press, Cambridge, p. 387

Capes, C.E. (1971), "Dense Phase Vertical Pneumatic Conveying," Can. J. Chem. Engng., 49, p. 182

Capes, C.E. and Nakamura, K. (1973), "Vertical Pneumatic Conveying, An Experimental Study with Particles in the Intermediate and Turbulent Regimes," Can, J. Chem. Engng, 51, pp. 31 - 38

Engstrom, F. (1980), "High-Sulphur Fuel Combustion in A Circulating Fludi Bed," Information by the Ahlstroem Company, Helsinki, Finland

Fan. L.-S., Satija, S. and Wisecarver, K. (1986), "Pressure Fluctuation Measurements and Flow Regime Transitions in Gas-Liquid-Solid Fluidized Beds," AICHE J., 32, p. 328

Geldart, D. (1973), "Types of Gas Fluidization," Pow. Tech., 7, pp. 285 - 292

Hartge, E.-U., Li, Y. and Werther, J. (1985), "Analysis of the local Structure of the Two Phase Flow in a Fast Fluidized Bed," Paper presented at the First Int'l Conference on Circulating Fluidized Beds, Halifax, Canada

Helmrich, H. (1979), "Reactionstechnische Untersuchungen chemischer Reactoren - insbesondere zirkulierender Wirbelschichtreactoren - zur Durch- fuehrung nichtkatalytischer Gas - Feststoffreactionen", Habilitationsschrift, Technische Universitaet Hannover

Hikita, T., Jkeda, M. and Asano, H. (1983), "Upward Transportation of Particles in Dense Phase," Paper presented at the IV Int'l. Conference on Fluidization, Japan

Hofbauer, H. (1982), "Untersuchungen an einer zirkulierenden Wirbelschicht mit Zentralrohr", CIT, 54, pp. 528 - 529

Judd, M.R. and P.D. Dixon (1974), "The Flow of fine, Dense Solids Down a Vertical Standpipe," AICHE Symp. Ser., 74, pp. 38 - 44

Kehoe, P.W.K. and J.F. Davidson (1971), "Continuously Slugging Fludized Beds," Inst. Chem. Engrs. (London) Symp. Ser. 33, pp. 97 - 116

Ketta, J.J. and Cunningham, W.A. (1981), "Catalytic Cracking", in "Encylopedia of Chemical Processing and Design", Marcel Dekker Publ., New York - Basel

Knowlton, T.M. and D.M. Bachovchin (1976), "The Determination of Gas-Solids Pressure Drop and Choking Velocity as a Function of Gas Density in a Vertical Pneumatic Conveying Line," in "Fluidization Technology," D.L. Kearins, Hemisphere Publishing Corporation, New York

Kuramoto, M., Ogata, H., Koya, T., Furusawa, T. and Kunii, D. (1981), "Circulation System of Fluidized Solids Within a Single Vessel," in proceedings to the second World Congress of Chem. Engng, Montreal, Canada, vol. 3

Kwauk, M., Ningde, W., Youchu, L., Bingyu, C. and Zhiyuan, S. (1985), "Fast Fluidization at ICM," Paper presented at the First International Conference on Circulating Fluidized Beds, Halifax, Canada, 1985

Lanneau, K.P. (1960), "Gas-Solids Contacting in Fluidized Beds," Trans. Inst. Chem. Engrs., 38, p. 125

Leung, L.S., Wiles, R.J. and Nicklin, D.J. (1969), "Transition from Fluidized to Packed Bed Flow in Vertical Hydraulic Conveying," Trans. Inst. Chem. Engrs., 47, p. T271 - T278

Leung, L.S., Wiles, R.J. and Nicklin, D.J. (1971), "Correlation for Predicting Choking Flowrates in Vertical Pneumatic Conveying," Ind. Eng. Chem. Process Des. Dev., 10, pp. 183 - 189

Leung, L.S. and Wiles, R.J. (1976), "A Quantitative Design Procedure for Vertical Pneumatic Conveying Systems," Ind. Eng. Chem. Process Des. Dev., 15, pp. 552 - 556

Lewis, W.K., Gilliland, E.R. and Bauer, W.C. (1949), "Characterisics of Fluidized Particles," Ind. Eng. Chem., 41, pp. 1104 - 1117

Li, Y. and M. Kwauk (1980), "The Dynamics of Fast Fluidization," in "Fluidization", Grace, J.R. and J.M. Matsen, Plenum Press, New York - London, p. 537

Li, Y., Chen, B., Wang, F., Wang, J. and Guo, M. (1981), "Rapid Fluidization," Int. Chem. Engng., 21, pp. 670 - 678

Liss, B., Graff, R.A. and Yerushalmi, J. (1981), "Design of High-velocity Fluid Beds for Flash Hydrogenation," Fuel Process. Techn., 5, pp. 1 - 24

Lurgi - Umwelt und Chemotechnik (1982), "Rauchgase im Muellkraftwerk", Umweltmagazin (West Germany), 2, p.42

Massimilla. L. (1971), "Behavior of Catalytic Beds of Fine Particles at High Gas Velocities," AICHE Sym. Ser., 69, pp. 11 - 13

Matsen, J.M., Howard, S. and Davidson, J.F. (1969), "Expansion of Fluidized Beds in Slug Flow," CES, 24, pp. 1743 - 1754

Matsen, J.M. (1737), "Flow of Fluidized Solids and Bubbles in Standpipes and Risers," Pow. Tech., 7, pp. 93 - 96

Matsen, J.M. (1976), "Some characteristics of Large Solids Circulation Systems," in "Fluidization Technology", D.L Kearins, Hemisphere Publ. Corp., New York

Matsen, J.M. (1982), "Mechanisms of Choking and Entrainment," Pow. Tech., 32, pp. 21 - 33

Matsen, J.M. (1983), "A Phase Diagram for Gas - Particle Flow," Paper presented at the IV Int'l. Conf. on Fluidization, Japan

Meller, M. M. (1984) "The Structure and Operation Characteristics of High Velocity Fluidized Beds," Ph.D. Thesis, City University of New York

Mohamed, M., Ta'eed, O. and Gibbs, B.M. (1985), "Cold Modelling of the Hydrodynamics of a Recirculating Fluidized Bed," Paper presented at the First International Conference on Circulating Fluidized Beds, Halifax, Canada, 1985

Molerus, O. (1982), "Interpretation of Geldart's Type A,B,C and D Powders by Taking into Account Interparticle Forces," Pow. Tech., 33, pp. 81 - 87

Monceaux, L., Azzi, M., Molodtsof, Y. and Large, J.F. (1985), "Overal and Local Characterization of Flow Regimes in a Circulating Fluidized Bed," Paper presented at the First International Conference on Circulating Fluidized Beds, Halifax, Canada, 1985

Morooka, S., Kago, T. and Kato, Y. (1983), "Flow Pattern of Solid Particles in the Freeboard of a Fluidized Bed," Paper presented at the IV Int'l. Conf. on Fluidization, Japan

Nakamura, K. and C.E. Capes (1976), "Vertical Conveying of Binary Particle Mixtures," in "Fluidization Technology", D.L. Kearins, Hemisphere Publ. Corp., New York

Paul, M. (1982), "Digitale Messwertverarbeitung", VDE-Verlag, Berlin-Offenbach

Rangachari, S. and R. Jackson (1982), "The Stability of Steady States in a One-Dimensional Model of Standpipe Flow," Pow. Tech., 31, pp. 185 - 196

Reddy, K.V.S. and D.C.T. Pei (1969), "Particle Dynamics in Solid - Gas Flow in a Vertical Pipe," Ind. Eng. Chem. Fund., 8, pp. 490 - 502

Reh, L. (1971), "Fluid Bed Processing," Chem. Eng. Progr., 67, pp. 58 - 64

Reh, L. (1974), "Highly Expanded Fluidbeds and Melting Cyclons for High-Temperature Reactions between Gases and Fine Particles," Reprints of the GVC/AICHE joint meeting and Jahrestreffen der Verfahrensingenieure, Munich

Reh, L. (1979), "High Temperature Fluid Bed Reactors in Processing, Environmental Protection and Enery Supply," Information of the Lurgi Company, Frankfurt a.M., West Germany

Reh, L., Plass, L. and Morchessaux, Ph. (1979), "Thermal Decomposition of Aluminium Chloride Hexahydrate for Aluminia Production," Information (C1326/6.79) of the Lurgi Company, Frankfurt a.M., West Germany

Reh, L. (1979), "Fluid Bed Combustion in Processing, Environmental Protection and Energy Supply," Paper presented at the Int'l. Fluidized Bed Combustion Symposium af the American Flame Research Commitee, Boston, Massachussetts

Reh, L. (1980), "Circulating Fluidbed Combustion, An efficient Technology For Energy Supply and Environment Protection," Conference Reprints: Fluidized Combustion: Systems and Applications, Institute of Energy, Symposium Series, Num. 4

Reh, L. (1983), "Neue Grosstechnische Anwendungen des Reaktorprinzips der zirkulierenden Wirbelschicht im Umweltschutz", Paper presented at the Jahrestreffen der Verfahrensingenieure, Nuremberg

Rhodes, M.J. and Geldart, D. (1985), "The Hydrodynamics of Re-Circulating Fluidized Beds," Paper presented at the first Int'l. Conference on Circulating Fluidized Beds, Halifax, Canada

Richardson, J.F. and W.N. Zaki (1954), "Sedimentation and Fluidization, Part I," Trans. Inst. Chem. Engrs., 32, pp. 35 - 53

Saxton, A.L and A.C. Worley (1970), "Modern Catalytic-Cracking Design," Oil and Gas J., 68, pp. 82 - 99

Schmidt, W., Beiswenger, H. and Kaempf, F. (1979), "Flexibility of Fluid Bed Calciner Process in View of Changing Demands in th Alumina Market," Am. Inst. of Mining, Metalurgical and Petroleum Engineers: 106th AIME Anual Meeting, New Orleans

Shao, M. (1986) "Radial and Axial Variation in Voidage in High Velocity Fluidized Beds," Ph.D. Thesis, City University of New York

Squires, A.M. (1962), "Species of Fluidization," CEP 58, pp. 66 - 73

Squires, A.M. (1975), "Application of Fluidization Beds in Coal Technology," Lecture Notes on Int'l. Seminar on Heat an Mass Transfer Problems in Future Energy Production, Dubrovnik, Yugoslavia

Squires, A.M., Kwauk, M. and Avidan, A.A. (1985), "Fluid Beds,: At last, Challenging Two Entrenched Practices," Science, 230, p. 1329

Shimano, S. (1983), "Lurgi Fluidized Bed Calciner for Sandy-Type Alumina," Paper presented at the IV Int'l. Conference on Fluidization, Japan

Sitnai, O. (1982), "Utilization of The Differential Records from Gas Fluidized Beds With Internals for Bubble Parameters Determination," CES, 37, pp. 1059 - 1066

Tutu, N.K. (1982), "Pressure Fluctuations and Flow Pattern Recognition in vertical Two Phase Gas - Liquid Flows," Int. J. Multiphase Flow, 8, pp. 443 - 447

Wein, W., Hoeffgen, H., Daradimos, G. and Maintok, K.-H. (1980), "Die zirkulierende atmosphaerische Wirbelschicht, eine Feuerungstechnologie fuer umweltfreundliche Kraftwerke", KFA-PLE Status- seminar "Umweltfreundliche Kraftwerkstechnologie", Juelich

Wein, W. (1982), "Verbrauchernahe Energieerzeugung durch ein Heizkraftwerk mit der umweltfreundlichen zirkulierenden, atmosphaerischen Wirbelschichtfeuerung", VGB Kraftwerkstechnik, 62, pp. 185 - 190

Weinstein, H., Graff, R.A., Meller, M. and Shao, M.J. (1983), "The Influence of the Imposed Pressure Drop across a Fast Fludized Bed," Paper presented at the IV Int'l. Conference on Fluidization, Japan

Weinstein, H., Shao, M.J., Schnitzlein, M. and Graff,R.A. (1985), "Radial Variation in Void Fraction in a Fast Fluidized Bed," Paper presented at the V Int'l. Conference on Fluidization, Elsinore, Denmark

Wen, C.Y. and L.H. Chen (1982), "Fluidized Bed Freeboard Phenomena: Entrainment and Elutriation," AICHE J., 28,pp. 117 - 128

Wen, C.Y. and R.F. Hashinger (1960), "Elutriation of Solid Paricles from a Dense-Phase Fludized Bed," AICHE J., 6, pp. 220 - 226

Wisecarver, K.D., Kitano, K. and Fan, S. (1985), "Pressure Fluctuations in a Multi-Solid Pneumatic Transport Bed," Paper presented at the First International Conference on Circulating Fluidized Beds, Halifax, Canada, 1985

Wilhelm, R.H. and M. Kwauk (1948), "Fluidization of Solid Particles," CEP, 44, pp. 201 - 218

Yerushalmi, J., McIver, A.E. and Squires, A.M. (1974), "The Fast Fluidzed Bed," Preprints of GVC/AICHE Joint Meeting and Jahrestreffen der Vahrensingenieure, Munich

Yerushalmi, J., Gluckman, M.J., Graff, R.A., Dobner, S. and Squires, A.M. (1976), "Production of Gaseous Fuels From Coal in The Fast Fludized Bed," in "Fluidization Technology," D.L. Kearins, Hemisphere Publ. Corp., New York

Yerushalmi, J. and A.M. Squires (1976), "The Phenomenon of Fast Fluidization," AICHE Sym. Ser., 73, pp. 44 - 50

Yersuhalmi, J., Turner, D.H. and Squires, A.M. (1976), "The Fast Fluidized Bed," Ind. Eng. Chem. Process Des. Dev., 47

Yerushalmi, J., Cankurt, N.T., Geldart, D. and Liss, B. (1978), "Flow Regimes in Vertical Gas - Solid Contact Systems," AICHE Sym. Ser., 74, pp. 1 - 13

Yerushalmi, J. and N.T. Cankurt (1978), "High-Velocity Fluidized Beds," Chem.-Tech., 9, pp. 564 - 572

Yerushalmi, J. and N.T. Cankurt (1979), "Further Studies of the Regimes of Fluidization," Pow. Tech., 24, pp. 187 - 205